# Mechanisms of Acid Mist Formation in Electrowinning

Thesis submitted by

**Reza Al Shakarji**

Bachelor of Science (Chemical Engineering Honours, JCU)

in February 2012

for the degree of Doctor of Philosophy

in the School of Engineering and Physical Sciences

James Cook University

Australia

# Statement of the contributions of others

**Thesis supervisory team:**

Professor Yinghe He, School of Engineering and Physical Sciences, James Cook University

Mr Simon Gregory, Manufacturing Superintendent, Xstrata Technology

**Statistical and theoretical support:**

Professor Yinghe He

Professor Peter Ridd

Dr Yvette Everingham

**Editorial support:**

Professor Yinghe He

Mr Simon Gregory

Dr Rosalind Gummow

Ms Elizabeth Tynan

# Statement of Access

I, the undersigned, the author of this thesis, understand that James Cook University will make it available for use within the University Library and, by microfilm or other means, allow access to users in other approved libraries. All users consulting with this thesis will have to sign the following statement:

In consulting this thesis I agree not to copy or closely paraphrase it in whole or in part without written consent of the author; and to make proper public written acknowledgement for any assistance which I have obtained from it. Beyond this, I do not wish to place any restriction on access to this thesis.

06/02/2012

---------- ----------

Reza Al Shakarji Date

# Sources Declaration

I declare that this thesis is my own work and has not been submitted in any form for another degree or diploma at any university or other institution of tertiary education. Information derived from the published or unpublished work of others has been acknowledged in the text and a list of references is given.

Every reasonable effort has been made to gain permission and acknowledge the owners of copyright material. I would be pleased to hear from any copyright owner who has been omitted or incorrectly acknowledged.

06/02/2012

---------- ----------

Reza Al Shakarji Date

# Acknowledgements

I would like to thank my family, especially my parents, who strongly encouraged me to undertake a postgraduate study. Their continuous and unlimited support helped me not to give up and continue my work regardless of the many great challenges that I had to overcome.

I am very appreciative of my academic supervisor, Professor Yinghe He, for his invaluable support and advice over the course of my PhD candidature. Professor He helped me, on many occasions, to overcome the challenges of my project and to explain a number of unusual and counter-intuitive observations I encountered in my experiments.

I would like to thank Xstrata Technology for their financial and technical support. Special thanks to the following Xstrata Technology staff who helped me to overcome a number of difficult technical challenges: Simon Gregory, Nigel Aslin, Christian Pastan, and Tony Ruddell.

I would like to express my gratitude to the technicians of the engineering workshops at James Cook University who assisted me with the design and fabrication of customized equipment for my experiments: Curtis Arrowsmith, James Galbraith, Warren O'Donnell, John Renehan, and Lloyd Baker.

I am grateful to the academic and administrative assistance provided by the staff of the School of Engineering and Physical Sciences of James Cook University especially: Professor Peter Ridd, Associate Professor Mohan Jacob, Ruilan Liu, Alison Ambrey, Paula Rodger, and Melissa Norton.

# Abstract

Acid mist is generated during electrowinning in the final stage of hydrometallurgical production processes of metals including copper, zinc and nickel. In electrowinning, oxygen bubbles are formed on the anode. Burst of these bubbles at the solution/air interface produces fine acid-containing liquid droplets which become airborne and disperse throughout the workplace. These droplets are known as acid mist. Acid mist poses a serious health hazard to the workers. It also results in severe structural and equipment corrosion, costing the industry millions of dollars every year.

Prior to this study, little quantitative information was available on acid mist generation and the process parameters that affect its amount. Moreover, while it was well acknowledged that the amount of acid mist was related to the size of the electrolytically generated bubbles, no systematic measurements had been made to quantify bubble size and its relationship with materials and process variables. The present work investigates the parameters that affect acid mist amount and bubble size, acid mist-bubble size correlation, acid mist generation mechanisms, and the effectiveness of typical acid mist suppression techniques.

Five variables are tested for their influence on the amount of acid mist generated, namely, solution temperature, FC-1100 (a surfactant widely used in copper electrowinning to suppress acid mist), electrical current density, solution acidity, and anode age. Among them, solution temperature and FC-1100 show significant effect. More than 90% of the variations in the acid mist generation can be explained by changes made in the two parameters and their interaction. To a lesser extent, electrical current density and solution acidity also affect the total amount of acid mist generated. Anode's age and most of the 3, 4, and 5-way parameter interactions show negligible influence on the amount of acid mist. Overall, acid mist increases with temperature and current density. In contrast, increasing the viscosity of the electrolyte solution decreases the amount of acid mist.

A technique is developed for the size measurement of oxygen bubbles formed on the anode in copper electrowinning. High resolution images of the bubbles are captured by utilizing a high speed camera, super bright LEDs, and a special viewing chamber. Regardless of the operating conditions, bubbles are found to be generated in a wide size distribution ranging from 20 μm to more than 400 μm in diameter with an overall average diameter of about 53 μm. Statistical analyses on the measurement results show that

addition of FC-1100 and solution temperature are the two most influential test parameters on the bubble size followed by the age of the anode. In contrast, current density and solution acidity have negligible effect on the bubble sizes.

In the absence of surfactants, the amount of generated acid mist decreases as the average bubble size increases. In contrast, in the presence of a surfactant such as FC-1100, acid mist shows little correlation with the average bubble size. The significant change in the bubble burst mechanism, due to the presence of surfactant molecules in the solution/air interface, is believed to be the reason for the suppression of the effect of bubble size on acid mist.

Theoretical assessment of the source of acid mist suggests that acid mist is formed almost entirely from airborne jet drops and not film drops as generally understood. Jet drops are created from the disintegration of a liquid jet that is formed after the collapse of the bubble cavity. The diameter of the jet drops, generated during copper electrowinning, is estimated to range from about 0.1 μm up to 54 μm. The maximum acid mist concentration, for a given air speed above the cell, is shown (theoretically and experimentally) to occur not at the solution/air interface but rather at a certain height above the solution line.

Floating plastic objects, such as small balls and beads, are widely used in industry to supress acid mist. The two important factors that influence the performance of such floating barriers are shown to be their coverage of the solution's surface area and their height above the solution line. When comparing single layered floating barriers, spherical shaped barriers reduce acid mist the most due to their higher buoyancy and higher coverage of the solution surface. In general, barriers made of high density polyethylene are 3.4% more effective in reducing acid mist than those made of polypropylene due to their lower density which enables them to be more buoyant in the solution and intercept acid mist more effectively.

Acid mist is reduced noticeably with the addition of FC-1100 to the solution up to 30 ppm. Further addition of FC-1100 makes much less difference in the suppression of acid mist. When FC-1100 is used in combination with floating barriers (such as spheres), the reduction in acid mist further improves by an average of 29% in comparison to the use of FC-1100 alone.

# Publications

**Journal papers:**

- Al Shakarji, R, He, Y & Gregory, S 2011, 'Statistical analysis of the effect of operating parameters on acid mist generation in copper electrowinning', *Hydrometallurgy,* vol. 106**,** pp. 113-118.
- Al Shakarji, R, He, Y & Gregory, S 2011, 'The sizing of oxygen bubbles in copper electrowinning', *Hydrometallurgy,* vol. 109**,** pp. 168-174.
- Al Shakarji, R, He, Y & Gregory, S 2012, 'Acid mist and bubble size correlation in copper electrowinning', *Hydrometallurgy,* vol. 113–114**,** pp. 39-41.
- Al Shakarji, R., He, Y., Gregory, S., 2012. *Performance Evaluation of Acid Mist Reduction Techniques*. Hydrometallurgy (under review).
- Al Shakarji, R., He, Y., Gregory, S., 2012. *Mechanism of acid mist formation in copper electrowinning,* (in preparation).

**Conferences:**

- Al Shakarji, R., He, Y., Gregory, S 2009, 'Mechanisms of acid mist formation', paper presented at the 5th International Seminar on Copper Hydrometallurgy, Antofagasta Chile, 13-15 May.
- Al Shakarji, R, He, Y & Gregory, S 2010, 'Measurement of Bubble Size Distribution in Copper Electrowinning Process by Image Analysis', *7th International Copper Conference*, GDMB, Germany, vol. 4, pp. 1237-1251.
- Al Shakarji, R., He, Y., Gregory, S 2010, 'Influential parameters in acid mist generation', paper presented at the Tankhouse Technology Conference, San Pedro de Atacama Chile, 15-18 November.
- Al Shakarji, R., He, Y., Gregory, S 2011, 'Performances of Mechanical Barriers in Reducing Acid Mist', paper presented at the *6th International Seminar on Copper Hydrometallurgy*, Vina del Mar Chile, 6-8 July.

# Table of Contents

# List of Tables



# List of Figures

# Nomenclature

| | |
|---|---|
| a | droplet's overall acceleration (m $s^{-2}$) |
| $a_d$ | droplet's acceleration due to air drag (m $s^{-2}$) |
| $a_f$ | initial area of a thin film |
| $a_g$ | droplet's acceleration due to gravity (m $s^{-2}$) |
| $A_H$ | Hamaker constant |
| C | coulombs (unit of electric charge) |
| $C_d$ | Drag coefficient |
| CCC | critical coalescence concentration |
| CMC | critical micelle concentration |
| CRL | Copper Refinery Ltd |
| $D_b$ | diameter of a bubble (mm) |
| $D_i$ | nominal bubble diameter for category i (μm) |
| $D_{drop}$ | diameter of a droplet (m) |
| $E^0$ | half-cell potential (Volts) |
| $E^0_{cell}$ | standard cell potential (Volts) |
| EW | electrowinning |
| F | Faraday constant ($9.649\times10^4$ C $mol^{-1}$) |
| $F_b$ | buoyancy force (N) |
| $F_d$ | drag force (N) |
| $F_i$ | inertia force (N) |
| $F_p$ | pressure force (N) |
| $F_s$ | surface tension force (N) |
| g | gravitational acceleration (m $s^{-2}$) |
| H | Henry coefficient (kg $m^{-1}$ $s^{-2}$) |

| | |
|---|---|
| $h_c$ | critical thickness of rupture (m) |
| I | electric current (Amperes) |
| $M_i$ | molar mass of species i (g $mol^{-1}$) |
| $\dot{m}_{Cu}$ | copper production rate (g $s^{-1}$) |
| $N_{film}$ | number of film drops |
| $N_i$ | number frequency of detected bubbles with a nominal diameter of $D_i$ |
| $N_j$ | number frequency of all the bubbles generated with a nominal diameter of $D_i$ |
| $N_{jet}$ | number of jet drops |
| NMR | nuclear magnetic resonance |
| NPE | nonyl phenol ethoxylate |
| $P_0$ | atmospheric pressure (Pa) |
| $P_B$ | pressure inside the bubble (Pa) |
| $P_C$ | capillary pressure (Pa) |
| $P_H$ | hydrostatic pressure (Pa) |
| $Q_{O_2}$ | oxygen production rate ($m^3$ $s^{-1}$) |
| R | universal gas constant (8.314 J $K^{-1}$ $mol^{-1}$) |
| r | bubble radius (m, µm) |
| $r_{base}$ | radius of the bubble's base (m, µm) |
| $R_{bubble}$ | radius of bubble (µm) |
| $R_{drop}$ | radius of droplet (µm) |
| Re | Reynolds number |
| Sc | Schmidt number |
| $s_{e\ drop}$ | speed of ejection of a droplet (m $s^{-1}$) |
| Sh | Sherwood number |
| STEL | short time exposure limit |
| SX | solvent extraction |

| | |
|---|---|
| T | temperature (Kelvin) |
| t | time (seconds) |
| TWA | time-weighted average |
| u | instantaneous velocity of a droplet (m $s^{-1}$) |
| $u_o$ | initial (ejection) velocity of a droplet (m $s^{-1}$) |
| $V_B$ | bubble volume ($m^3$) |
| $V_i$ | total oxygen volume of detected bubbles with a nominal diameter of $D_i$ |
| $V_j$ | total oxygen volume of all the bubbles generated with a nominal diameter of $D_i$ |
| $V_{tot}$ | total volume of the oxygen generated during electrolysis |
| w | weight of the electrodeposit (grams) |
| z | instantaneous height of a droplet above the solution (m) |
| $z_o$ | initial (ejection) height of a droplet above the solution (m) |
| $\gamma$ | surface or interfacial tension (mN $m^{-1}$) |
| $\eta$ | efficiency |
| $\theta$ | contact angle (degrees) |
| $\rho_{O_2}$ | density of oxygen gas (g $m^{-3}$) |
| $\rho_G$ | density of gas |
| $\rho_L$ | density of liquid |

# Chapter 1: Introduction

Most metals occur in nature in oxidized form in their ores and thus must be reduced to their metallic forms. In hydrometallurgical processes, the ore is normally dissolved following some pre-processing in an aqueous electrolyte and the resulting solution is electrolysed. The metal is deposited on the cathode while the anodic reaction is usually oxygen evolution. Metals such as copper, zinc, and nickel are naturally present as metal sulphides. Most metal sulphides or their salts are electrically conductive and this allows electrochemical redox reactions to efficiently occur in the aqueous solutions.

Electrowinning is an important process for the economical purification of non-ferrous metals such as copper, zinc and nickel. Currently, there are 57 copper electrowinning tankhouses worldwide (similar to that shown in Figure 1.1) producing more than 4.5 million tonnes of pure copper per annum (ICSG 2010). In 2010, the worldwide zinc and nickel production exceeded 12 million and 1.5 million tonnes per annum, respectively (Wallace 2011, Miller 2012).

In electrowinning, a current is passed from an inert anode through the metal-containing aqueous solution so that the metal is extracted as it is deposited onto the cathode. As part of the electrowinning process, large volumes of oxygen gas in the form of micro-bubbles are generated at the inert anodes. The burst of these oxygen bubbles at the free surface of the solution ejects fine acidic droplets into the air which become airborne and disperse throughout the workplace (the fog that can be seen in Figure 1.1). This acid-containing mist not only poses a serious health hazard to the workers but also causes severe corrosions of the cathodes, anodes, hanger bars and other equipment of the tankhouse.

**Figure 1.1** A typical 400,000 tonne capacity copper electrowinning tankhouse (Piedras Verdes in Mexico) with clearly visible acid mist in the air

There have been many attempts to eliminate or minimize acid mist in electrowinning operations. Polyethylene balls, suction hoods, mats, brushes and wipers, chemical reagents and forced ventilation are examples of such attempts (Mella et al. 2006, Davis and Eng 2002, Hooper 2008, Sunwest 2004, 3M 2007). However, the majority of these methods attempt to treat the symptoms of acid mist rather than the root causes of mist formation. This is because little is known about the acid mist generation mechanism and only a handful of scientific papers have directly discussed this topic.

## 1.1 Background

Copper production worldwide has increased exponentially in recent years. Total copper production was less than 500,000 metric tonnes in 1900 and exceeded 18 million metric tonnes in 2009 (ICSG 2010). With the ever increasing demand for copper, especially by China and India, copper prices have also increased significantly in recent years. The price of copper has surged by over 450% between 2002 and 2010 (ICSG 2010).

Copper is extracted from its ore by pyrometallurgy or hydrometallurgy, depending on the ore type. About 25% of primary copper production comes from the hydrometallurgical processing of copper ore. Hydrometallurgy is mainly used to process copper oxide ores such as cuprite ($Cu_2O$) and tenorite (CuO) (Davenport et al. 2002). Hydrometallurgical processes involve leaching, solvent extraction (SX) and electrowinning (EW) as illustrated in Figure 1.2.

In leaching, dilute sulphuric acid (about 10 g $L^{-1}$ $H_2SO_4$) is sprinkled over a heap of crushed ore (Robinson et al. 1994). The acid reacts with the oxidised minerals as it flows slowly through the ore to the collection ponds. The resulting solution (also known as the pregnant solution) contains 1-6 g $L^{-1}$ copper, 0.5-5 g $L^{-1}$ $H_2SO_4$, and some impurities such as Fe and Mn (Davenport et al. 2002).

The copper concentration in the pregnant solution is too low for electrochemical purification of copper. Hence, SX is employed to reduce the impurities and to produce high concentration copper electrolyte. The resulting electrolyte solution from SX, known as rich electrolyte, has a copper ion concentration of about 45 g $L^{-1}$.

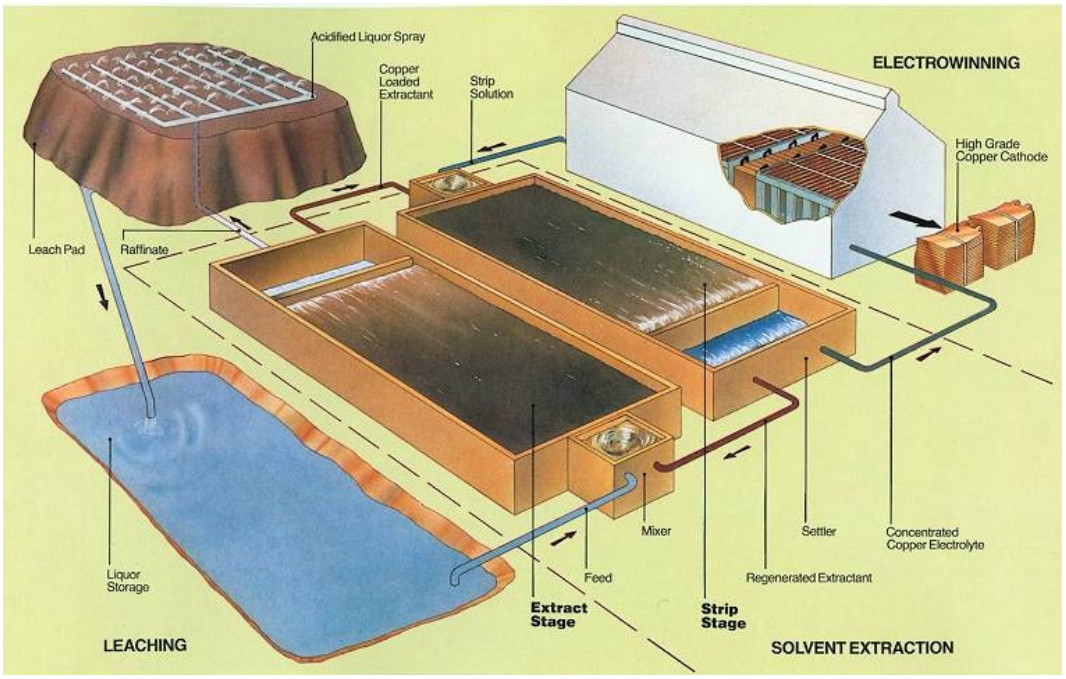


**Figure 1.2** A schematic view of copper leaching, solvent extraction, and electrowinning operations (PMOS 2003)

Electrowinning is employed to produce pure metallic copper from the rich electrolyte. Polymer concrete cells are first filled with the copper-rich electrolyte which has been heated to about 45 ˚C. Anodes (made of inert lead alloys) and cathodes (made of stainless steel) are then placed in the cell. When the anodes and cathodes are connected to a direct current power source, copper cations from the electrolyte solution deposit on the surface of the cathode and form sheets of pure copper metal. The produced copper sheets are then stripped from the cathodes by mechanical means. These copper sheets have a purity greater than 99.99% (Robinson et al. 1994) which is known as Grade A copper in the London Metal Exchange market.

During electrowinning, oxidation reaction occurs at the anode and oxygen bubbles nucleate at the surface of the anode. Once these bubbles reach a certain size, they detach from their nucleation sites and rise through the electrolyte solution. The wetted oxygen bubbles burst at the free surface of the solution and produce fine acid-containing liquid droplets as illustrated in Figure 1.3. These droplets become airborne and form acid mist which disperses throughout the tankhouse atmosphere by natural or forced convection.

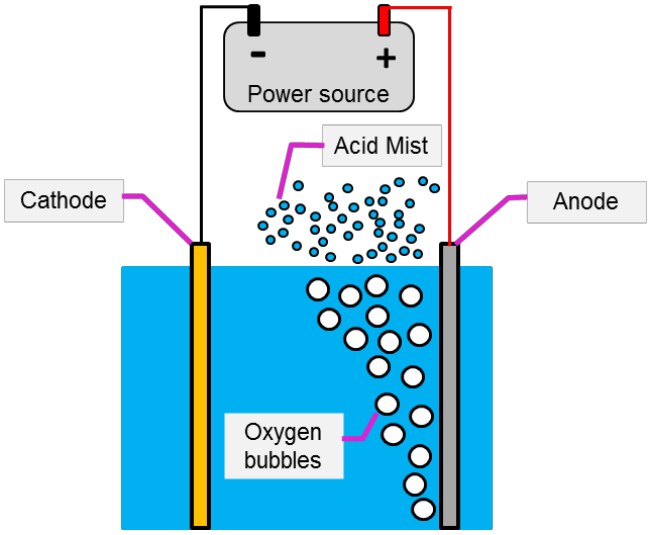


**Figure 1.3** A schematic view of copper electrowinning process and acid mist formation

A current density of 280-340 A $m^{-2}$ is applied during electrowinning which is similar to that of electrorefining. However, the electrical potential required for electrowinning is much higher than that of electrorefining. The electrical potential employed during electrowinning is about 2 V whereas that of electrorefining is only about 0.3 V (Davenport et al. 2002). This high voltage requirement is the main reason for the high energy consumption of the electrowinning operation. For instance, to produce one tonne of copper, the energy requirement for electrowinning is about 2000 kWh whereas that of electrorefining is 300-400 kWh (Davenport et al. 2002). Nevertheless, the overall investment and operating costs of hydrometallurgical processes are considerably lower than those of conventional pyrometallurgical processes. The reason is that hydrometallurgy does not involve high energy consuming processes, such as smelting, that are employed in pyrometallurgy. The lower capital and operating costs were the driving force for the rapid adoption of hydrometallurgical processes in the 1990's, particularly for the production of copper in Chile (Davenport et al. 2002).

## 1.2 Thesis Objectives

In order to solve the acid mist problem in copper electrowinning operations, it is imperative to develop a fundamental understanding of the mechanisms of acid mist formation. The impact of acid mist on workers' health, building structures and equipment, in addition to the rapid increase in SX-EW operations worldwide for copper production, highlight the importance of such a study. No specific publications could be found in the literature that examine the mechanism of oxygen bubble formation and burst during the copper electrowinning process. The primary goal of this thesis is to

systematically investigate the mechanisms of acid mist generation during copper electrowinning process, and its correlation to materials and process variables. In this context, the specific aims of this thesis are to:

1. Determine the level of significance of a range of operating parameters on the amount of acid mist being generated.
2. Determine bubble sizes produced under different operating conditions and quantify the effect of operating parameters on the average bubble size and bubble size distribution.
3. Investigate the relationship between bubble size and the amount of acid mist generated.
4. Investigate the effect of geometry and material properties of mechanical barriers, floating on the surface of the solution, on the acid mist amount.

## 1.3 Thesis outline

This thesis is presented as a series of chapters that have already been published or currently being reviewed for publication in international journals and conferences. The authorship of the chapters is shared with my academic and industry supervisors, Professor Yinghe He and Simon Gregory, respectively. Professor Yinghe He and Simon Gregory have assisted me with the experimental design, interpretation of the experimental results, and editing my reports.

**Chapter 1** gives a brief overview of the history of copper production and prices worldwide. The two major methods of producing primary copper, pyrometallurgy and hydrometallurgy, are also briefly discussed.

**Chapter 2** presents the most relevant and recent literature on acid mist and the electrolytically generated bubbles. Generation, negative impacts, and minimization of acid mist are discussed in detail. Also, literature on bubble nucleation, growth, size measurement, and burst are presented and critically analysed in this chapter.

**Chapter 3** describes a series of experiments that were conducted to determine the most influential parameters on acid mist. The relationship between the amount of acid mist generated and five process parameters is analysed quantitatively. Mechanistic explanation for each parameter's high (or low) influence on acid mist generation is also given. The content of this chapter has been published in Hydrometallurgy (Al Shakarji, R., He, Y., Gregory, S., 2011. *Statistical analysis of the effect of operating parameters on acid mist generation in copper electrowinning*. Hydrometallurgy, vol. 106, pp. 113-118).

**Chapter 4** describes a novel technique that was developed to measure bubble sizes by image analysis. Accurate estimations of the rate of bubble generation at various electrical current densities are also presented. In addition, the effect of changing the electrical current density on both the amount of acid mist and on the size distribution of bubbles is analysed. The content of this chapter has been published in the proceedings of the 7th International Copper Conference which was held in Hamburg Germany in 2010 (Al Shakarji, R., He, Y., Gregory, S 2010, 'Measurement of Bubble Size Distribution in Copper Electrowinning Process by Image Analysis', *Electrowinning and –refining: proceedings from the 7th International Copper Conference*, GDMB, Hamburg Germany, pp. 1237-1251).

**Chapter 5** offers accurate and extensive data on the size of the oxygen bubbles that were generated under various operating conditions. The influence of each of the five test variables, on bubble size, is quantified and the reasons for its effects are discussed. The content of this chapter has been published in Hydrometallurgy (Al Shakarji, R., He, Y., Gregory, S., 2011. *The sizing of oxygen bubbles in copper electrowinning*. Hydrometallurgy, vol. 109, pp. 168-174).

**Chapter 6** examines the correlation between the average bubble size and the amount of acid mist generated. This is done by analysing the acid mist and bubble size measurements at various operating conditions (i.e. data from Chapters 3 and 5). The content of this chapter has been published in Hydrometallurgy (Al Shakarji, R., He, Y., Gregory, S., 2012. *Acid mist and bubble size correlation in copper electrowinning*. Hydrometallurgy, vol. 113-114, pp. 39-41).

**Chapter 7** investigates jet drops as the source of acid mist. Size distribution, ejection speed, and maximum height reached by these droplets are also presented. Moreover, the effect of air suction rate, above the cell, on the concentration of acid mist at various heights is also examined.

**Chapter 8** quantifies and compares the effectiveness of various acid mist suppression techniques. Mechanistic explanations for the differences seen in the performance of floating barriers are also presented in this chapter. The content of this chapter has been submitted to Hydrometallurgy for publication (Al Shakarji, R., He, Y., Gregory, S. *Performance Evaluation of Acid Mist Reduction Techniques*. Hydrometallurgy, under review).

**Chapter 9** summarizes the important findings of this PhD research project. Based on the experiences gained from this PhD project, a number of recommendations are also made for future research.

# Chapter 2: Literature Review

## 2.1 Electrowinning of copper

To electrowin copper, the copper-containing solution from the solvent extraction process is sent to the electrowinning cells. Cells usually are constructed from polymer concrete to withstand the corrosivity of the electrolyte solution and to resist the mechanical wear due to material handling within the cell (CTI-ANCOR 2001). In each cell, anodes and cathodes are aligned in parallel. Cathodes are positioned so that the distance between any two cathodes is 90-100 mm (Houlachi et al. 2007).

When electrodes are connected to the power source, the reduction reaction occurs at the cathode and copper ions deposit onto the surface of the cathode. At the anode, oxidation reaction takes place and oxygen is liberated from the electrolyte. The overall electrowinning reaction is as following:

$$CuSO_{4\,(aq)} + H_2O_{\,(aq)} \rightarrow Cu_{\,(s)} + H_2SO_{4\,(aq)} + \tfrac{1}{2}\, O_{2\,(g)} \qquad E^0_{cell} = -0.89\, V \qquad (\mathbf{2.1})$$

The negative cell voltage in equation 2.1 means the reaction is non-spontaneous and extra energy is needed to overcome the thermodynamics. Although the theoretical voltage required for the reaction is about 0.9 V, in practice an electric potential of about 2 V is employed to extract copper from its solution. This discrepancy is due to the oxygen evolution overpotential (~0.5 V), copper deposition overvoltage (~0.05 V), and electrical resistance of the electrolyte (~0.5 V) (Davenport et al. 2002).

### 2.1.1. Cathode

More than two-thirds of the SX-EW plants employ permanent cathode technology in their electrowinning tankhouses (Houlachi et al. 2007). Currently, there are three different permanent cathode technologies: ISA Process, Kidd Process, and Outotec Ew. All three technologies utilize 316L stainless steel, with 2B finish, for the blade of the cathode.

The reduction reaction, which takes place at the cathode, during copper electrowinning is shown in equation 2.2.

$$Cu^{2+}_{\,(aq)} + 2e^- \rightarrow Cu_{\,(s)} \qquad E^0 = +0.34\, V \qquad (\mathbf{2.2})$$

The current density applied to the cathode is 200-300 A $m^{-2}$. The cathode current efficiency (η), which ranges from 88% to 92%, depends on the operational conditions of

the tankhouse (Davenport et al. 2002). The rate of copper production, $\dot{m}_{Cu}$ (g $s^{-1}$), can be predicted by equation 2.3 derived from the Faraday's law:

$$\dot{m}_{Cu} = \eta \frac{IM_{Cu}}{zF} \qquad (2.3)$$

In equation 2.3, $I$ is the electrical current (in ampere), $M_{Cu}$ is the molar mass of copper (63.45 g $mol^{-1}$), $z$ is the number of electrons required to reduce a copper ion, and $F$ is the Faraday constant (96,485 A s $mol^{-1}$).

A cathode consists of a blade and a hangar bar. The size and the geometry of the cathode depend on the cell design. The blade of a typical cathode is approximately 1100 mm long, 1000 mm wide, and 3 mm thick (Houlachi et al. 2007).

If copper deposits on the edges of the cathode blade, stripping copper from the cathode becomes a difficult task. To avoid this problem, the side edges of the blade are masked by ABS or PVC strips and the bottom edge is either waxed or V-grooved (Houlachi et al. 2007). These edge masks prevent copper from depositing on the blade's edges and result in two separate copper sheets on each side of the blade.

### 2.1.2. Anode process

Anodes' design and geometry depend on the tankhouse configuration and cell specification. A typical lead anode is a rectangular cube which is 1100 mm long, 900 mm wide and 6 mm thick (Davenport et al. 2002). The useful life of an anode strongly depends on the operating conditions of the tankhouse. The average life of an anode is 3-5 years; however some plants reported anode life up to ten years (Houlachi et al. 2007).

Lead alloys are the preferred anode material to electrowin copper from acidic sulphate solution. Insolubility, corrosion and passivation resistance, relatively low cost, and acceptable operating voltage are some of the important characteristics of lead alloy anodes. About 86% of the electrowinning plants utilize cold rolled lead-Tin-Calcium (Pb-Sn-Ca) alloy as their anode, and the remaining 14% use cast lead anode (CTI-ANCOR 2001).

Tin in the lead alloy anode reduces creep and corrosion and improves conductivity (Houlachi et al. 2007). Calcium, added to the alloy, improves the mechanical properties and decreases the potential of the anode but it also increases the rate of corrosion (Houlachi et al. 2007). Cold rolling the alloy, which elongates the grains, increases the strength and corrosion resistance of the anode (Davenport et al. 2002).

The electrolysis of water molecules at the anode leads to the liberation of oxygen gas as illustrated in equation 2.4:

$$H_2O_{(aq)} \rightarrow \frac{1}{2} O_{2(g)} + 2H^+ + 2e^- \qquad E^0 = -1.23\ V \qquad \textbf{(2.4)}$$

The rate of oxygen production, $Q_{O_2}$ ($m^3\ s^{-1}$), can be estimated as:

$$Q_{O_2} = \frac{IM_{O_2}}{zF\rho_{O_2}} \qquad \textbf{(2.5)}$$

In equation 2.5, $I$ is the electrical current (in ampere), $M_{O_2}$ is the molar mass of oxygen (32 g $mol^{-1}$), $z$ is the number of electrons involved in the generation of one oxygen molecule, $F$ is the Faraday constant (96,485 A s $mol^{-1}$), and $\rho_{O_2}$ is the density of oxygen gas ($\rho_{O_2} = 1308$ g $m^{-3}$ at 45 $^oC$ and 101325 Pa).

To reduce the high energy requirements of copper electrowinning, alternative anodic reactions can be introduced. The cell potential, for example, can be reduced to less than half (from 1.8 V to 0.77 V) by adding sulphurous acid to the copper electrolyte solution (Subbaiah et al. 2000). Since sulphur dioxide is oxidised at the anode, instead of water molecules, no oxygen evolution is expected and therefore no acid mist should be generated during the electrowinning process. However, although this technique reduces the power consumption, it doubles the production of sulphuric acid which has to be removed from the electrolyte solution (Subbaiah et al. 2000).

One of the problems of using lead alloy anodes is the particle flake off. The main reason for particle flake off is the formation of a porous lead sulphate ($PbSO_4$) layer on the surface of the anode (Moskalyk et al. 1999). These particles, apart from polluting the electrolyte solution, can deposit on the cathode surface and reduce the quality of the copper deposit.

To minimize lead spalling and achieve a lead free copper cathode, more stable anodes have been introduced to the market in recent years. These include: activated lead (Pb coated with Ir-$O_2$), dimensionally stable anode (Ti coated with Ir-$O_2$ or Ir-Co), and Mesh-on-Lead anodes (Subbaiah et al. 2000). However, the high capital and maintenance cost of these anodes is usually their main disadvantage.

### 2.1.3. Electrolyte

#### *Composition*

In copper electrowinning, electrolyte flows in and out of each cell at a rate of 0.18-0.25 $m^3$ $min^{-1}$. Electrolyte that enters the cell has the following characteristics (Houlachi et al. 2007):

- Copper; 40-45 g $L^{-1}$
- $H_2SO_4$; 165-185 g $L^{-1}$
- Temperature; 40-50 $^oC$
- Iron ions ($Fe^{+2}$, $Fe^{+3}$); 0.15-2 g $L^{-1}$
- Guar gum addition; 200-300 g per tonne of cathode
- $Co^{+2}$ addition; 100-150 ppm
- $Cl^-$ ions; 20-30 ppm

Guar gum is a levelling agent which is compatible with solvent extraction and is added to the electrolyte solution to promote dense and level copper deposit (Davenport et al. 2002).

Cobalt in the electrolyte solution minimizes lead contamination of the copper deposit and also extends anode life (Davenport et al. 2002). The reason is that in the presence of cobalt ions a continuous $PbSO_4$ + α-$PbO_2$ film is formed on the surface of the lead alloy which protects the anode from further oxidation (Nguyen et al. 2008). The presence of cobalt ions in the electrolyte solution also makes the anodic film dense and compact whereas the absence of cobalt ions results in a thick and porous anodic film.

Nguyen et al. (2008) also investigated the effect of the cobalt ion concentration on the electrical potential of the anode. The anode potential was found to reach the steady state quicker as the cobalt ion concentration increased. At 0 ppm it took approximately one hour to reach a steady state potential of 2.15 V whereas at concentrations above 100 ppm a steady state potential of less than 2 V was achieved within the first few minutes.

Chloride promotes dense and fine grain growth of copper deposit (Davenport et al. 2002). Chloride ions are either already in the electrolyte, from copper ore, or they are maintained by adding HCl to the electrolyte solution. Chloride ions, despite their usefulness, are reduced to chlorine gas at high enough concentrations and pit corrode the stainless steel blade. Therefore, chloride ion concentration are kept below 30 ppm to

prevent pit corrosion of the cathode blade and to prevent the deposited copper from sticking to the blade and resisting detachment (Houlachi et al. 2007).

### *Circulation*

Electrolyte flow manifolds are widely used in copper electrowinning cells. Although flow manifolds improve fluid mixing within the cell, gas sparging has long been investigated as a possible mean of enhancing the efficiency of copper electrowinning (Rigby et al. 2001). Some fundamental studies have shown that gas sparging decreases the thickness of the concentration boundary layer, near the cathode, and increases the mass transfer coefficient up to ten fold (Rigby et al. 2001).

In gas sparging, the pumped air is released in form of bubbles at the bottom of the electrowinning cells. These bubbles rise and burst at the free surface of the solution. There have been no studies, to the best of author's knowledge, to quantify the effect of gas sparging on the amount of acid mist. Most likely, the amount of acid mist will increase when air sparging is used due to the increase in the number of bubbles bursting at the solution/air interface resulting in the ejection of more acid-containing droplets into the air. However, if the sparged bubbles are large enough (larger than 5 mm) and coalesce with oxygen bubbles (generated by electrolysis), less droplets are ejected into the air above the solution and the amount of acid mist could actually decrease.

Investigation on different manifold and sparging designs has been mainly focused on improving fluid mixing within the cell. Another primary goal for such research is to increase copper production by employing higher electrical current densities. Under normal electrowinning conditions, applying current densities higher than 300 A $m^{-2}$ would increase nodule formation on the cathode resulting in low quality copper. However, with the aid of appropriate manifold and sparger designs, high quality copper can be produced at higher current densities. Rigby et al. (2001) claim that copper of acceptable quality can be produced at current densities of up to 600 A $m^{-2}$ by employing their specially designed venturi bolt sparger that produces bubbly electrolyte (i.e. air-electrolyte jet).

## 2.2 Acid mist related problems

The anodic process of copper electrowinning involves the generation of millions of oxygen bubbles on the surface of the anode. These oxygen bubbles rise through the

solution and burst at the free surface of the electrolyte producing small and highly acidic airborne droplets known as acid mist.

Acid mist is highly corrosive and results in the corrosion of cathode plates, anode's hanger bar, tankhouse equipment and building structures. It also poses a serious health hazard. Sulphuric acid mist was confirmed as a human carcinogen in 1992 by the International Agency for Research on Cancer (HSIS 2009). Acid mist disperses throughout the tankhouse of the electrowinning plant, by natural or forced convection, and causes extreme discomfort to the skin, eyes and respiratory systems of the tankhouse workers. Occupational Safety and Health Administration (OSHA) recommends a time-weighted average (TWA) exposure limit of 1 mg of sulphuric acid per $m^3$ of air, and a short term exposure limit (STEL) of 3 mg per $m^3$ of air (OSHA 2003). These exposure limits are also adopted by European countries and Australia as well as USA (HSIS 2009). However, American Conference of Governmental Industrial Hygienists (ACGIH) in 2004 proposed a TWA exposure limit of 0.2 mg per $m^3$ of air (3M 2007).

If acid mist is not managed properly and exhausted outside the tankhouse without proper treatment, it can have negative impacts on the surrounding plants, soil and underground water. The negative impact of acid mist on the cost of copper is also significant. Copper electrowinning tankhouses, for example, spend millions of dollars every year to install and run ventilation fans and hoods, to replace corroded equipment, and to purchase specialized personal protective equipment for the tankhouse workers.

## 2.3 Acid mist generation mechanisms

### 2.3.1. Bubble burst

When a bubble rises through the bulk liquid and reaches the surface of the liquid, a thin film is produced on top of the bubble. The stability and lifetime of this thin film is influenced by a number of factors such as surfactant concentration, surface diffusion, surface tension gradient and drainage rate (Pugh 1996).

Pugh (1996) suggests that gravity is the main driving force for liquid film drainage. Gravity acts directly on the film or indirectly through capillary suction at the junctions between bubbles. Generally, drainage rate decreases as the bulk viscosity of the solution increases (Pugh 1996). Viscosity can be increased by adding a solute, such as glycerine, or by adding a certain type of surfactants to the aqueous system capable of producing gel networks.

Increasing surface viscosity and surface elasticity of the solution can also decrease the drainage rate (Pugh 1996). These two factors can be increased by increasing the adhesive and cohesive bonding at the surface by means of highly packed surfactant molecules at the liquid/gas interface. Polymeric surfactants or mixed surfactant systems can maintain high cohesion forces in the film surface. It should be noted that surface viscosity mainly influences the drainage rate of thin films whereas bulk viscosity affects the drainage rate of thick films (Pugh 1996).

As mentioned before, liquid films become thinner under the effect of drainage. A liquid film may rupture when it reaches a critical thickness ($h_c$). The critical thickness of rupture can be estimated by using Van der Waals intermolecular forces, surface tension and disjoining pressure (Pugh 1996):

$$h_c = 0.267\left(\frac{a_f A_H^2}{6\pi\gamma\Delta p}\right)^{1/7} \qquad (2.6)$$

In equation 2.6, $a_f$ is the initial area of the film, $A_H$ is the Hamaker constant, $\gamma$ is the surface or interfacial tension, and $\Delta p$ is the excess pressure in the film.

### 2.3.2. Aerosol formation

When a bubble bursts at the free surface of a liquid, it usually produces two types of drops: film drops and jet drops. Film drops are created from the shattering of the film cap of the bubble (Figure 2.1a). After the collapse of the bubble cavity, liquid rushes towards the centre and rises from the surface of the solution as a liquid jet (Figure 2.1b). The disintegration of this liquid jet forms a series of droplets known as jet drops.

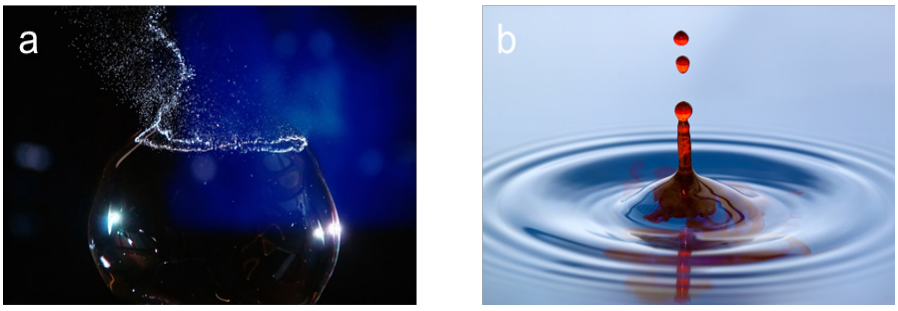


**Figure 2.1** Examples of (a) film drops which are formed during the bubble burst and (b) jet drops which are formed after the collapse of the bubble cavity (von der Höh 2010)

The type and the number of drops, produced after the collapse of a bubble, are strongly influenced by the size of the parent bubble (Blanchard and Syzdek 1988, Resch

and Afeti 1991, Spiel 1994a) as illustrated in Figure 2.2. Larger bubbles tend to produce film drops upon their burst whereas smaller bubbles tend to produce jet drops.

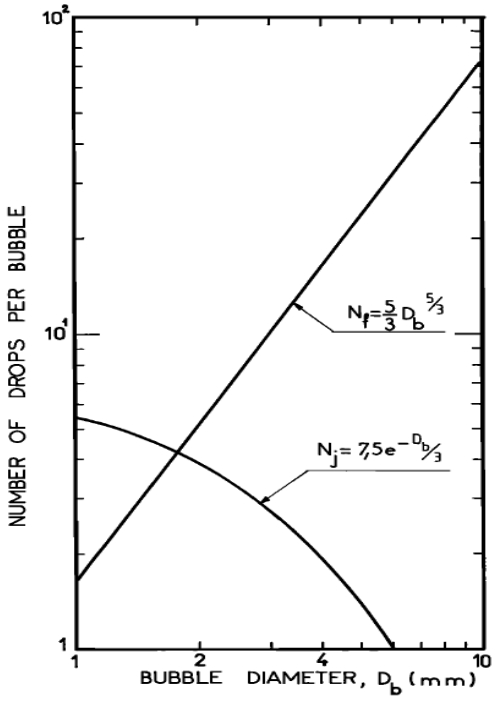


**Figure 2.2** Dependency of the number of film drops ($N_f$) and jet drops ($N_j$) on the size of the parent bubble (Resch and Afeti 1991)

Figure 2.2 shows that for bubbles smaller than 1.8 mm in diameter, jet drop formation is predominant ($N_j >> N_f$). The reason could be that for a given liquid/gas system, a smaller bubble has lower rising velocity which means it releases less energy upon its burst at the liquid/air interface in comparison to a larger bubble. Due to this lower energy release, less portions of the bubble's cap can be freed up from the bulk solution and as such, lesser numbers of film drops are produced. On the other hand, a smaller bubble produces smaller and thinner liquid jet, after its collapse, which disintegrates easily producing smaller and higher number of jet drops in comparison to a larger bubble.

The number of film drops ($N_{film}$) and jet drops ($N_{jet}$) can be estimated based on the diameter of the parent bubble ($D_b$ in mm):

$$N_{film} = \frac{5}{3} D_b^{5/3} \qquad (\mathbf{2.7}) \qquad \text{(Resch and Afeti 1991)}$$

$$N_{jet} = 7.5 exp\left(-\frac{D_b}{3}\right) \qquad (\mathbf{2.8}) \qquad \text{(Blanchard and Syzdek 1988)}$$

Equations 2.7 and 2.8 are based on studies conducted on bubbles collapsing in seawater or freshwater. Although the composition of seawater (and freshwater) used by various researchers is not the same, the type and size of the produced droplets are fairly similar (Blanchard and Syzdek 1988, Resch and Afeti 1991, Rossodivita and Andreussi 1999, Spiel 1994b, Spiel 1998). Since copper electrolyte solution has similar surface tension and viscosity as seawater, it is reasonable to assume that the collapse of bubbles in the copper electrolyte solution is not significantly different from that in seawater.

No data could be found in literature specifying the range of bubble sizes that are generated in copper electrowinning. Therefore, it is not possible at this stage to predict what type of droplets (film drops or jet drops) is produced upon the burst of oxygen bubbles in the copper electrowinning solution.

### 2.3.3. Factors affecting acid mist generation

Although it is well known that the amount of acid mist changes with the process variables, there are very few publications that quantify the relationships. The electrical current density is the only known process parameter, qualitatively, that has a noticeable effect on the amount of acid mist. Bubble size is thought to be the other major factor in determining the amount of acid mist generation. Liow et al. (2007) investigated the effect of bubble size on the amount of acid mist by sparging air in synthesized copper electrolyte solution. The acid mist flux was found to be inversely proportional to the bubble diameter (Liow et al. 2007). Bubbles that were used in the aforementioned study, however, were 10-100 times larger than those generated in the copper electrowinning process. Since the droplet formation mechanism is strongly influenced by the bubble size (Blanchard and Syzdek 1988, Resch and Afeti 1991, Spiel 1994a), the conclusions drawn from the work of Liow et al. (2007) cannot be reliably applied to the acid mist formed in copper electrowinning.

FC-1100 is another factor that is known to reduce the amount of acid mist. Quantitative analyses on the effectiveness of this chemical reagent in reducing acid mist, however, are scarce. The effect of other process parameters such as solution temperature, solution acidity, and anode age are yet to be determined.

## 2.4 Bubble nucleation and growth

### 2.4.1. Bubble nucleation

Nucleation of gas bubbles occurs when the liquid is supersaturated with dissolved gas. The driving force for gas bubble nucleation is the excess of chemical potential of the liquid in comparison to that of the gas (Volanschi et al. 1996).

Supersaturation is strongly influenced by parameters such as interfacial tension, electrode material, electrode surface topology, and surfactant concentration. Since gas supersaturation at the electrode-liquid interface is higher than that of the bulk liquid, gas bubbles always nucleate at the electrode rather than in the bulk liquid during electrolysis (Volanschi et al. 1996).

Tiny air cavities, trapped in the surface irregularities of the electrode, act as bubble nucleation sites during electrolysis (Vogt et al. 2004). These nucleation sites become active and allow bubble growth when interfacial equilibrium is disturbed. Different types of anodes form anodic layer of different morphology during electrolysis. The morphology of these anodic layers ranges from being loose and coral-like on the Pb-S anode to fibrous on Pb-Ca-Sn anode to dense and fine-grained on Pb-$Co_3O_4$ anode (Hrussanova et al. 2004). It is likely that oxygen bubble nucleation and growth would not be the same on different types of anodes due to surface morphology differences of the anodes. Hrussanova et al. (2004), however, only studied the rate of corrosion of the aforementioned anodes and did not investigate the oxygen bubbles or the acid mist generated by those anodes.

The site of nucleation on a flat electrode cannot be accurately determined. It seems that nucleation sites are randomly distributed on the electrode surface (Volanschi et al. 1996). In recent years, however, new types of microelectrodes have been designed that have a single nucleation site capable of generating monosized gas bubbles (Wedin et al. 2003). These electrodes are employed to study the nucleation process as well as the dynamic rheological properties of liquids.

A bubble nucleus becomes active and starts to grow if its radius is larger than a critical value (also known as the critical nucleation radius). The critical nucleation radius ($R_c$) is directly proportional to the Sherwood number (Sh) and indirectly proportional to the Reynolds number (Re) of the bubble (Vogt et al. 2004):

$$\mathrm{R_c} = \frac{2\gamma}{\mathrm{H}} \frac{\rho_L RT}{\rho_G M_L} \frac{\mathrm{Sh}}{\mathrm{Re.Sc}} \qquad (\mathbf{2.9})$$

In equation 2.9, $\gamma$ is the interfacial tension (N m$^{-1}$), $H$ is Henry coefficient (kg m$^{-1}$ s$^{-2}$), $\rho_L$ is the density of the liquid (kg m$^{-3}$), $\rho_G$ is the density of the gas (kg m$^{-3}$), $R$ is the universal gas constant (8.314 J K$^{-1}$ mol$^{-1}$), $T$ is temperature (K), $M_L$ is the molar mass of the liquid (g mol$^{-1}$), and Sc is the Schmidt number.

Sherwood number is directly related to the mass transfer coefficient, k, whereas Reynolds number is directly related to the current density, I/A. The increase in the k value is much smaller than the increase in the I/A value (Vogt et al. 2004). Therefore, the critical radius of nucleation becomes smaller as the current density is increased. In other words, as the current density increases, more nucleation sites will become active.

Experimentally, microelectrodes are employed to measure mass transfer and study the hydrodynamic conditions of bubble nucleation. In this method, fluctuations in low frequency electrical current are measured and used to map the mass transfer inhomogeneity across a bubble's surface (Simison et al. 1999). A limitation of this method is that measurement is restricted to a specific point where microelectrode is placed.

Electrochemical optical method, which was developed recently, is an alternative method of studying the hydrodynamic conditions at a surface. In this method, luminol is electrochemically oxidised near the electrode and the light emitted from the reaction is used to image the mass transfer process (Simison et al. 1999). Some of the advantages of the electrochemical optical method include simple apparatus setup, use of conventional camera and image processing technique, and that the method does not require an external source of light.

### 2.4.2. Bubble growth on the anode

The growth of a spherical bubble can be described by the Rayleigh-Plesset equation (dots represent time derivatives) (Oguz and Prosperetti 1993):

$$r\ddot{r} + \frac{3}{2}\dot{r}^2 = \frac{1}{\rho_G}(\mathrm{P_B} - \mathrm{P_c} - \mathrm{P_h}) \qquad (\mathbf{2.10})$$

In equation 2.10, $r$ is the bubble radius (m), $\rho_G$ is the density of the gas (kg m$^{-3}$), $P_B$ is the pressure inside the bubble (Pa), $P_C$ is the capillary pressure (Pa), and $P_h$ is the hydrostatic pressure (Pa).

The capillary pressure can be determined from the Young-Laplace equation:

$$P_c = \frac{2\gamma}{R} \qquad (2.11)$$

where $\gamma$ is the interfacial tension (N $m^{-1}$) and $R$ is the universal gas constant (8.314 J $K^{-1}$ $mol^{-1}$).

The hydrostatic pressure ($P_h$) is the sum of the atmospheric pressure ($P_0$) and the liquid head pressure (Najafi et al. 2008):

$$P_h = P_0 + \rho_L g h \qquad (2.12)$$

where $\rho_L$ is the density of the liquid (kg $m^{-3}$) and $g$ is the gravitational acceleration (m $s^{-2}$).

There are a number of forces that act upon a bubble growing on a solid substrate. The balance of these forces determines the detachment size of the bubble (Jones et al. 1999):

$$F_d + F_s = F_i + F_p + F_b \qquad (2.13)$$

The drag force ($F_d$ exerted by the solution surrounding the bubble due to the bubble growth) and the surface tension force ($F_s$) act downward and hold the bubble on the substrate. The inertia ($F_i$), pressure ($F_p$), and buoyancy ($F_b$) forces act upward and separate the bubble from its substrate (Jones et al. 1999).

At low growth rates in a quiescent solution, the drag and inertia forces can be neglected (Jones et al. 1999). Moreover, it can be shown that when bubble radius exceeds 10 µm, the pressure force can be neglected and removed from the bubble's force balance. Therefore, the detachment size of a bubble can be approximated by equating the vertical components of the surface tension force and the buoyancy force:

$$2\pi r_{base}\gamma sin\theta = \Delta\rho g \frac{4}{3}\pi r^3 \qquad (2.14)$$

In equation 2.14, $r_{base}$ is the radius of the bubble's base (m), $\gamma$ is surface tension (N $m^{-1}$), θ is the contact angle (degrees), $\Delta\rho$ is the density difference between liquid and gas (kg $m^{-3}$), and r is the detachment radius of the bubble (m).

Based on the free body diagram (Figure 2.3), it can be shown that for a symmetrical bubble $r \sin\theta = r_{base}$. Therefore, equation 2.14 can be rearranged to estimate the detachment radius of a bubble:

$$r = \sqrt{\frac{3\gamma}{2\Delta\rho g}} \sin\theta \qquad (2.15)$$

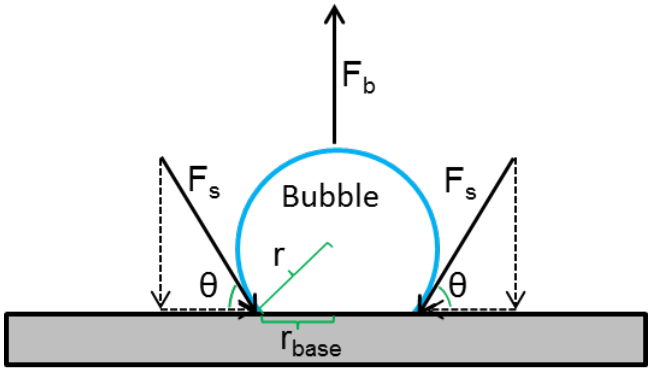


**Figure 2.3** Free body diagram of a symmetrical bubble growing on a horizontal substrate

One should note that equations 2.14 and 2.15 were developed for a single bubble growing on a horizontal substrate whereas the lead anode used in the copper electrowinning process, and also in the present work, is positioned vertically in the solution producing millions of bubbles per second. The free body diagram in Figure 2.4 illustrates the surface tension and buoyancy forces acting on a bubble growing on a vertical substrate.

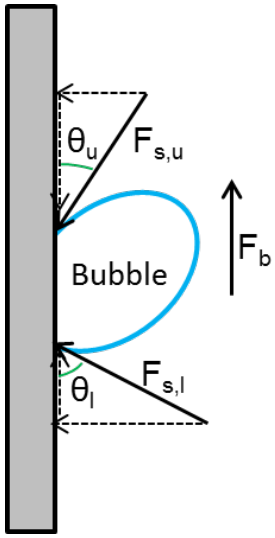


**Figure 2.4** Proposed free body diagram of a bubble growing on a vertical anode

If a bubble grew symmetrically about its horizontal axis, on a vertical anode, the upper and lower contact angles ($\theta_u$ and $\theta_l$ in Figure 2.4) would be equal. In this case, the vertical components of the upper and lower surface tension forces ($F_{s,\,u}$ and $F_{s,\,l}$) would cancel each other out and there would be no force to oppose the buoyancy force. Therefore, theoretically no bubble could nucleate and grow on the anode, which is obviously not the case.

It is therefore postulated that bubble growth on the vertical anode must be asymmetrical with the upper contact angle being much smaller than the lower contact angle as illustrated in Figure 2.4. In this case the resulting surface tension force in the vertical direction acts downward and opposes the buoyancy force making it possible for the bubble to grow on the surface of a vertical anode.

Experimental work by Najafi et al. (2008) shows that the upper and lower contact angles of a bubble growing on an inclined micropipette are in fact different and that the bubble attains an asymmetrical position. In addition, the resulting vertical components of the detachment resistive forces are always smaller for an inclined micropipette in comparison to those of a micropipette with no inclination (Najafi et al. 2008). This means that the detachment size of a bubble growing on an inclined substrate will always be smaller than that predicted by equation 2.15.

### 2.4.3. Bubble growth by coalescence

When bubbles approach each other, after detachment from their nucleation sites, their surfaces deform and the shape of the bubble caps changes from convex to concave which leads to the formation of a dimple as illustrated in Figure 2.5 (Valkovska et al. 1999). The dimple is unstable and flows out quickly and a plane-parallel film is formed. The liquid film continues to thin until it reaches a critical thickness at which it ruptures and bubbles coalesce.

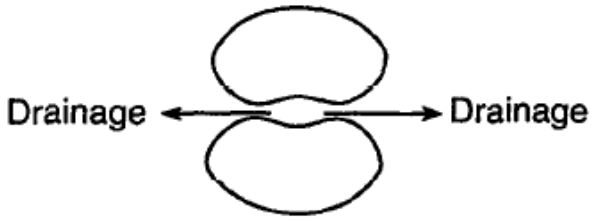


**Figure 2.5** Dimple formation and film drainage (Pugh 1996)

The above procedure is usually observed when relatively large bubbles, of the order of 1 mm, are involved (Valkovska et al. 1999). In contrast, the shape deformation of small bubbles is negligible and they remain almost spherical up to the moment of coalescence. Although bubble size is an important factor in shape deformation, there are other factors that can strongly influence the coalescence rate. Interfacial surface tension, surfactant type and concentration, viscosity, and external forces are examples of such influential factors.

A frother can significantly influence the final size of a bubble by affecting the degree of coalescence. When bubble size measurements are plotted versus frother concentrations, two distinctive regions are observed (Grau and Heiskanen 2005). At very low frother concentrations, the mean bubble diameter decreases dramatically as the frother concentration is increased. At higher frother concentrations, bubble sizes remain relatively unchanged despite the increase in frother concentration. The intersection between these two distinctive regions corresponds to the critical coalescence concentration (CCC) (Grau and Heiskanen 2005). At CCC, coalescence conditions in the solution have reached their maximum and therefore no further decrease in bubble size is observed beyond this point.

Bubble coalescence is also affected by the presence of electrolytes in the solution. At low electrolyte concentrations, the long-range electrostatic forces are dominant (Henry et al. 2006). The electrostatic forces are not ion-specific which means the intermolecular interactions are based on the valency of the ion rather than the type of the ion. On the contrary, the ion-specific interactions, which are short-range interactions, become dominant at high electrolyte concentrations (Henry et al. 2006).

Marcelja's theory suggests that different bubble coalescence behaviour, related to different electrolytes, can be explained by the fact that different ions have different affinities for the air/solution interface. Based on Marcelja's theory, when both ions of a salt have the affinity to stay at subsurface region, or when both are concentrated at the interface, bubble coalescence will barely be affected by the electrolyte. In contrast, when one ion favours the interface and the other ion favours the subsurface region, bubble coalescence will be inhibited in such solution.

A typical copper electrolyte solution contains a number of different ions such as $Cu^{2+}$, $Fe^{2+}$, $Co^{2+}$, $Mg^{2+}$, $H^{+}$, $SO_4^{2-}$, $Cl^{-}$. Some of these ions such as $SO_4^{2-}$ have an affinity for the free surface of the solution while others such as $Mg^{2+}$ have an affinity for the subsurface region. This separation of ion species between surface and subsurface is expected to result in the inhibition of bubble coalescence according to Marcelja's theory.

## 2.5 Bubble size measurement

Bubble size is known to influence the size and the number of the after-collapse droplets (Liow et al. 2007, Resch and Afeti 1991, Rossodivita and Andreussi 1999, Spiel 1994a) which in turn influence the amount of acid mist. However, there has been only one publication that deals explicitly with the relationship between acid mist amount and average bubble size. It shows that the acid amount from the burst of the bubbles is inversely related to the average bubble size (Liow et al. 2007).

Since the introduction of the froth floatation process, a number of techniques have been developed to determine the bubble size distributions accurately within an operating cell. These methods include photographic techniques, electroresistivity measurements, gas hold up and pressure measurements (O'Connor et al. 1990). Two of these techniques, which are more often used, are discussed in further details below.

The UCT (University of Cape Town) technique is based on an optical method for bubble size measurements. UCT has a belled-end capillary tube which draws up the rising bubbles from within the liquid medium (O'Connor et al. 1990). Bubble diameters are calculated by using the data collected from the photo-transistor detectors, installed on the capillary tube, and normalizing the results with respect to the total gas volume. UCT can process a total of about 7000 bubbles at a rate of 50 bubbles per second.

For accurate bubble size determination by UCT technique, the applied vacuum and the capillary bell geometry must be chosen carefully. An incorrect setup in either of these two factors can lead to bubble coalescence or bubble breakage in the capillary which results in errors in bubble size distribution measurements. Tucker (1994) suggests that the opening of the sampling port (i.e. the capillary entrance) must be at least three times bigger than the diameter of the largest expected bubble. O'Connor (1990) performed six repeat experiments on an air/water system to determine the precision of the UCT technique. The reproducibility of the bubble diameter distribution results was found to be excellent for the two-phase system.

Photographic techniques are employed very often to visualize fluid's behaviour and flow patterns. The HUT (Helsinki University of Technology) method was first introduced in 2002 for the determination of bubble size distribution in a two-phase system. HUT combines the bubble sampling techniques with the digital image processing procedures to determine the bubble diameter (Grau and Heiskanen 2002). Matrox Inspector, a commercial image analysis software, is utilized to automate image capture and analysis.

Prior to image analysis, a sharpening filter is applied to the digital images to facilitate bubble identification and labelling (Grau and Heiskanen 2002).

A comparison between UCT and HUT techniques showed that, for narrow bubble size distributions in a two-phase system, both techniques produced very similar results (Grau and Heiskanen 2002). However, when the two-phase system contained a wide range of bubbles sizes, major discrepancies were observed in the results obtained by UCT and HUT. Digital images revealed that the discrepancy was due to bubble break-up in the fine capillary tube of the UCT device (Grau and Heiskanen 2002). It was shown that a bubble that was too large would either not enter the capillary and go undetected, or break up at the tip of the capillary and only a fraction of it enters the capillary tube of UCT. Grau and Heiskanen (2002) claim that the HUT system does not have the bubble break-up problem and therefore, it can provide much more accurate results when dealing with a wide range of bubble diameters.

The McGill bubble size analyser is also based on the imaging technique and it consists of a capillary and a viewing chamber. The distinctive feature of the McGill device is that its viewing chamber is inclined 15 degrees from the vertical axis. The inclination of the chamber forces the bubbles to spread in a single plane along the viewing window and therefore reduces the overlapping of bubbles and out of focus photographs (Girgin et al. 2006).

A study by Hernandez-Aguilar et al. (2004) showed that UCT technique provides more accurate estimations for single bubble measurements, for bubbles of less than 2 mm diameter, in comparison to McGill technique. UCT has a small tendency to overestimate the bubble size (about 1% error for 1.3 mm bubble) while McGill has the tendency to underestimate (about 4% error for 1.3 mm bubble) (Hernandez-Aguilar et al. 2004). Nevertheless, both methods exhibit relatively high accuracy, with less than 5% error, and prove to be capable of producing reliable bubble size estimations.

One of the simplest forms of representing an image is the binary form (i.e. the black and white form). A grey scale image can easily be converted into a binary image by thresholding the intensity component so that pixels above the threshold are white and those below are black (Lin et al. 2008). The binary image analysis is especially suitable when dealing with a large number of bubbles, such as those encountered in floatation cells. This technique also has the advantage of being easy to obtain and has low storage

requirements. MATLAB can be employed to extract image features and obtain data such as number of bubbles and bubble size distributions.

The image analysis software used with the McGill device is Empix Northern Eclipse (Bailey et al. 2005b). The software is programmed to automatically recognize an enclosed and relatively circular object in a grey scale image as a bubble. To distinguish a single bubble from a cluster (i.e. several joint bubbles), an entity known as the shape factor is often employed by the image analysis software. Shape factor determines the degree of sphericity of an object and is defined as following:

$$Shape\ factor = \frac{4\pi(Area)}{(Perimeter)^2} \qquad (2.16) \qquad \text{(Bailey et al. 2005a)}$$

Thus, for a perfectly spherical bubble, the shape factor equals one. In McGill bubble size analyser, the minimum standard shape factor is 0.7 (Bailey et al. 2005a).

It is important to note that employing shape factor will result in reasonably accurate data only when dealing with a narrow range of bubble sizes. Bailey et al. (2005a) suggest using a combination of two filters instead of relying on the shape factor. Since a single bubble in a grey scale image has only one bright spot (i.e. a hole), the first filter is set to remove objects from the image that have no hole or more than one hole. The second filter discards an object when its area is much smaller than the area of a circle with the same maximum diameter. Bailey et al. (2005a) claim that by using these two filters, instead of shape factor, a significant improvement is achieved in determining wide bubble size distributions.

## 2.6 Factors affecting bubble sizes

### 2.6.1. Contact angle

Contact angle measures the wetting tendency of a liquid on a solid and is closely related to the surface tension. A liquid droplet on a solid surface has two tendencies: 1) to spread and cover the surface; 2) to round up and minimize its own area to achieve the minimum free energy (Hunter 2001). The final shape of the droplet and the degree of wetting depend on the relative magnitude of the two tendencies.

The contact angle of a liquid on a solid can greatly affect the spreading of a bubble's contact base which in turn influences the bubble growth and detachment processes. Pugh (1996) noticed that hydrophilicity of the solid surface has a significant influence on bubble size in that bubbles developed on a hydrophobic surface can grow to a much

bigger size than those formed on a hydrophilic surface. The reason is that the base of the bubble can expand more easily on the solid surface when the liquid is of non-wetting nature. In contrast, no contact base was observed for a hydrophilic surface and therefore, bubbles were of much smaller size at the detachment time (Pugh 1996).

There are several methods of measuring a contact angle. The easiest method is based on the formation of a sessile or pendant drop on the solid's surface. The contact angle is determined by photographing the drop and magnifying the image (Hiemenz 1977). Alternatively, a telescope with a goniometer eyepiece may be used on the drop to directly approximate the contact angle.

The *tilted plate* method is another technique employed to measure the contact angle. In this method a smooth solid is inserted in the liquid and held at the liquid/gas interface. The angle of inclination of the plate is then varied until the liquid forms a horizontal contact with the solid. At this stage, the angle formed between the solid plate and the liquid is taken as the contact angle.

It should be noted that the equilibrium contact angle is different from the contact angle observed during bubble growth. The latter is known as the dynamic contact angle. Porter (1994) emphasizes that Young's equation and the spreading coefficient can only characterize wetting under equilibrium conditions. Since in many practical applications of wetting, such as detergents, equilibrium conditions cannot be established, the kinetics of the wetting process is of high importance. There are a number of practical tests, such as Draves wetting test, that characterize wetting under dynamic conditions rather than equilibrium (Porter 1994).

### 2.6.2. Surface Tension

Surface tension is one of the main forces acting on a growing bubble, as mentioned before in Section 2.4.2. Surface tension is a measure of a liquid's surface resistance to a change in its area. Surface tension existence is due to the energy differences between the molecules at the surface and those in the bulk phase of a material (Hunter 2001).

Various chemicals can affect the surface tension of a solution differently. For example, surface tension of water increases when a salt such as NaCl is added (Permprasert and Devahastin 2005). In contrast, the addition of a certain class of chemicals known as surfactants can lower the surface tension of an aqueous solution drastically.

Surface tension is the main force that opposes the buoyancy force (equation 2.14), and assists a bubble in remaining attached to the substrate and growing larger. By lowering the surface tension, there is less resistance to the buoyancy force and as a consequence, a bubble detaches from its nucleation site prematurely. In other words, lowering the surface tension will result in the generation of smaller bubbles as shown by the experimental work of many researchers (Grau et al. 2005, Kazakis et al. 2008, Xie et al. 2009, Xu et al. 2009).

There are several methods that can be used to measure the surface tension of a liquid; *Du Nouy ring* method, *Wilhelmy's plate* method, *Sessile drop* method, *Capillary rise* method, and *Drop-weight* method to name a few. The choice of the method depends on factors such as the nature of the liquid, testing conditions, and the surface stability when deformed.

Du Nouy and drop-weight methods, unlike other techniques, involve liquid detachment from a support. The liquid detachment process, which results in the creation of a new surface, occurs in short period of time and may not allow the equilibrium requirement to be satisfied (Hiemenz 1977). These non-equilibrium conditions could introduce large measurement errors when dealing with solutions that contain a surfactant since surface tension is highly affected by the concentration of the surfactant at the surface of the solution.

It is essential to distinguish between static and dynamic surface tension. The former relates to the equilibrium conditions whereas the latter relates to situations far from equilibrium (Volanschi et al. 1996). The abovementioned surface tension measurement techniques are based on the assumption that the system is at equilibrium.

A surface with changing area is required to measure the dynamic surface tension. To create a changing surface, a gas bubble is grown in the liquid, normally on a micro electrode, either by sparging or by electrolysis (Volanschi et al. 1996). The presence of the gas bubble on the micro electrode induces changes in both the electrode overpotential and the impedance (Volanschi et al. 1996). Either of these changes can be accurately monitored and used to determine the dynamic surface tension of the solution.

The *maximum bubble pressure* is another technique for measuring the dynamic surface tension. Since the measurement occurs under rate dependant surface expansion conditions, the measured surface tension includes parameters such as surface dilation viscosity, surface shear viscosity and elasticity forces (Pugh 1996).

### 2.6.3. Use of surfactants

#### *Surfactant types and properties*

Surface active agents, or surfactants, are materials that have the tendency to accumulate at the solution/air interface. A surfactant can influence the amount of acid mist directly by changing the bubble burst mechanism or indirectly by changing the final bubble sizes. The existence of surfactant molecules in a solution can reduce the final size of bubbles in two different ways: by reducing the surface tension force which results in early detachment of bubbles from their nucleation sites; by inhibiting coalescence in the bulk solution.

Many properties of a surfactant are determined by the relative sizes and shapes of the hydrophilic and hydrophobic parts of the surfactant's molecules (Porter 1994). Adsorption, micelles, solubility, and wetting are some of the properties that characterize a surfactant.

At high enough surfactant concentrations a unimolecular layer of the surfactant is formed at the interface. The surfactant concentration at which the unimolecular layer is formed is known as the critical micelle concentration (CMC) (Porter 1994). Surface viscosity and surface elasticity are two measurable parameters and are often utilized to characterize the dynamics of monolayer surfactants. Surface viscosity represents the restoration of equilibrium after a stress being imposed on the system. In other words, surface viscosity is a measure of energy dissipation in the surface. Surface elasticity, on the other hand, is a measure of the energy stored in the surface layer.

CMC can be determined in several ways. The easiest method is based on the surface tension measurements. In this method, the surface tension measurements are plotted against the surfactant's concentration. The concentration at which a sharp change in the slope of the plot occurs is the CMC value for that particular system (Song et al. 2005).

The other method is very similar to the first one except that the conductivity of the solution is plotted versus the surfactant's concentration. CMC can then be obtained from the discontinuity of conductivity data. Nuclear magnetic resonance (NMR) is another alternative to estimate CMC. NMR is suitable for systems of mixed surfactants since such systems exhibit changes in phase behaviour which can be detected by NMR spectra (Song et al. 2005).

The micellar structure and aggregation number of a particular surfactant in a solution can have a profound effect on the viscosity of the solution. Very high increase in viscosity can be achieved over a narrow range of the surfactant's concentration. For example, a slight increase in ether sulphate concentration changes the micellar structure from spherical to hexagonal and as a result, the viscosity increases by about 1000 times (Porter 1994).

A common type of classification categorises surfactants based on the polarity of their hydrophilic group into four groups of anionic, cationic, non-ionic and amphoteric (Porter 1994). However, there are surfactants with quite different chemical structure that do not fit into the above categories. Polymeric surfactants, fluorochemical compounds, and Gemini surfactants are examples of such specialty surfactants.

Surfactants can appreciably influence the wetting power of a solution. The reason for such influence is that the ability to wet or not to wet is determined by the surface tension of the solution and the adsorption of surfactants to the surface can greatly reduce the surface tension. Surfactants with small molecules are shown to provide better wetting compared to surfactants with large molecules (Porter 1994). The reason for such behaviour could be due to the fact that smaller molecules diffuse faster through the solution and therefore, surface tension is reduced at a higher rate.

Fluorinated surfactants, similar to conventional surfactants, are often composed of hydrophilic and hydrophobic groups. However, due to high electronegativity of fluorine atoms, these compounds exhibit some exceptional properties:

- Insensitivity to low pH or hard water (Holmberg et al. 2003)
- Immiscibility with both polar and non-polar solvents (Porter 1994)
- Compatibility with aqueous ions (Holmberg et al. 2003)
- High thermal and chemical stability due to the strong covalent C-F bond (Porter 1994)
- High surface tension reduction of aqueous systems due to very low inter-molecular forces between the fluorinated molecules (Porter 1994)

FC-1100, which is widely used to suppress acid mist in copper electrowinning tankhouses, is an amphoteric fluorosurfactant (3M 2007). The high chemical stability of FC-1100, due to its high energy C-F bond, facilitates its use under high electrical current density, high acid concentration and relatively high temperature conditions of copper electrowinning process. FC-1100 is defined as moderately surface active at low

concentration (3M 2007). Hence, it exhibits no (or low) foaming behaviour at target concentrations of 25-100 ppm. More importantly, FC-1100 is compatible with solvent extraction and remains in the interface of the aqueous and organic solutions (3M 2007).

Despite their exceptional properties, fluorochemical surfactants are very expensive and do not biodegrade easily (Porter 1994). Also, their concentration in the solution cannot be easily measured and highly specialized instruments are required. Therefore, the use of these surfactants should only be considered when their properties are really required.

### *Foam formation*

Most surfactants result in foam formation on the surface of the solutions. Foam is a two-phase system, gas bubbles in a liquid, and is thermodynamically unstable (Porter 1994). The foam formation process involves the expansion of the liquid's surface area. The work required to create a new area is directly related to the surface tension. Therefore, the lower the surface tension, the less energy required to expand the surface area and hence, the more foam is formed.

Dowfax is a foaming reagent which reduces acid mist by stabilizing oxygen bubbles into a layer of foam on the surface of the electrolyte. Dowfax belongs to the alkyl phenol ethoxylate family which are classified as non-ionic surfactants (Porter 1994). The effects of nonyl phenol ethoxylate (NPE), which is from the same family of surfactants as Dowfax, on the electrowinning of zinc were investigated by Hosny (1993). The experiments were conducted at various zinc/acid ratios, surfactant concentrations and electrical current densities. The addition of NPE was found to increase the cell voltage and energy consumption and therefore, decreases the current efficiency of the zinc extraction process (Hosny 1993). Although no attempt was made to measure the effect of NPE on the amount of acid mist, Hosny (1993) observed the formation of non-coalescing bubbles of low rise velocity. Such bubbles create a barrier and lower the conductivity which explains the cell voltage increase in the presence of NPE.

NPEs are available in large volumes and at low prices on the international market but their biodegradability is questionable. When comparing different nonyl phenol products, nonyl phenol+6 Ethylene oxide (EO) exhibits maximum surface active properties and it lowers the surface tension of an aqueous system to about 28 mN $m^{-1}$ (Porter 1994). NPEs have excellent compatibility with all aqueous ions and they are stable to hot dilute acid and alkali.

To explain the stability of foams, Gibbs surface elasticity and Marangoni effect are often used together (Porter 1994). It should be noted that Gibbs theory is based on equilibrium conditions whereas Marangoni effect is dynamic and accounts for the diffusion rate of the surfactant. Both Gibbs and Marangoni effects, despite their differences, suggest that when a liquid film is stretched, the local surface tension increases and causes the liquid to flow from the thicker sections to the thinner section and restores the film (Porter 1994). The existence of a local surface tension gradient also means that there is a gradient in the local concentration of surfactant molecules.

If the total surfactant concentration is too low, the local concentration gradient in the stretched film will be low (Porter 1994). Low concentration gradient results in a low surface tension gradient. Since the local surface tension difference is low, there would be little or no restoring force and the film rupture cannot be prevented. When surfactant concentration is too high, much higher than CMC, surfactant molecules diffuse rapidly and minimize the local concentration gradient and the restoring force. Rapid diffusion of surfactant molecules also produces dangerously thin films and causes poor foaming behaviour (Pugh 1996). Therefore, the Gibbs-Marangoni effect explains why in many applications maximum foam stability is achieved near the CMC level.

### 2.6.4. Process conditions

The effect of some variables, such as current density, on the amount of acid mist can be predicted qualitatively. By increasing the electrical current density, the rate of oxidation reaction increases at the anode leading to the generation of more oxygen bubbles and more bursts at the free surface of the solution which in turn increases the amount of acid mist. Although current density and the amount of liberated oxygen at the anode are correlated by Faraday's law, no publications could be found that quantitatively correlate the electrical current density and the amount of acid mist.

The effect of temperature on bubble size and acid mist is less predictable than that of current density. The reason is that temperature not only affects reaction kinetics but also characteristics of the electrolyte solution (such as surface tension and viscosity). Hrussanova et al. (2004) studied the temperature and current density effects on the corrosion rate of different types of anodes. Increasing temperature and current density were found to depolarise the oxygen evolution reaction and increase the rate of corrosion of all the examined anodes. At low temperature and current density conditions (25 $^{o}$C and 100 A $m^{-2}$), the crystallites at the anode surface were found to be rounded and the anodic

film was dense. In contrast, at high temperature and current density conditions (45 $^{o}$C and 500 A $m^{-2}$), low density coral-like anodic film was observed (Hrussanova et al. 2004).

Gas sparging can also influence the process dynamics by reducing the electric double layer at the anode/solution interface. Thus far, the primary goal of investigating different manifold and sparging designs has been focused on improving fluid mixing within the cell to increase copper production at higher electrical current densities (Rigby et al. 2001). No literature data could be found in relation to the effect of bubble size and rate of sparging on the amount of acid mist, sparging near the anode instead of cathode, effect of sparging on the electrical resistance of the electrolyte, and coalescence of the sparged bubbles with the electrolytically generated oxygen bubbles.

## 2.7 Acid mist minimization strategies

There have been many attempts to eliminate or minimize acid mist in the electrowinning operations. The most commonly used acid mist suppression techniques are discussed in the following subsections.

### 2.7.1. Floating barriers

Plastic balls and beads are the most common means of mechanical interference. More than 56% of the electrowinning plants worldwide use plastic balls and over 33% use polypropylene beads (CTI-ANCOR 2001). These plastic objects float on the surface of the electrolyte and allow wetted oxygen bubbles to coalesce and burst less violently which reduces the amount of airborne electrolyte. The main reason for the widespread adoption of plastic balls and beads is their availability in large quantities at low cost.

Balls and beads are good mist eliminators only in thick layers (Mella et al. 2006). Using thick layers of plastic balls and beads, however, could result in thin upper cathode deposit making it difficult to strip the produced copper from the cathode. Another disadvantage of using balls and beads is the difficulty in housekeeping. The plastic balls and beads are small, 2-20 mm, and easily slip into the pipes and pumps blocking the flow of electrolyte and damaging the equipment. Sometimes, they stick to the cathodes and fall to the floor when cathodes are being transported. When on the floor, these small plastic objects can create a hazardous environment for the tankhouse workers (Mella et al. 2006).

### 2.7.2. Hoods and mats

Hoods and special mats are used in some tankhouses to capture acid mist directly above the electrowinning cells. A hood is installed above each cell at an arbitrary height of 750 mm to 1500 mm whereas a mat is laid on top of the cell to cover anodes and cathodes. These systems are typically employed in cold climates to reduce energy consumption associated with heating the electrolyte (Davis and Eng 2002). Although these close capture methods can significantly lower the mist generation, they have a number of disadvantages. One main disadvantage is that hoods and mats must be removed when cathodes are harvested, and placed back when blank cathodes are inserted into the cell. This repeated action consumes time and is also labour intensive. Hoods and mats are often blocked by copper sulphate crystals which obstruct the air flow and significantly reduce the effectiveness of the acid mist reduction process. The very high capital cost associated with the purchase, installation and maintenance of the required equipment is another disadvantage of using hoods and mats. For example, a 1.2 m x 6 m mat manufactured by 3M can cost up to 10,000 AUD (Hooper 2008).

### 2.7.3. Brushes and Wipers

Another form of mechanical interference adopted by several tankhouses is brushes and wipers. Sunwest Supply claims that its mist suppression system is cost effective and of high performance. This system consists of brushes pinned to the hangar bar of each anode. The brushes surround the upper section of the anode and extend to the adjacent cathodes on each side. The bristles entrap the fine electrolyte droplets of the rising acid mist but allow oxygen to pass through (Sunwest 2004). Sunwest Supply reports that its system not only reduces acid mist, but also reduces heat loss and evaporation of the electrolyte by providing a heat blanket over the cell. Some of the disadvantages of this system include relatively high capital costs, and an increase in the local concentration of oxygen and fire risks. Moreover, continuous and effective mist capture requires continuous in-situ washing of the bristles to clean the mist and return it to the electrolyte (Mella et al. 2006). This in-situ washing is both time consuming and labour intensive. Constant washing may also negatively affect the quality of copper deposit and, therefore, the ease of the stripping process due to the dilution of the electrolyte near the free surface.

### 2.7.4. Chemical reagents

Chemical reagents such as FC 100, FC-1100, Dowfax, and Mersolate are used in some tankhouses as mist suppressants (Mella et al. 2006). Over 42% of copper electrowinning

plants use some type of surfactant to suppress acid mist (CTI-ANCOR 2001). These surfactants reduce acid mist by either reducing the surface tension or by forming a foam blanket over the free surface of the electrolyte solution.

FC 100 and FC-1100 reduce the surface tension to about 33 mN $m^{-1}$ (3M 2007). The lowered surface tension results in liquid drainage from the bubble prior to burst and therefore less acid is carried to the atmosphere (3M 2007). These surfactants, although effective in mist reduction, are very expensive. Moreover, these surfactants must be added to the electrolyte solution at very low concentrations and well mixed with the electrolyte to be effective. Another difficulty in using these chemicals is that the concentration of the surfactant in the solution has to be monitored regularly and maintained at an optimal level for effective mist reduction, which usually is a difficult and expensive task.

Dowfax and Mersolate are foaming reagents. These surfactants reduce acid mist by stabilizing oxygen bubbles into a layer of foam on the surface of the electrolyte solution. Although the foam layer captures a large portion of the escaping electrolyte droplets, it is difficult to maintain a uniform layer thickness to cover the entire electrolyte surface (Mella et al. 2006). If the foam layer is too thin, fine electrolyte droplets escape the surface and become airborne. On the other hand, a too thick foam layer may touch the hanger bars and electrical contacts and cause severe corrosion and lower the cell productivity. In addition, there are potential safety hazards associated with foaming agents in SX-EW operations. These hazards arise from the entrapment of oxygen bubbles in the foam layer which, in turn, increases the local concentration of oxygen. Oxygen, combined with organic and fatty acids carried over from SX processes can easily ignite when short circuits occur in the cells (CTI-ANCOR 2001). High cost and extensive use of water are other disadvantages of foaming agents.

### 2.7.5. Forced ventilation (dilution)

Dilution is one of the main strategies utilized to manage acid mist. Over 42% of the copper electrowinning tankhouses worldwide have some type of ventilation system to reduce acid mist (CTI-ANCOR 2001). In ventilation systems, large flows of air dilute the mist and the contaminated air is exhausted to the ambient. The main forced ventilation systems are Push-pull and Cross-flow systems designed by Cominco Ltd and DESOM Inc., respectively (Mella et al. 2006). Cross-flow design in combination with plastic balls and surfactants is very common in Chile (CTI-ANCOR 2001). However, when the level of plastic balls and surfactants is too low, the rate of electrode corrosion increases. Forced

ventilation cools the electrolyte solution which leads to an increase in the energy consumption to maintain the desired electrolyte temperature (Mella et al. 2006). Moreover, high air flows in forced ventilation can be extremely uncomfortable for the tankhouse workers since they must wear masks and protective clothing to avoid breathing problems and skin irritations. Another disadvantage is the high installation and running costs of ventilation systems. For example, a Cross-Flow ventilation system required for an average size tankhouse, consisting of 164 cells, was quoted to cost over 2.5 million USD (Davis and Eng 2002).

## 2.8 Summary

Acid mist is still one of the most problematic aspects of raw metal production via electrowinning. There have been many attempts to eliminate or minimize acid mist in electrowinning operations. Some of these techniques are only partially effective in reducing acid mist (such as floating barriers and ventilation fans), some are too expensive (such as hoods and chemicals), and others are time and labour intensive (such as brushes and mats). The majority of these methods attempt to treat the symptoms of acid mist rather than the root cause of mist formation. This is because little is known about the acid mist generation mechanism and only a handful of scientific papers have directly or indirectly discussed this topic. To solve the acid mist problem effectively, a fundamental understanding on the mechanism of the acid mist formation and quantitative information on the effect of process variables on the acid mist amount must be developed. The data obtained from such fundamental studies can be utilized to design more efficient and effective methods of mist minimization.

# Chapter 3: Effect of operating parameters on acid mist generation


## Abstract

Acid mist is generated during the final stage of hydrometallurgical metal refining processes including the electrowinning of copper. In this chapter, the effect of five process parameters and their interactions on the amount of acid mist generated is analysed quantitatively. The amount of acid mist generated was measured under 32 different operating conditions. It was found that solution's temperature and mist suppressant chemical had significant effect on the amount of acid mist generated. More than 90% of the variations in the acid mist generation can be explained by changes in the two parameters and their interaction. To a lesser extent, electrical current density and solution acidity also affected the total amount of acid mist generated. Anode's age and most of the 3, 4, and 5-way parameter interactions were found to have negligible influence on the amount of acid mist. Overall, acid mist was found to increase with temperature and current density. In contrast, increasing the viscosity of the solutions tends to decrease the amount of acid mist.


*Keywords:* Copper electrowinning; Acid mist; Oxygen evolution; Surface tension; Viscosity

## 3.1 Introduction

In electrowinning of copper, a direct electrical current is passed between an anode and a cathode that are submersed in a copper-rich solution (Robinson et al. 1994). At the inert anode, water molecules are electrolysed and oxygen bubbles are formed on the surface of the anode. These oxygen bubbles grow and eventually detach from the surface and rise in the bulk of the solution. These bubbles burst at the free surface of the solution and produce highly acidic droplets of which the fine ones become airborne and form an acid mist throughout the tankhouse of the electrowinning plant.

Acid mist is highly corrosive and results in the corrosion of cathode plates, anode's hanger bar, tankhouse equipment and building structures. Acid mist also poses a serious health hazard and causes extreme discomfort to the skin, eyes and respiratory systems of the tankhouse workers (HSIS 2009). The Occupational Safety and Health Administration (OSHA) recommends a time-weighted average (TWA) exposure limit of 1 mg of

sulphuric acid per $m^3$ of air, and a short term exposure limit (STEL) of 3 mg $m^{-3}$ (OSHA 2003).

There have been many attempts to eliminate or minimize acid mist in copper electrowinning operations (Mella et al. 2006). Polyethylene balls, suction hoods, mats, brushes and wipers, chemical reagents and forced ventilation are examples of such attempts (Mella et al. 2006, Davis and Eng 2002, Hooper 2008, Sunwest 2004, 3M 2007). Qualitatively, the use of chemical reagents such as FC-1100, Mistop, Dowfroth, and alkylated ethoxylates has been rated as the most effective method of suppressing acid mist (Bender 2010). However, there have been no systematic studies to quantitatively compare the effect of different operating parameters, including the use of a chemical reagent, on the amount of acid mist generated. Most of the published works to date, have only examined the effect of one or two parameters individually without considering any possible interaction effects on the amount of acid mist (Sigley et al. 2003, San Martin et al. 2005b, San Martin et al. 2005a, Hosny 1993, Cheng et al. 2004, Alfantazi and Dreisinger 2003).

This chapter examines, quantitatively, the relationship between the amount of acid mist generated and five operating parameters. These parameters are the age of the anode, electrical current density, solution temperature, sulphuric acid concentration of the solution, and the presence of a typical chemical mist suppressant (i.e. FC-1100). The results are useful for the design of more efficient methods or systems for acid mist minimization at electrowinning tankhouses.

## 3.2 Methodology

### 3.2.1. Equipment setup

The copper electrowinning process was replicated in a bench-scale cell. This cell (C2 in Figure 3.1) was constructed of 10 mm thick clear acrylic and had a capacity of 6 litres. During each test, electrochemical reactions resulted in continuous copper depletion and acid generation in the solution. Therefore, a peristaltic pump was utilized for gradual and continuous addition of fresh solution, from C1 container to C2, to maintain consistency in the composition of the solution. A horizontal slit in the side of C2 was utilized to keep the level of the solution in the container constant.

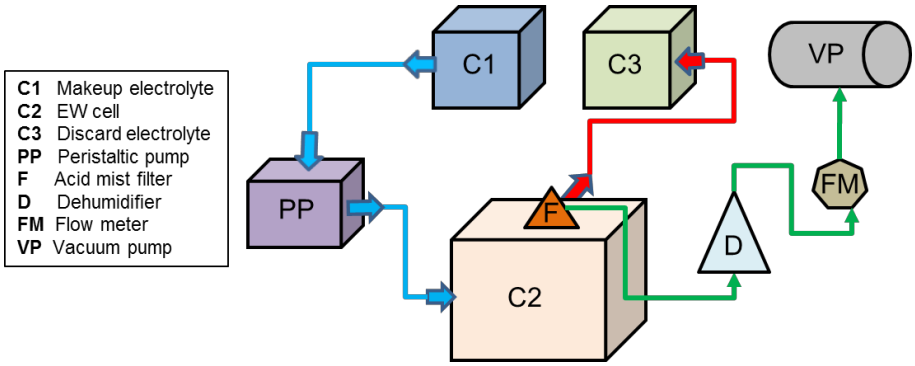


**Figure 3.1** A schematic view of equipment setup

Four submersed heaters were placed in the corners of C2 to keep the solution at a constant temperature for the duration of each test. To replicate industrial operations, Pb-Ca-Sn alloy and 316L stainless steel were used as anode and cathode, respectively (Houlachi et al. 2007). For each set of experiments a fresh batch of solution was synthesized that contained 45 g $L^{-1}$ Cu, 15 mg $L^{-1}$ Guar gum, 20 ppm Cl and 100 ppm Co. The synthesized solution was similar to the electrolyte solutions found in most copper electrowinning tankhouses worldwide (Robinson et al. 1994). The sulphuric acid concentration in the solution, however, was one of the five selected variables and its concentration differed from that of a typical copper electrolyte solution.

Nitro cellulose filters were used to capture acid mist. These filters were 47 mm in diameter and had a pore size of 0.45 µm which ensured the capture of very fine acidic droplets. For each experiment, a fresh filter chapter was installed at 45 mm above the free surface of the electrolyte solution inside the electrowinning cell (C2). The filter was held by an inverted funnel (F in Figure 3.1) and connected to a vacuum pump (VP) via a pneumatic tube. For precise air flow measurements, the drawn air was dehumidified by passing it through an enclosed flask that contained silica beans (D). A flow meter (FM) with a built in valve was installed on the pneumatic tube to ensure a constant air flow of 5 L $min^{-1}$ through the filter for the duration of each experiment.

At the end of each test, the used nitro cellulose filter was removed from the cell and placed in 25 mL of deionized water and agitated for about 60 minutes. The pH of the solution was then measured and the amount of the captured acid was calculated as grams of sulphuric acid per cubic meter of air drawn through the filter.

### 3.2.2. Experimental design

The main goal of the present work was to compare, quantitatively, the effect of different operating parameters on the amount of acid mist generated during a typical copper electrowinning process. To fully explore the main effect of each individual parameter as well as any possible interaction effects, the 2K factorial method was utilized to determine the required experimental conditions (Montgomery 2005). In this method, the examined parameters are tested at two levels (low and high). The bigger the difference between the low and high levels of a parameter, the more reliable its effect measurements would be (Montgomery 2005). Table 3.1 illustrates the examined parameters and their low and high level values.

**Table 3.1** The selected test variables and their values

| No | Examined Parameter | Low | High |
|---|---|---|---|
| 1 | Anode age (months) | 0 | 6 |
| 2 | Current density ($A.m^{-2}$) | 200 | 400 |
| 3 | Temperature ($^oC$) | 30 | 60 |
| 4 | Acidity ($g\ L^{-1}$) | 100 | 250 |
| 5 | FC-1100 (ppm) | 0 | 30 |

The values shown in Table 3.1 were selected so that the midpoint between low and high levels of each parameter represented the typical value used in most copper electrowinning tankhouses (Houlachi et al. 2007). For example, the temperature of the electrolyte solution is usually kept at about 45 $^oC$. Thus, the low and high limits of temperature for the experiments were set at 30 $^oC$ and 60 $^oC$, respectively.

Based on the 2K factorial method, 32 parameter combinations were required to fully examine the effect of five parameters at two levels. For reliable data analysis, a minimum of two replicates were needed for each test condition. Hence, 64 tests were conducted to determine the influence of each parameter on the generation of acid mist and also to identify any significant interactions amongst the selected parameters.

## 3.3 Results and Discussion

### 3.3.1. Descriptive statistical analysis

In all 64 experiments at 32 different operating conditions, the least amounts of detected acid mist were 0.03 and 0.02 mg acid per $m^3$ of air. These two tests were repeats, conducted with an old anode at low current density in a solution with low acidity, low temperature and high concentration of FC-1100.

The highest amounts of detected acid mist were 114.42 and 117.08 mg acid per $m^3$ of air. These two repeats were conducted with a new anode at high current density in a solution with low acidity, high temperature and no FC-1100.

The test results proved to be highly repeatable. The average relative error between the repeats of medium-high acid mist concentration tests was 18%. The smallest relative error was 0.001%. For the very low acid mist concentration tests, however, the average relative error between the repeats was 41%. This high relative error was essentially due to the resolution limit of the measurement method.

To distinguish the effect of individual parameters, the average amount of collected acid mist for each level of a parameter was calculated. The bar graph in Figure 3.2 illustrates the results where each bar represents the average amount of acid mist collected from 32 independent experiments.

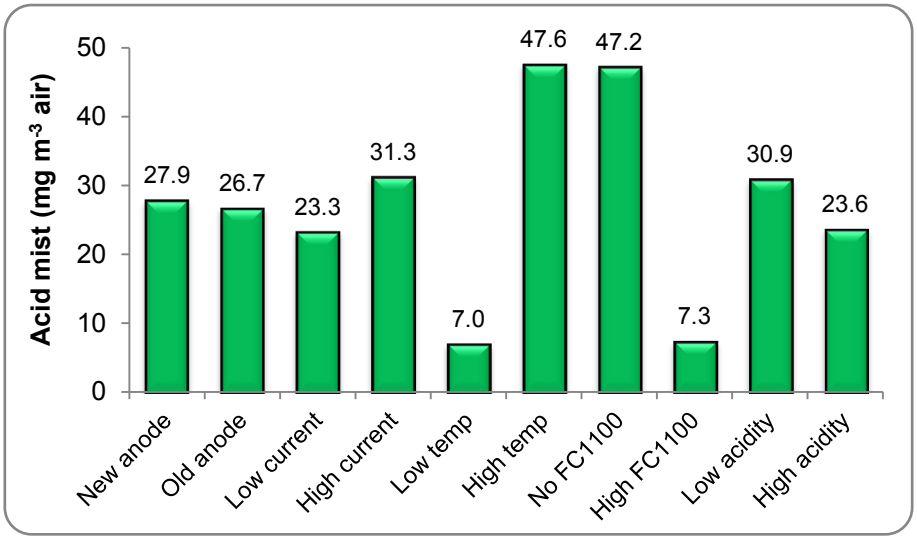


**Figure 3.2** Mean acid mist generation at different operating conditions

In Figure 3.2, it can be seen that highest amounts of acid mist were generated when the solution was kept at high temperature or when no FC-1100 was added to the electrolyte solution. To a lesser extent, high current density, low sulphuric acid concentration in the solution and new anode also favoured higher acid mist generations.

High temperature solutions produced the most amounts of acid mist. Temperature is known to affect the rheological properties of fluids. Surface tension and viscosity of the electrolyte solution were known to strongly influence the final size and the burst process of the oxygen bubbles (Xie et al. 2009, Xu et al. 2009). Thus, to find an explanation for the strong influence of temperature on acid mist, the effects of temperature on both the surface tension and the viscosity of the solution were evaluated and the results are discussed in details in Section 3.3.3.

The second highest amount of acid mist belonged to the tests where no FC-1100 was added to the solution. The addition of 30 ppm of FC-1100 reduced the acid mist amount from 47.2 to 7.3 mg acid per $m^3$ of air. As will be seen later, this reduction in the amount of acid mist in the presence of FC-1100 is believed to be caused by a change in the burst mechanism of bubbles at the free surface of the solution through changes in the surface viscosity and surface elasticity.

The third highest acid mist concentration belonged to high current density experiments. Based on Faraday's law, electrical current is directly related to the rate of chemical reactions that occur during an electrochemical process (Harris 2007). Decomposition of water molecules at the surface of the anode is the main anodic reaction that takes place during the copper electrowinning process. Therefore, based on Faraday's law, doubling the electrical current density will double the total volume of the generated oxygen bubbles.

Our previous experimental work suggested that changing the electrical current density had negligible effect on the final sizes of the bubbles that detached from the anode (Al Shakarji et al. 2010). Consequently, doubling the current density will approximately double the number of oxygen bubbles generated. This increase in the number of bubbles (per unit time) with current density results in a net increase in the number of bubbles that burst at the free surface of the solution which in turn produces a higher number of airborne acidic droplets (i.e. acid mist) per unit time per unit surface area of the solution.

### 3.3.2. Quantitative statistical analysis of test parameters on acid mist generation

A 5-way ANOVA analysis was conducted on the raw experimental data to determine the full effect of test parameters on the amount of acid mist generated. This analysis returned p values less than 0.05 (i.e. significant at 95% level) for 18 of the 32 possible parameter combinations. Cohen classifies the magnitude of a parameter's effect into three categories of small, medium and large (Cohen 1988). These categories correspond to $R^2$ values of 0.01, 0.09 and 0.25, hence accounting for 1%, 9% and 25% of the total variance, respectively (Cohen 1988). To quantify the influence of the aforementioned 18 conditions on acid mist generation, the $R^2$ value was calculated for each case based on its Pearson's r value (Field 2005). The top ten cases (with respect to $R^2$) are shown in descending order in Figure 3.3.

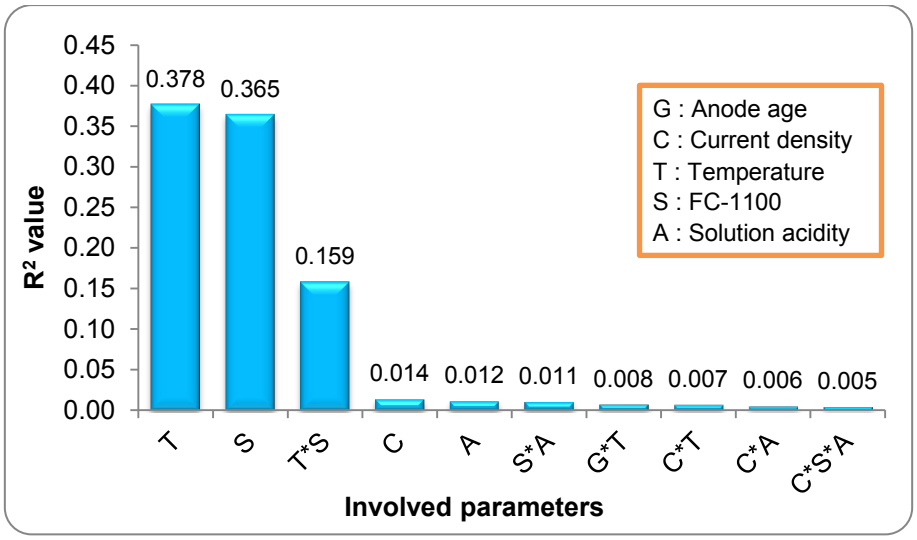


**Figure 3.3** Quantified influence of different parameters and parameter combinations on the amount of acid mist generated

The quantitative analysis (Figure 3.3) shows that temperature, FC-1100 and the interaction of these two parameters are the most influential parameters in determining the amount of acid mist generated. To a lesser degree, current density and solution acidity also affected the generation of acid mist. Anode's age with an $R^2$ value of $8 \times 10^{-5}$ was determined to be a parameter with negligible effect on the amount of acid mist generated.

The ANOVA analysis returned an overall adjusted $R^2$ value of 0.986, which meant 98.6% of the variation in acid mist recorded in the series of experiments could be explained by changes in the five parameters. The uncontrolled variables and

instrumentation errors accounted for only 1.4% of the measured acid mist variations which implied the experiments were conducted at a highly controlled environment.

The influence of individual test parameters as well as that of important interactions (shown in Figure 3.3) on acid mist is discussed in more details in the following sections.

### *Effect of temperature and FC-1100 on acid mist*

Based on Cohen's classification, both temperature (T) and FC-1100 (S) parameters with $R^2$ values of 0.378 and 0.366, respectively, proved to have large effects on the amount of acid mist generated. The interaction of these two influential parameters (T*S) with an $R^2$ value of 0.159 had a medium effect on acid mist. These effects can be seen graphically in Figure 3.4.

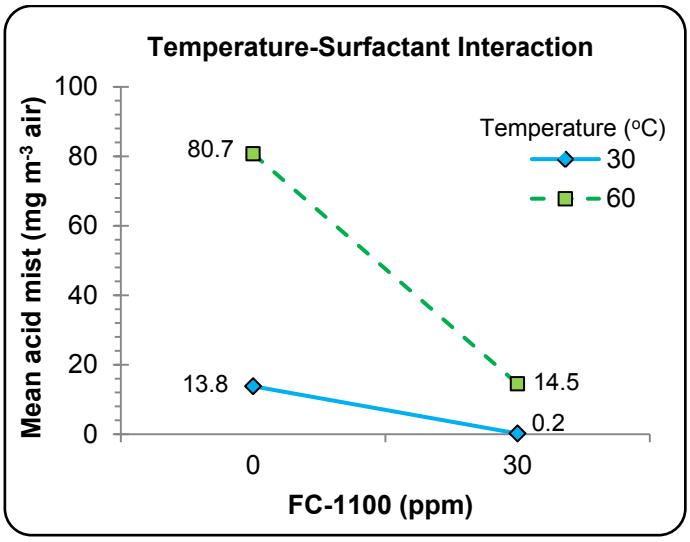


**Figure 3.4** The temperature-FC1100 interaction based on mean acid mist values

Figure 3.4 also shows that the presence of FC-1100 in the electrolyte solution strongly influenced the effect of temperature on the amount of acid mist generated. In the absence of FC-1100, a 30 °C increase in the solution temperature increased the amount of acid mist by almost 67 mg $m^{-3}$ of air whereas in the presence of FC-1100 the same increase in the solution temperature resulted in only 14.3 mg more acid mist per $m^3$ of air.

The vast difference in the slopes of the two lines in Figure 3.4 indicated the strong interaction between temperature and FC-1100. The T*S interaction alone accounted for nearly 16% of the variations seen in the amount of acid mist generated. Overall, temperature (T), FC-1100 (S), and T*S have a combined $R^2$ value of 0.903 which means

that changes made in these three parameters are sufficient to explain more than 90% of the variations seen in the amount of acid mist generated.

### *Effect of current density on acid mist*

Current density with an $R^2$ value of 0.014 was the fourth influential parameter in the amount of acid mist generated. In absolute terms, the effect of current density on acid mist is much less than that of temperature and FC-1100 and based on Cohen's classification the effect of current density is considered small. Nevertheless, in relative terms, current density is an important factor as the amount of acid mist generated at 400 A $m^{-2}$ was 34% more than that generated at 200 A $m^{-2}$ (Figure 3.2).

To compare the magnitude that current density and FC-1100 affect the amount of acid mist generated, the averaged acid mist measurements were plotted at different current densities with or without the presence of FC-1100. The results are shown in Figure 3.5.

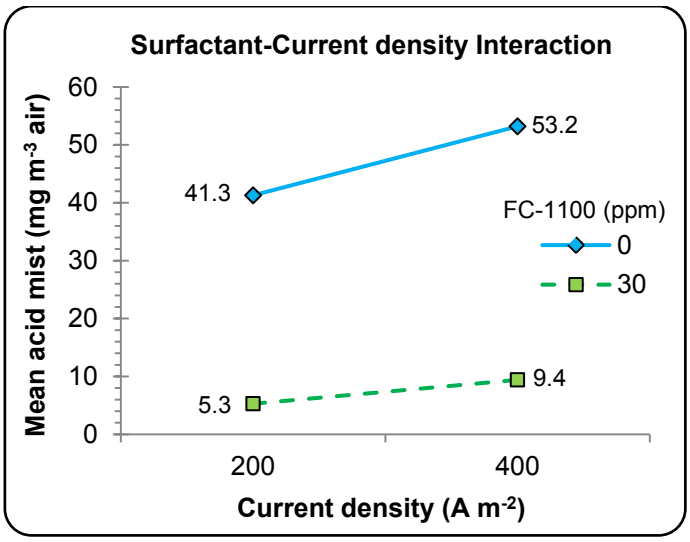


**Figure 3.5** The effect of FC-1100 on acid mist at different current densities

Figure 3.5 confirms again a substantial reduction in acid mist at both low and high current densities when FC-1100 is added to the electrolyte solution. Since there is no significant difference in the slope of the two lines in Figure 3.5, it means that current density has no significant influence on the effect of FC-1100 on acid mist generation, i.e. little interaction effect between the current density and FC-1100.

Figure 3.5 also shows that, regardless of the presence of FC-1100, an increase in current density increases the amount of acid mist generated. However, the acid amount did not double when the current density was doubled. This is because acid mist is

produced from the burst of bubbles that ejects droplets into the air of which some become airborne. The amount of mist generated from the simultaneous bursts of two neighbouring bubbles is known to be less than the sum of mist amount from the bursts of two individual bubbles separately, due to interferences between the bursts of the bubbles. At a higher current density, the likelihood for a number of neighbouring bubbles to burst simultaneously is higher. Consequently, even though the number of oxygen bubbles must be doubled when the current density is doubled, based on Faraday's Law and that the bubble size does not change with current density, the acid mist amount is expected to be less than double.

### *Effect of solution acidity on acid mist*

The ANOVA analysis returned an $R^2$ value of 0.012 for the solution acidity which meant this parameter was the fifth most influential parameter in acid mist generation, which is comparable to that of the current density (0.012 vs. 0.014). This means that the acidity of the solution is approximately as influential as the current density in acid mist generation.

The C*A interaction is listed as one of the top ten influential parameters (Figure 3.3). This interaction is confirmed from the considerable difference in the slope of the two lines shown in Figure 3.6. For high acidity solutions, doubling the current density from 200 to 400 A $m^{-2}$ only resulted in 13% increase (equivalent to 0.087 standard deviations) in the amount of acid mist. In contrast, doubling the current density in low acidity solutions resulted in a staggering 54% increase (equivalent to 0.395 standard deviations) in the amount of acid mist.

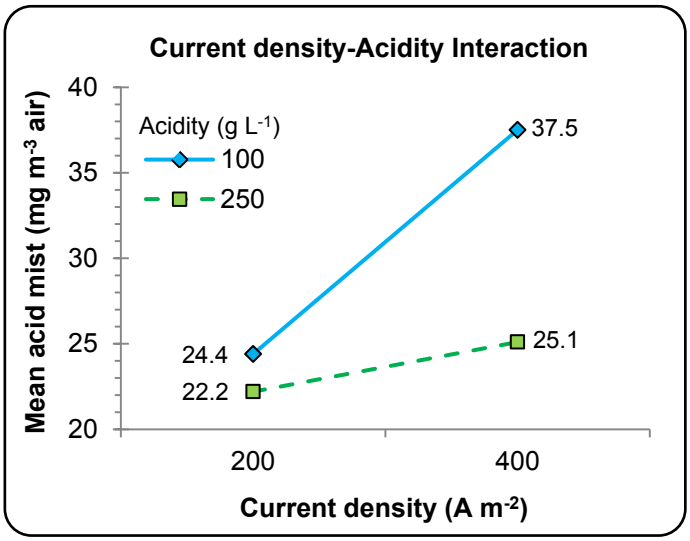


**Figure 3.6** The effect of solution acidity on acid mist at different current densities

Figure 3.7 shows the effects of solution temperature and acidity on the acid mist amount. It again confirms the profound effect that temperature has. Further, the two lines in Figure 3.7 have similar slopes (1.46 for low acidity solutions and 1.24 for high acidity solutions), which suggests that the interaction between temperature and acidity is negligible.

The plots in both Figure 3.6 and Figure 3.7 reveal an interesting phenomenon that low acidity solutions consistently resulted in higher amount of acid mist than high acidity solutions did, regardless of the applied current density and temperature. This apparent counter-intuitive result will be explained in detail in Section 3.3 below.

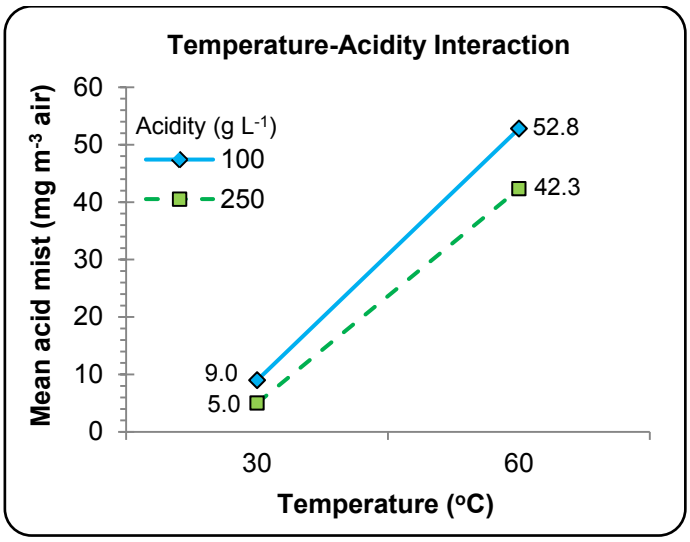


**Figure 3.7** The effect of solution acidity on acid mist at different temperatures

### 3.3.3. The role of surface tension and viscosity in acid mist generation

The previous two sections presented statistical observations on the influence of operational variables and their interactions on the amount of acid mist generated. This section offers mechanistic explanations to the results obtained in this investigation.

#### *Effect of Surface Tension*

Qualitatively, temperature and FC-1100 are both known to affect the surface tension of a solution. To quantify their effect on the electrolyte, the surface tension of 7 samples was measured by the Wilhelmy's plate method at two different temperatures. The averaged results are shown in Figure 3.8.

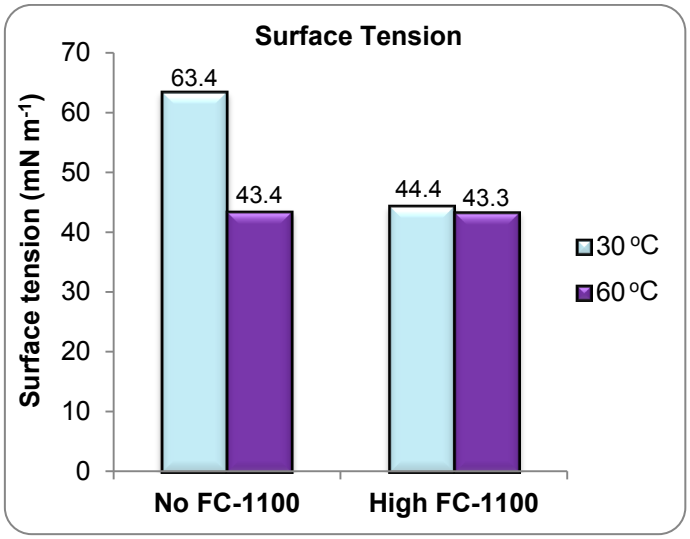


**Figure 3.8** The effect of temperature and FC-1100 on surface tension

It can be seen that temperature strongly influences the surface tension of the electrolyte in the absence of FC-1100. On average, the surface tension decreases by 32% when the temperature is raised from 30 to 60 $^{o}$C in the absence of FC-1100. In contrast, in the presence of FC-1100 at 30 ppm, the temperature change has a negligible effect (less than 3%), as shown in Figure 3.8. These observations are similar to those seen in Figure 3.4 in that, in the absence of FC-1100, the difference caused in the amount of acid mist by temperature change is much larger. Both figures demonstrate a strong interaction between temperature and FC-1100.

It is important to note that, while both increasing solution temperature and addition of FC-1100 cause a significant decrease in the surface tension of the electrolyte, their effect on acid mist generation is the opposite. For example, at 30 $^{o}$C the addition of 30 ppm FC-1100 reduces surface tension to 44 mN.m$^{-1}$ and results in 0.41 standard deviations reduction in acid mist generation. Increasing the temperature from 30 to 60 $^{o}$C, in the absence of FC-1100, also reduces the surface tension to almost the same value (43 mN m$^{-1}$). However, this has resulted in an increase of 2.01 standard deviations in acid mist amount.

In the absence of a surface active agent, lower surface tension or lower surface energy, means lower amount of energy required for the generation of new surfaces. In other words, at a lower surface tension, it is more likely to generate higher number and smaller size of liquid droplets from the burst of bubbles. In addition, previous studies also show that the amount of liquid droplets produced from the burst of gas bubbles increases exponentially with decreasing diameter of the bubbles (Liow et al. 2007, Liow and Gray

1996). That is, the burst of smaller gas bubbles produces more liquid droplets, or mist. In this study, when the temperature is increased, the surface tension is reduced. This has resulted in not only an increase in the likelihood to produce a higher number and smaller size of liquid droplets, but also a reduction in the size of the oxygen bubbles detaching from the anode, causing an increase in the amount of acid mist produced.

In contrast, the reduction in surface tension from the presence of surface active agents not only reduces the final bubble sizes but also changes the bubble burst mechanism at the free surface of the solution. When a bubble rises through the bulk solution and reaches the free surface of the solution, a thin film is produced in the top of the bubble. The stability and lifetime of this thin film is influenced by a number of factors such as surfactant concentration, surface diffusion, surface tension gradient, and drainage rate (Pugh 1996). Generally, drainage rate decreases with the increase in bulk viscosity, surface viscosity and surface elasticity of the solution (Pugh 1996). The latter two factors can be increased significantly by the presence of surfactant molecules at the liquid-gas interface (Pugh 1996). Therefore, it is proposed that the presence of FC-1100 molecules in the solution reduces acid mist mainly via its effects on the thin film drainage rate through a change in the surface viscosity and surface elasticity rather than its effect on final bubble sizes. The slower film drainage and higher surface elasticity in the solutions containing FC-1100 result in the generation of a smaller number of airborne acid droplets (i.e. lesser amounts of acid mist).

### *Effect of Viscosity*

To investigate the counter-intuitive inverse relationship between the solution acidity and the amount of acid mist generated shown in Figure 3.6 and Figure 3.7, the viscosity of 12 electrolyte samples (7 low acidity and 5 high acidity solutions) was measured at three different temperatures. The averaged viscosity measurements for the two types of the electrolyte solution are shown in Figure 3.9.

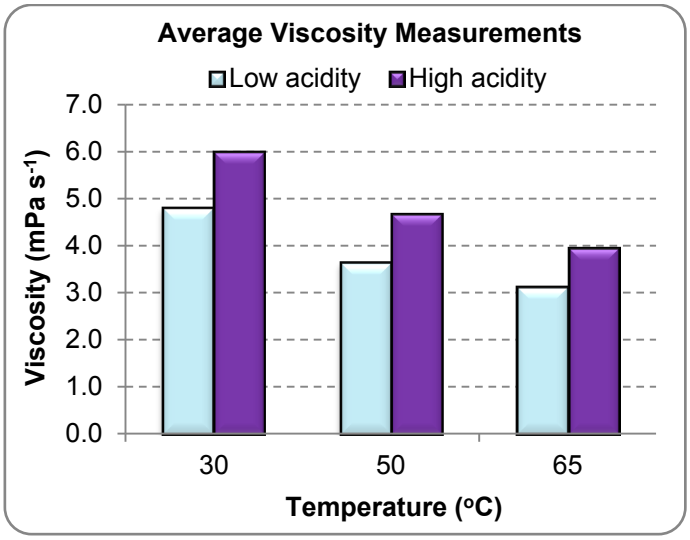


**Figure 3.9** The effect of solution acidity on its viscosity at different temperatures

Figure 3.9 shows that the viscosity of a solution increases with the increase of its acid concentration but decreases with an increase in temperature. The results shown in Figure 3.6 and Figure 3.7, that is, more acid mist is generated by low acid concentration solutions regardless of the applied current density and temperature, can be explained by the fact that the amount of acid mist generated is inversely related to the viscosity of the solution.

While no quantitative relationships between the liquid viscosity and the droplet size and size distribution from the burst of bubbles can be offered at present, it is certainly true qualitatively that, the burst of more viscous liquid films or bubbles will produce less number, but in larger sizes, of droplets. This is simply because more viscous liquid films are more difficult to break-up. Further, based on Stokes' law, the terminal velocity of a rising bubble in a liquid is inversely related to the viscosity of the liquid due to the higher drag force exerted on the bubble by the surrounding liquid. As such, the average ascending oxygen bubble velocity in a more viscous liquid is lower than that in a less viscous liquid. Bubbles reaching the free surface at a lower speed would have less dynamic energy to "throw" the droplets from the bubble burst and make them air-borne. The results shown in Figure 3.6 and Figure 3.7 imply that, at the high acidity level (high viscosity), the number of electrolyte droplets that become airborne is much less than that from the low acidity level.

It must be noted, however, that the substantial increase in acid mist with increasing temperature is not solely due to the decrease in viscosity. Based on Figure 3.7 and

Figure 3.9 it can be seen that a 20% decrease in viscosity due to lower acid concentration in the solution results in 0.22 standard deviations increase in acid mist whereas the 34% decrease in viscosity due to temperature rise results in 1.22 standard deviations increase in acid mist. This significant increase must be attributed to the compound effect of a simultaneous decrease in both the viscosity and surface tension of the solution caused by the temperature increase.

## 3.4 Conclusions

The effect of five different operating parameters on acid mist generation was analysed using a full matrix experimental design. The temperature of the solution and the presence of FC-1100 in the solution proved to be the most influential parameters in the amount of acid mist generated. More than 90% of the variations in the acid mist generation can be explained by changes in the two parameters and their interaction.

To a lesser extent, electrical current density and solution acidity also affected the total amount of acid mist generated. Anode age and most of the 3, 4, and 5-way parameter interactions were found to have negligible influence on the amount of acid mist.

Overall, acid mist was found to increase with temperature and current density. In contrast, addition of FC-1100 to the solutions decreased the amount of acid mist. However, it is critical to note that it is the ability of FC-1100 to increase the surface elasticity and surface viscosity, not its ability to reduce surface tension, that is responsible for the reduction of acid mist generation. The bubble burst mechanism at the free surface of the solution, which is mainly influenced by surface elasticity and surface and bulk viscosity of the solution, proved to be a critical factor in the amount of acid mist generated.

# Chapter 4: Measurement of Bubble Size Distribution by Image Analysis


## Abstract

During electrowinning of copper, oxidation reaction occurs at the surface of the lead anode and oxygen gas is liberated. The size and the burst mechanism of the oxygen bubbles are known to have significant effects on the generation of acid mist. However, little is known about the actual size and its distribution of the oxygen bubbles that are generated under typical operating conditions of a copper electrowinning tankhouse.

This chapter presents a technique for the measurement of oxygen bubbles formed in a copper electrowinning process. Live images of the generated oxygen bubbles were captured by utilizing a high speed camera, super bright LEDs and a special viewing chamber. A MATLAB based software was developed to analyse the images and to determine the size of the bubbles.

The effect of electrical current density on the size of the oxygen bubbles was experimentally investigated. Results show that regardless of the current density applied, bubbles were found in various sizes ranging from 33 μm up to 278 μm. They also revealed that current density had negligible effect on bubble size distribution. The mean bubble diameter for all three different current densities was found to be between 65 and 68 μm.

Experimentally measured amount of acid mist was found to increase linearly with the increase of current density. Based on Faraday's Law, the total volume oxygen generated at the anode is linearly related to the current density. Since the current density had negligible effect on the bubble size, it was postulated that the total number of bubbles generated at the anode was also linearly related to current density.


*Keywords:* Electrowinning; Bubble size measurement; Image analysis; Acid mist

## 4.1 Introduction

In electrowinning of copper, water molecules are hydrolysed and oxygen bubbles are formed at the anode surface. These oxygen bubbles grow and eventually detach from the anode surface and rise in the bulk of the electrolyte. These bubbles burst at the free surface of the electrolyte and produce highly acidic electrolyte droplets of which the fine

ones become airborne and form an acid mist throughout the tankhouse of the electrowinning plant.

Although it is known that bubble size directly affects the amount of acid mist being generated (Frazer 2006), no publications could be found in relation to the size of the bubbles that are generated during copper electrowinning process. Further, current density is known to influence the amount of acid mist generated. However, there have been no studies to quantitatively relate current density to the amount of acid mist.

This chapter presents a method for the determination of bubble sizes. The method combines the use of a high speed camera and super-bright LED lighting, for the capture of live images of the oxygen bubbles, with digital processing of the images to determine the size of the bubbles. This chapter also examines, quantitatively, the relationship between the amount of acid mist generated and current density applied. The acid mist amount is further related to the number of oxygen bubbles based on Faraday's Law.

## 4.2 Methodology

### 4.2.1. Equipment setup

Figure 4.1 shows the pieces of equipment and their arrangement used in this investigation. Essentially, the copper electrowinning process was replicated in a bench-scale cell as explained in Section 3.2.1.

To replicate industrial operations Pb-Ca-Sn alloy and 316L stainless steel were used as anode and cathode, respectively (Houlachi et al. 2007). A clear acrylic frame was constructed for each of the electrodes to control the exposure of the electrode's surface to the solution. The use of these frames ensured a consistent and precise electrical current density for all the experimental runs. The electrodes were placed about 50 mm apart. A double junction reference electrode was placed near the anode to monitor the anodic potential during each experiment.

An electrolyte solution (45 g $L^{-1}$ Cu, 180 g $L^{-1}$ $H_2SO_4$, 15 mg $L^{-1}$ Guar gum, 20 ppm Cl, 100 ppm Co) was prepared that replicated a typical electrolyte solution used in a copper electrowinning tankhouse (Robinson et al. 1994).

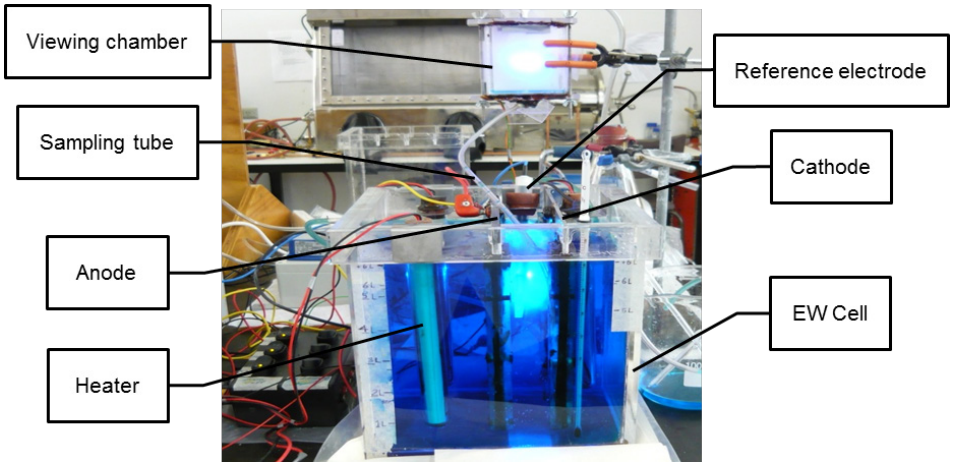


**Figure 4.1** Equipment setup

Capturing live images of the generated oxygen bubbles proved to be an extremely difficult task because these bubbles were typically less than 100 μm in diameter and they were produced in very large numbers on the surface of the anode.

A number of different approaches were tried. The successful method was based on the transfer of the oxygen bubbles from the original cell to a viewing chamber (VC). This method was similar, in concepts, to the HUT method that was discussed in Section 2.5. The VC was a relatively small and thin fully sealable box made of 2 mm thick clear acrylic. A clear PVC tube connected the top end of the VC to a vacuum pump while a flexible siliconee tube connected the bottom end of the VC to the main electrowinning cell (sampling tube in Figure 4.1). The end of the silicone tube was free and could be placed at any location near the surface of the immersed anode.

When the vacuum pump was turned on, the bubble containing electrolyte was drawn through the silicone tube and transferred from the main cell to the VC. Because the VC was very thin and also slightly tilted from its vertical asymptote, oxygen bubbles usually formed a single layer, making photographing of the bubbles much easier. In contrast, the bubbles in the main cell formed multiple layers which made it difficult to obtain clear images. A control valve on the clear PVC tube enabled the control of the vacuum power and hence the number of bubbles entering the VC.

A thin, 130 μm in diameter, copper wire was fixed inside the VC adjacent to the electrolyte's entrance. The diameter of this wire was used as a reference to determine the size of the bubbles captured in each image.

High speed photography of micro sized bubbles required a strong light source that could penetrate the electrolyte solution. Super bright blue LEDs were utilized to provide sufficient background light. A semi clear white acrylic sheet was fixed to the back wall of the VC to disperse the light of the LEDs and to provide even illumination for the region of interest. A high speed camera (RedLake MotionXtra HG-100K) was placed perpendicular to the surface of the VC. A constant current DC power supplier (GW Instek, model: SPS-1230) was used to deliver the required electrical current for the electrowinning process. The cell voltage and current were monitored by high sensitivity multimeters (Digitech QM1538) that were connected to the anode and the cathode.

### 4.2.2. Experimental design

The main goal of the present work was to determine the effect of electrical current density on the size of the bubbles as well as its effect on the amount of acid mist generated. Three different levels of current density were applied (200, 300 and 400 A $m^{-2}$). Two individual experiments were performed at each of the above mentioned current densities (i.e. 6 independent experiments in total).

Each experiment was run for 30 minutes and acid mist was collected for the entire duration of the experiment. Acid mist was captured by nitro cellulose filters and then quantified by pH measurements, of the solution containing the filters, as explained in Section 3.2.1.

Bubble size observations (i.e. image captures) were conducted approximately once every seven minutes (i.e. four independent observations for each experiment). The bubble sizing process is explained in more detail in the following section.

### 4.2.3. Bubble size measurement: Image acquisition and processing

For each electrowinning test, a set of images were captured approximately every seven minutes. High shutter speed was used to ensure the clarity and sharpness of the bubbles in the images. Each set of images contained 750 photos that were captured at 250 frames per second.

Manual bubble sizing was attempted by using the ‘Measure and Label’ Plug-in in ImageJ (version 1.40). In this method, a circle had to be drawn around each individual bubble. The software would then label each of the identified bubbles and measure the diameter of the corresponding circles. High accuracy and selectivity (i.e. ignoring the out of focus bubbles) were the main advantages of the manual bubble sizing technique. This

technique, however, was time and labour intensive. The processing of a typical image, for example, that contained 100 bubbles would take about 2 hours.

As a different approach, a MATLAB based code was developed (named 'The Bubble Detector') to automate the image analysis. The Bubble Detector, unlike ImageJ, was capable of processing grey scale bubble images without the need of converting them to binary format. The Bubble Detector analysed each image in the following steps:

1. Improved the image quality by eliminating the uneven illumination effects and the background noise
2. Enhanced the bubbles contrast and smoothed out the image
3. Detected the edges of all the objects that appeared in the image
4. Filled the holes of the detected enclosed objects and ignored the open or too small objects
5. Distinguished circular objects (i.e. bubbles) from other objects in the image
6. Calculated the area and the diameter for each of the detected bubbles based on the size of the reference wire
7. Highlighted the detected bubbles on the original image and exported the results to an Excel file

The Bubble Detector was tested on several images. In all cases, the software successfully detected almost all the bubbles that appeared in each image. The processing time of each image was reduced to a few seconds which was a big advantage over the manual image processing technique.

## 4.3 Results and Discussion

### 4.3.1. Bubble size measurements

The bubble sizes were determined by the aforementioned MATLAB code that was specifically developed for this purpose. The raw data from each image (i.e. bubbles diameters in μm) were then analysed by Excel and SPSS software.

#### *Descriptive statistical analysis*

Overall, more than 9000 bubbles were detected and their sizes measured. A summary of the descriptive statistical analysis for each of the electrical current densities is shown in Table 4.1.

**Table 4.1** Descriptive statistical analysis summary of the measured bubble sizes

| | | **Current Density (A m$^{-2}$)** | | |
|---|---|---|---|---|
| | | **200** | **300** | **400** |
| **Bubble Diameter (μm)** | Mean | 66 | 68 | 65 |
| | Mode | 39 | 46 | 41 |
| | Standard Deviation | 21.97 | 24.27 | 23.06 |
| | Sample Variance | 482 | 589 | 532 |
| | Skewness | 1.27 | 1.89 | 1.20 |
| | Range | 214 | 240 | 150 |
| | Minimum | 33 | 39 | 35 |
| | Maximum | 247 | 278 | 185 |
| | Count | 4,754 | 2,561 | 1,795 |
| | Confidence Level (95%) | 0.63 | 0.94 | 1.07 |

In Table 4.1 it can be seen that the average size of bubbles was about 66 μm and it did not change significantly with current density. In all three cases, bubbles existed in a wide range of sizes ranging from 33 μm up to 278 μm. The standard deviations were about one third of the mean values. The wide ranges of bubble size were the reason for the relatively large standard deviations. The positive skewness in all three cases indicated that a big percentage of the bubbles were smaller than the mean value. The 95% confidence levels for the mean values were rather small which indicated the samples were good representatives of the main populations. The reason for such narrow confidence intervals was the very large sample sizes.

To ease the comparison between the three test groups, the bubble measurement results were presented with boxplots (Figure 4.2).

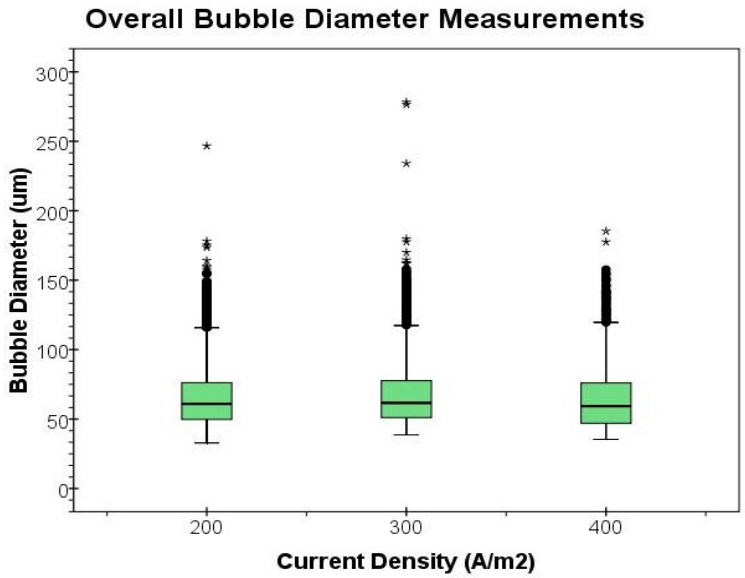


**Figure 4.2** Boxplot representation of bubble size measurements for different current densities

The boxes, in Figure 4.2, were similar in size which indicates about 50 percent of the bubbles (i.e. bubble sizes between the lower and the upper quartiles) had a diameter of 50-70 µm regardless of the applied electrical current density. It could also be seen that the whiskers of each box were unequal. Since all the three lower whiskers were shorter than their upper counterpart, it was concluded that all the three sample populations were skewed to the left (i.e. positive skewness). There were a number of observations that were 1.5-3 box lengths from the lower quartile. These observations were denoted by circles and stars, respectively (Figure 4.2). Reasons for the existence of these extremely large bubbles are discussed in more details later.

Based on the bubble size measurements, a histogram was plotted for each of the three current density levels. These histograms illustrated the number frequency of the detected bubbles at different size categories. The histogram for the 300 A $m^{-2}$ tests is shown in Figure 4.3 as an example.

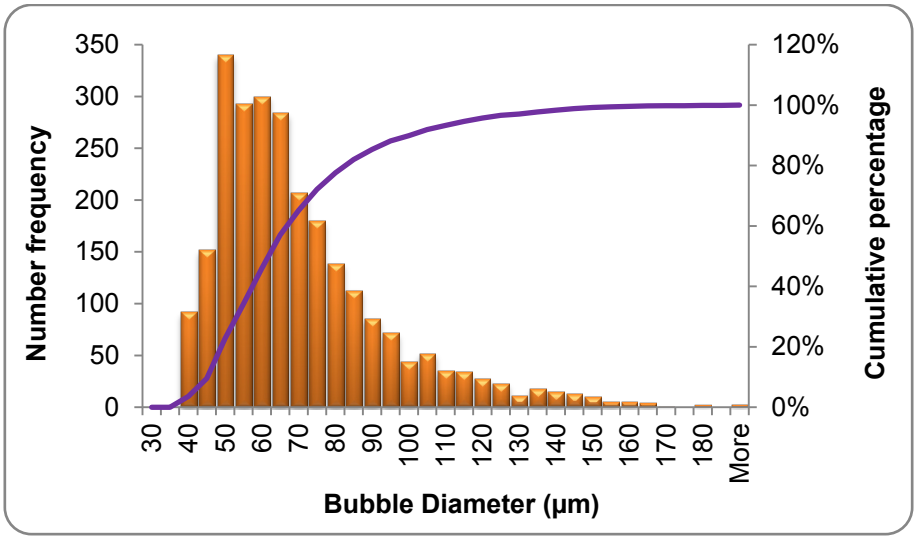


**Figure 4.3** Number frequency and cumulative percentage plots of bubble size distribution at 300 A $m^{-2}$

The frequency graph in Figure 4.3 (i.e. the orange bars) followed the general bell shape of a size distribution graph. However, it can be seen that only about 20% of the detected bubbles ranged from 80 µm to 280 µm which created a tail to the right hand side of the bar graph. Bubbles of 50-70 µm size had the highest frequencies which explained the overall mean value of 68 µm for this population.

From the cumulative percentage graph (the purple line in Figure 4.3) it can be seen that about two third of the bubbles were less than 70 µm in diameter and about 90% of the population had a diameter of 100 µm or less. For the 300 A $m^{-2}$ tests, only 6 of the detected bubbles were larger than 170 µm which accounted for 0.23% of the overall sample population.

To compare the spread of the sample populations of different current densities, frequency percentage plots were used. For each current density, the number frequencies were divided by the total number of detected bubbles (i.e. the sample size) to obtain the corresponding frequency percentage plot. The resulting plots are shown in Figure 4.4.

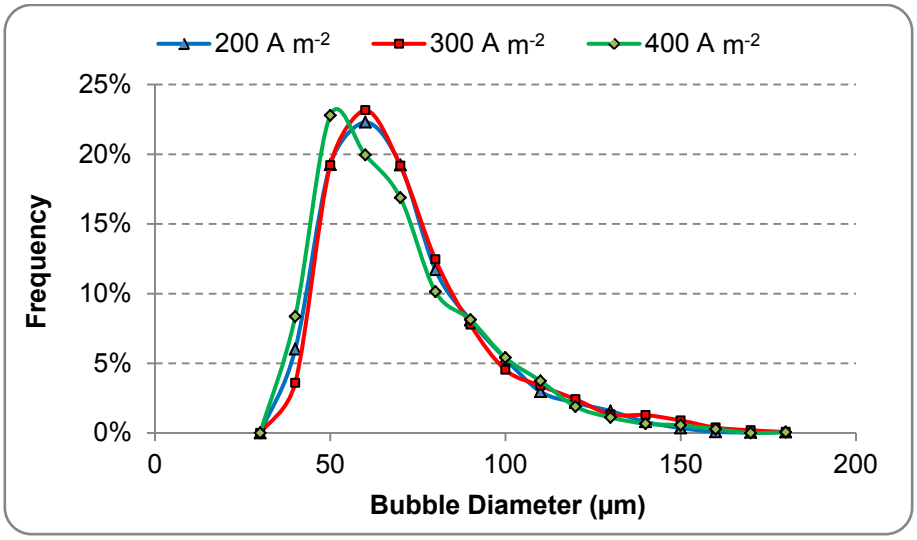


**Figure 4.4** Bubble size distribution at three different current densities

The obtained frequency percentage plots, Figure 4.4, were very similar in shape. The 200 A $m^{-2}$ and 300 A $m^{-2}$ plots were almost identical and the 400 A $m^{-2}$ plot was only slightly drifted to the left. This drift to the left was due to the fact that at 400 A $m^{-2}$ a slightly higher percentage of the detected bubbles were smaller than 50 µm in comparison to the other two current densities. Thus, the descriptive statistical analysis returned slightly lower mean and median values for the 400 A $m^{-2}$ group. Despite the small differences observed in the size distribution plots, the high similarity in size and the shape of the frequency graphs and the width of the size distribution indicated that current density had negligible effect on the size of the generated oxygen bubbles during copper electrowinning process.

The relatively wide bubble size distribution was not an expected outcome. Literature suggests that there are three main forces that act upon a growing bubble (Oguz and Prosperetti 1993). These forces are buoyancy, capillary and hydrodynamic forces (Oguz and Prosperetti 1993). The buoyancy force tends to detach the bubble, from its nucleation site, whereas the capillary and hydrodynamic forces tend to resist bubble detachment (Najafi et al. 2008). It is the balance of these three forces that determines the detachment size of a bubble. Neither the buoyancy nor the surface tension changed significantly during the electrowinning tests. This leaves capillary force to be the only factor that caused the spread of the bubble size distribution.

When measuring bubble size distribution through the viewing-chamber arrangement, a major issue is to ensure no changes occurred to the bubbles in the transfer process, i.e. no bubble breakage or coalescence. The diameter of the sampling tube and the applied

vacuum are two important factors in bubble size measurements. An incorrect setup in either of these two factors could lead to bubble coalescence or bubble breakage in the transfer tube which would result in bias bubble size distribution measurements (O'Connor et al. 1990). Tucker (1994) suggested that bubble breakage was significant when the diameter of the sampling tube was not large enough for the big bubbles to easily pass through (Tucker et al. 1994). The diameter of the sampling tube, shown in Figure 4.1, was three orders of magnitude larger than the biggest detected bubble. Therefore, no bubble breakage was expected to occur at the entrance of the sampling tube. Through the valve on the PVC tube, the suction rate of the solution from the main cell was controlled at sufficiently low level to ensure no breakage of bubbles during their transfer from the main cell to the VC.

Literature suggested that bubble coalescence is highly unlikely in a solution where different ionic species are present at high concentrations (Henry et al. 2006). Since the utilized copper electrolyte solution contained several ion species at high concentrations, bubbles were not likely to coalesce while inside the solution.

To confirm the measured bubble size in the viewing chamber was a true reflection of what was at the anode, video footages were taken from the surface of an operating anode. They confirmed that neither breakage nor coalescence took place in the electrolyte or in the transfer process.

A closer examination of the anode surface, while operating inside the solution, revealed that some of the bubbles stayed attached to the surface of the anode long after their nucleation and continued to grow to very large sizes (more than 400 µm in diameter in some cases as shown in Figure 4.5).

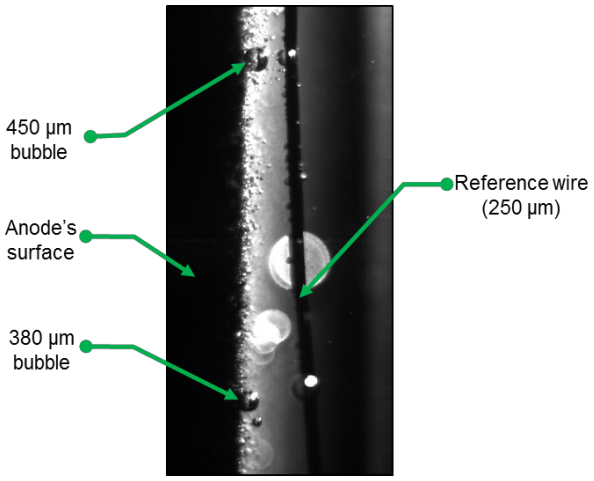


**Figure 4.5** A side view of very large bubbles growing on the surface of the anode

From Figure 4.5, it was evident that the heterogeneous surface of the anode was the major factor in generating bubbles in a wide range of sizes. The effect of the nucleation site properties (such as material composition and surface roughness) were outside the scope of this chapter.

### *Estimating the number of bubbles generated at different current densities*

As mentioned before, the oxygen bubbles generated during copper electrowinning are directly related to acid mist. However, there are no publications that indicate the nature of this relationship.

Equation 2.5 was used to calculate the volume of the oxygen generated (per second) for the applied current density ($V_{tot}$). The observed bubbles from each test group were categorized based on their sizes (i.e. 30-35 µm, 35-40 µm, 40-45 µm, etc.). The total oxygen volume for each category ($V_i$) was then calculated as the product of the nominal bubble volume (i.e. $\frac{\pi}{6}D_i^3$) and the number frequency of that category (i.e. $V_i = N_i\frac{\pi}{6}D_i^3$).

To calculate the volume fractions, volume of each category was divided by the total sum of the volumes of all categories of the test group (i.e. $\%V_i = \frac{V_i}{\sum V_i}$). These volume fractions were then multiplied by $V_{tot}$ to determine the volume contribution of each bubble size category ($V_j$). Finally, $V_j$ and $D_i$ were used to determine the true number of bubbles generated at each category (i.e. $N_j = \frac{6V_j}{\pi D_i^3}$).

The results of the oxygen generation and bubble numbers calculations for three different current densities are illustrated in Figure 4.6.

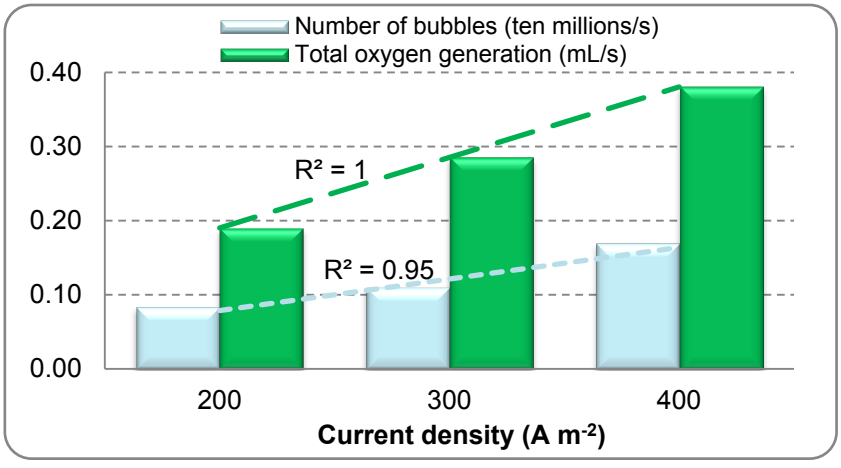


**Figure 4.6** Oxygen volume and bubble number calculation results for three different current densities

From the results in Figure 4.6, it was clear that both the volume of the generated oxygen and the total number of bubbles increased as the current density increased.

For the oxygen generation data, a straight line of best fit returned an $R^2$ value of 1 (Figure 4.6). In other words, current density accounted for 100% variations in the volume of the generated oxygen (Field 2005). This was an expected outcome since oxygen generation was calculated from the modified Faraday's law (equation 2.5) which stated a linear relationship between the rate of oxygen generation and the amount of electrical current used during the electrowinning process.

For the number of generated bubbles data, a straight line of best fit returned an $R^2$ value of 0.95 (Figure 4.6). In other words, current density accounted for more than 95% of the variations seen in the number of generated bubbles (Field 2005). The main reason for not achieving a straight line of perfect fit (i.e. $R^2 = 1$) for the number of generated bubbles was the slight differences seen in the size distribution at different current densities (Figure 4.4). Errors in bubble sizing (due to the sampling method and also size determination by pixel counting, and the very stochastic nature of the bubble generation process) also contributed to the non-perfect results.

### 4.3.2. Acid mist results

To quantify the relationship between current density and the amount of generated acid mist, 12 independent experiments were conducted (including the 6 bubble sizing experiments mentioned earlier). The electrolyte's composition and temperature were kept constant for all experiments. The only variable was the electrical current density which was applied at three different levels (200, 300 and 400 A $m^{-2}$). The generated acid mist was captured and quantified as explained in Section 3.2.1. The overall acid mist measurements are shown in Figure 4.7.

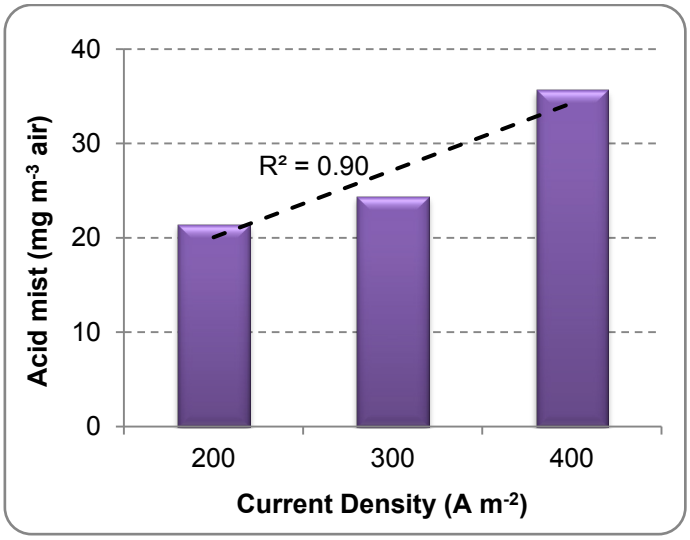


**Figure 4.7** Average acid mist generation at different current densities

Although it was known, through experience, that more acid mist is generated at higher current densities there has been no quantitative data, thus far, to determine the nature of this relationship. Figure 4.7 not only demonstrates the increase in acid mist amount at higher current densities but also suggests a linear relationship between the amount and the electrical current density. It can be seen that current density accounted for about 90% of the variations in acid mist (i.e. $R^2 = 0.90$ in Figure 4.7).

The rate of increase in acid mist with the increase in current density seemed similar to that of the total number of generated bubbles. To quantify this similarity, acid mist results were plotted against the bubble numbers calculated previously (Figure 4.8).

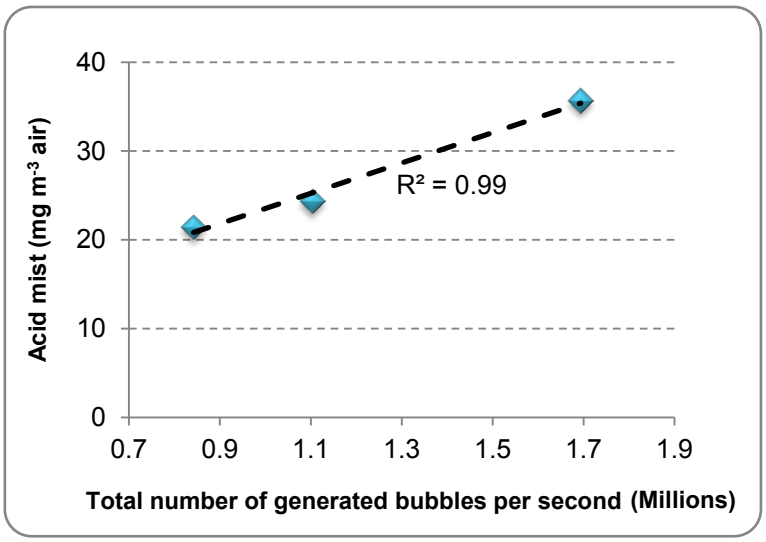


**Figure 4.8** Acid mist versus the total number of generated bubbles

It can be seen (in Figure 4.8) that when acid mist was plotted versus the total number of generated bubbles, a straight line could be fitted to the data almost perfectly (an $R^2$ value of 0.99). In other words, the number of generated bubbles accounted for 99% of the variations in acid mist. The small differences in size distribution at different current densities (Figure 4.4) as well as measurement errors account for the remaining 1% variations seen in the measured acid mist values.

## 4.4 Conclusions

Acid mist is a serious issue for the copper electrowinning tankhouses worldwide. Although oxygen bubbles that are generated at the anode are known to be the major contributor to acid mist, no systematic studies have been conducted to investigate the nucleation, growth and burst mechanism of these bubbles.

In present work, live images of the ascending oxygen bubbles were captured. A MATLAB based software was developed to analyse the images and to determine the size of the bubbles. Bubbles were found in various sizes ranging from 33 μm up to 278 μm. The heterogeneous surface of the anode was identified as the main factor for such wide bubble size distribution.

Bubble sizing at different current densities revealed that current density had negligible effect on bubble size distribution. The average bubble diameter at three different current densities was found to be between 65 and 68 μm.

At higher current densities more acid mist was detected. The number of generated bubbles was accurately predicted, at different current densities, based on the bubble size distribution data. Both the amounts of generated acid mist and the total number of generated bubbles were found to be linearly related to current density.

# Chapter 5: Effect of process parameters on bubble sizes


## Abstract

Oxygen bubbles are formed on the anode in the copper electrowinning process. Burst of the bubbles produces acid mist in the tankhouse. While it is well acknowledged that the amount of acid mist is related to the size of the bubble, no systematic measurements have been made to quantify bubble size and its relationship with materials and process variables. This chapter presents results of bubble size measurement under different operating conditions. For each of the operating conditions tested, bubbles were detected in a wide size distribution ranging from 20 μm to more than 400 μm in diameter. Statistical analyses on the measurement results showed that addition of FC-1100, a surfactant widely used in copper electrowinning to suppress acid mist, and solution temperature were the two most influential test parameters on the bubble size followed by the age of the anode. In contrast, current density and solution acidity had negligible effect.


*Keywords:* Copper electrowinning; Oxygen evolution; Imaging; Bubble size; Contact angle; Surface tension

## 5.1 Introduction

Previous research results suggest that the amount of acid mist being generated is related to the size of the bursting bubbles (Liow et al. 2007). For electrowinning processes, although it is known that some operating parameters such as solution temperature can influence the size of the bubbles, there have been no systematic studies to quantify the effect of operating parameters on the size and size distribution of bubbles.

This chapter reports the results of bubble size measurement under different operating conditions. It also examines, quantitatively, the relationship between the median bubble size and five operating parameters in copper electrowinning. These parameters are anode age, electrical current density, solution temperature, sulphuric acid concentration of the solution, and the presence of a typical chemical mist suppressant such as FC-1100.

## 5.2 Experimental

### 5.2.1. Equipment setup

The copper electrowinning process was replicated in a bench-scale tank (EW cell) as explained in Section 3.2.1. The equipment used in this investigation and its arrangements are shown in Figure 5.1.

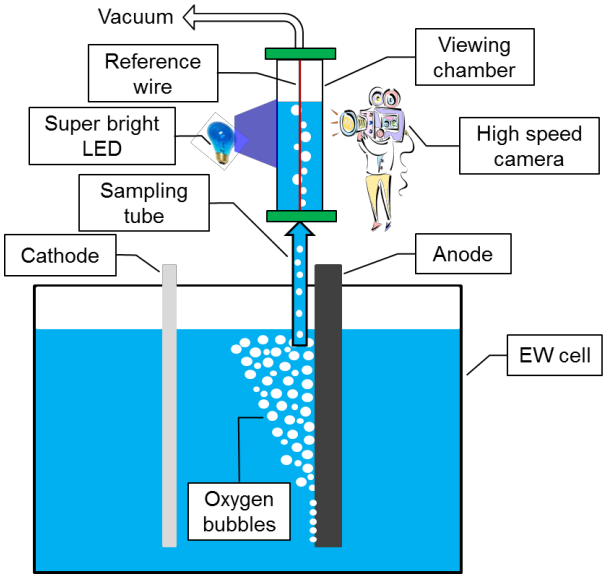


**Figure 5.1** A schematic view of equipment setup (not to scale)

For each set of experiments a fresh batch of solution was synthesized containing 45 g $L^{-1}$ Cu, 15 mg $L^{-1}$ Guar gum, 20 ppm Cl, 100 ppm Co, and various amounts of sulphuric acid. The concentration of Cu, Guar gum, Cl, and Co in the synthesized solution was similar to the electrolyte solutions found in most copper electrowinning tankhouses worldwide (Robinson et al. 1994). The sulphuric acid concentration in the solution, however, was one of the five selected variables and its concentration differed from that of a typical copper electrolyte solution.

To measure bubble sizes via image analysis, the generated oxygen bubbles were transferred from the EW cell to a viewing chamber. A high-speed camera (RedLake MotionXtra HG-100K) with a special macro lens and super bright blue LEDs were utilized to capture images of the rising bubbles in the viewing chamber. For more detail on bubble imaging please refer to Section 4.2.3.

### 5.2.2. Experimental design

The experimental design of this series of experiments was identical to that explained in Section 3.2.2 (i.e. 2K factorial method, 5 parameters, and 32 experimental conditions). Overall, 64 tests were conducted to determine the significance of each parameter and also to identify any significant interactions among the selected parameters.

For each of the 64 experiments, at least two sets of high resolution photos were taken by the high-speed camera. The images were taken at 10 minutes intervals at a rate of 250 frames per second while the experiment was being conducted. To ensure that the same bubbles were not accounted for more than once, only one photo was selected per 100 consecutive frames (i.e. 3 to 5 photos were selected from each set of images of each experiment) for image analysis.

### 5.2.3. Bubble sizing process

A flexible silicone tube (sampling tube in Figure 5.1) was used to transfer the bubble-containing solution from the EW cell to the viewing chamber. One end of the sampling tube was placed about 10 mm underneath the free surface of solution near the surface of the anode while the other end was connected to the bottom of the viewing chamber. By applying a gentle vacuum to the viewing chamber, the bubble containing solution was drawn from the EW cell to the viewing chamber at low flow rates. The large internal diameter of the sampling tube (5 mm) and the low solution flow rate, from the EW cell to the viewing chamber, ensured no bubble breakage or coalescence occurred during the bubble transfer process. Thus, bubbles observed in the viewing chamber were true representatives of those generated in the EW cell.

The high speed camera was then used to capture 800×600 pixel images. Each image taken from the rising bubbles in the viewing chamber contained about 100 bubbles on average (more than 300 bubbles in some cases). A MATLAB based program was developed to automate the analyses of the captured images. The developed program was able to process the images in grey scale format directly from the camera. The software was designed to take into account the uneven background illumination and to distinguish the boundaries of each bubble from its surroundings as explained in detail in Section 4.2.3.

A thin copper wire, 130 μm in diameter, was fixed inside the viewing chamber adjacent to the solution's entrance. The diameter of this wire was used as a reference to

determine the size of the bubbles captured in each image. The developed software was able to process each image in a few seconds and export the raw data of bubble diameters (in µm) to an Excel file. The software also indicated the detected bubbles with blue lines along the boundaries of each bubble and displayed the bubble diameter (in µm) next to it (Figure 5.2). These processed images were used to visually inspect the results of the bubble sizing process.

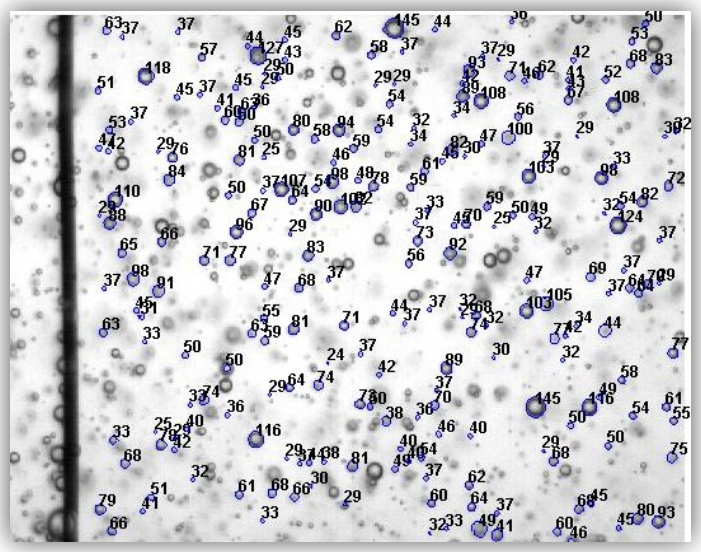

**Figure 5.2** A processed image with 250 detected bubbles and the reference wire (the vertical black line) appearing on the far left

To ensure the accuracy of the developed bubble sizing program, ImageJ (an open source image analysis software) was used to manually determine the bubble sizes of three randomly selected images. The results of the automated and manual bubble sizing were statistically identical.

## 5.3 Results and discussion

### 5.3.1. Overall statistical analysis

In total, more than 54,000 bubbles were sampled and their sizes measured. The diameter of the bubbles ranged predominantly from 26 µm up to 182 µm, on average, for each of the 64 experiments. However, there were cases where the smallest detected bubble was 20 µm and the largest one was 404 µm. On average, 50% of the detected bubbles had a diameter of 53 µm or less (i.e. the grand median value). A typical bubble size distribution and cumulative percentage graph is shown in Figure 5.3.

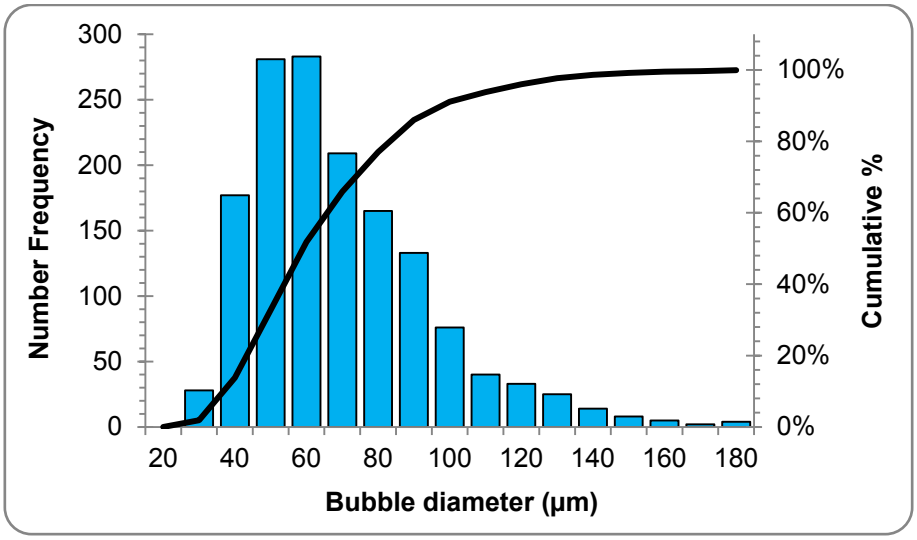


**Figure 5.3** Bubble size distribution and cumulative percentage graph for experiment No 9 (parameter values: new anode, 200 A $m^{-2}$ current density, 60 $^{o}$C solution, no FC-1100 and 100 g $L^{-1}$ sulphuric acid concentration)

There was a relatively strong positive skewness (1.7 on average) in all the collected data samples, similar to that shown in Figure 5.3. Therefore, median values were selected instead of mean values to represent the average bubble size for each experiment. The small difference between the medians of replicates of a test condition, which ranged from 0.00 µm up to 5.24 µm with the average being 2.17 µm, was a good indication of the high repeatability of the conducted experiments.

Figure 5.4 illustrates the median bubble diameter (the bold black line inside each box), the lower and upper quartiles (the lower and upper edges of each box), the lower and upper extremes (the lower and upper whiskers), and also the outliers (the stars) for each of the 32 experimental conditions. The values of median bubble diameters ranged from 43 µm to 66 µm. Regardless of the applied operating conditions, 95% of the generated bubbles were less than 106 µm in diameter. It must be noted that the outliers were neither the result of error in the bubble sampling process nor the image analysis procedure. Live video footage taken from the surface of an immersed operating anode proved the existence of such unusually large bubbles. These outliers are discussed in more details in Section 4.3.1 (Al Shakarji et al. 2010).

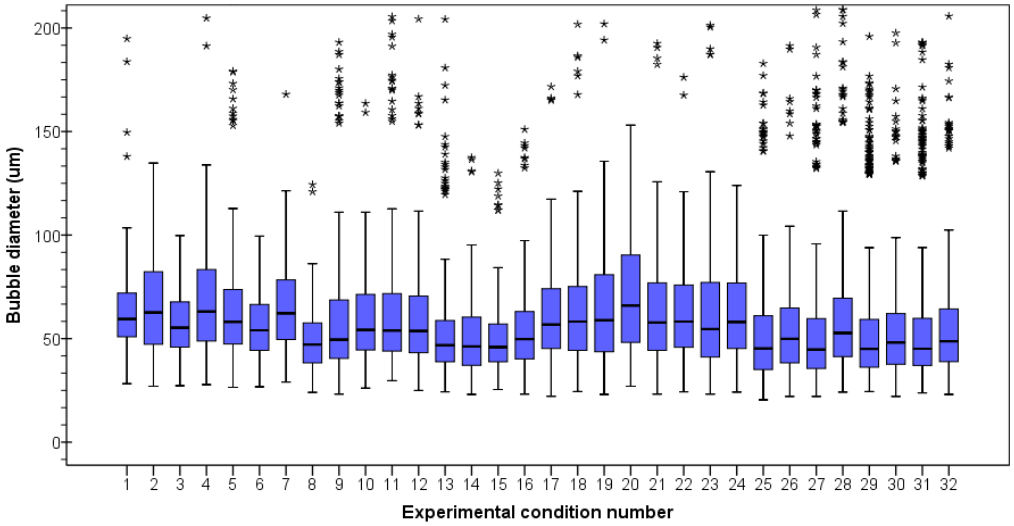


**Figure 5.4** Bubble size distribution under 32 different operating conditions

A 5-way ANOVA analysis was performed on the raw experimental data to determine the full effect of test parameters on the average bubble size. To quantify the magnitude of the effect of each of the 32 parameter combinations, Pearson's r value was calculated for each case based on its ANOVA's mean square value (Field 2005). Cohen classifies the magnitude of a parameter's effect into three categories of small, medium and large (Cohen 1988). These categories correspond to Pearson's r values of 0.1, 0.3 and 0.5 respectively (Cohen 1988). Parameter combinations with Pearson's r value greater than 0.10 are shown in Figure 5.5.

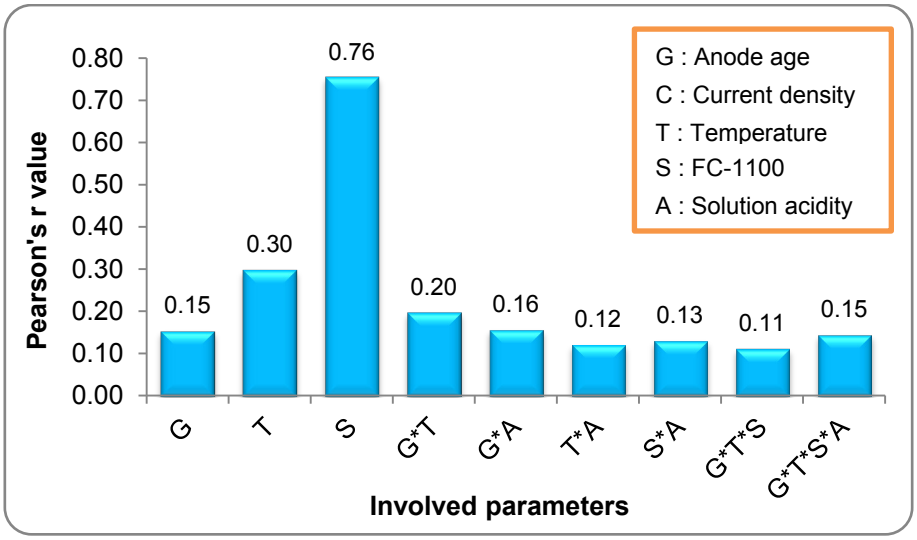


**Figure 5.5** Quantitative comparison of the most influential parameters and parameter interactions on the average bubble size

FC-1100 and solution temperature, having the highest r values in Figure 5.5, were the most influential parameters in determining the final bubble sizes. To a lesser extent, anode age also influenced the final bubble sizes. Current density and solution acidity, with Pearson's r values of 0.04 and 0.05 respectively (not shown in Figure 5.5), had negligible effect on the detachment size of bubbles.

The full factorial ANOVA analysis not only examined the effect of individual parameters but also all the possible parameter interactions. This analysis returned an $R^2$ value of 0.951, which meant the variations made in the test parameters of the conducted experiments could explain more than 95% of the bubble size variations measured in the test series.

### 5.3.2. Effect of individual parameters on bubble size

To assess the effect of individual test parameters on the bubble size, the average median bubble diameter for each level of a parameter was calculated. Each bar in Figure 5.6 represents the averaged median bubble diameter from 32 independent experiments.

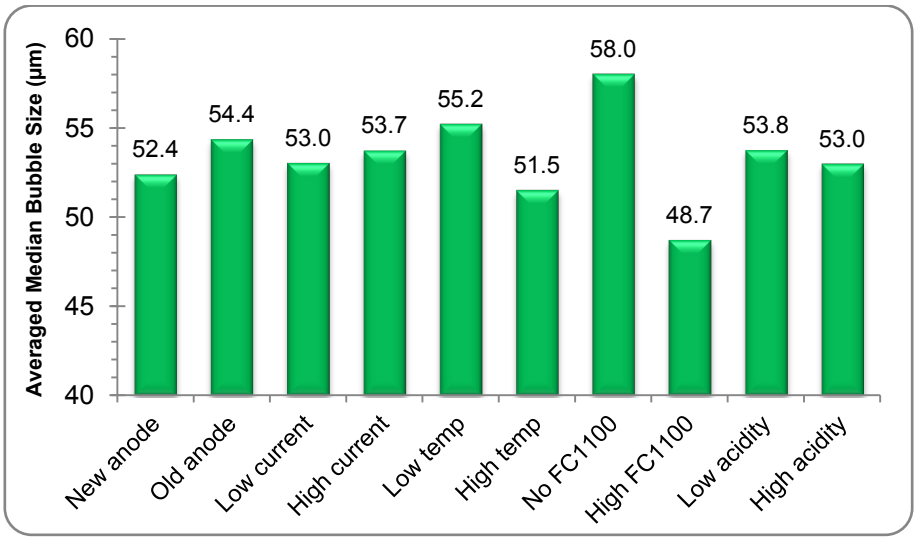


**Figure 5.6** Average bubble diameter at different operating conditions

### *FC-1100*

FC-1100 was the only parameter that had a large effect, based on Cohen's classification, on the average bubble sizes. The presence of FC-1100 in the solution reduced the average bubble diameter by 9.3 µm. This result was largely attributed to the ability of FC-1100 to reduce the surface tension of the electrolyte from 63 mN $m^{-1}$ to 44 mN $m^{-1}$. The near parallel solid lines in Figure 5.7 implied that, within the tested range, the effectiveness of FC-1100 in reducing the final bubble sizes was independent of the solution temperature.

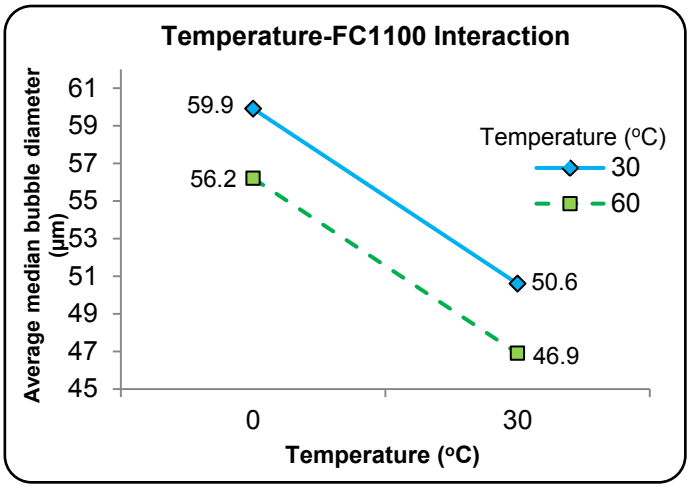


**Figure 5.7** The effect of FC-1100 on bubble size at different temperatures

The bubble size distribution, in addition to the average bubble size, was also considerably reduced in the presence of FC-1100 (Figure 5.8). It was proposed that the presence of FC-1100 molecules reduced the surface tension of the solution to a degree that resulted in less variation in the three phase contact angle on the anode, leading to the generation of more uniformly sized bubbles (i.e. smaller standard deviation).

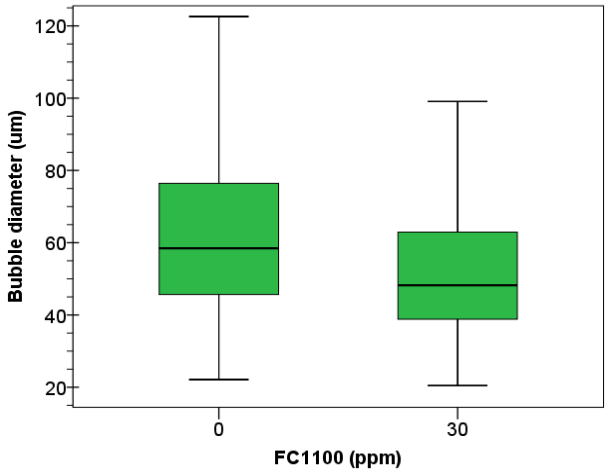


**Figure 5.8** Effect of FC-1100 on bubble size distribution (not including outliers)

### *Temperature*

Solution temperature with a Pearson's r value of 0.30 was the second most influential parameter in determining the final size of a bubble (Figure 5.5). Changing the solution temperature caused a relatively large difference in the average bubble diameter. Raising the temperature of the solution from 30 $^{o}$C to 60 $^{o}$C resulted in 3.7 µm reduction in the average bubble sizes, equivalent to 0.150 standard deviations (Figure 5.6).

Similar to the presence of FC-1100, when temperature of the solution was raised from 30 $^{o}$C to 60 $^{o}$C, surface tension of the electrolyte solution decreased from 63 mN m$^{-1}$ to 44 mN m$^{-1}$. Therefore, it was postulated that the decrease in the average bubble size at higher temperature was mainly due to the decrease in the surface tension of the solution. The large reduction in surface tension due to temperature rise was also expected to result in less variation in the three phase contact angle, leading to the generation of more uniformly sized bubbles. This expectation was confirmed by data presented in Figure 5.9 where bubble size distribution was noticeably less (smaller box and whiskers) in high temperature electrolyte solution.

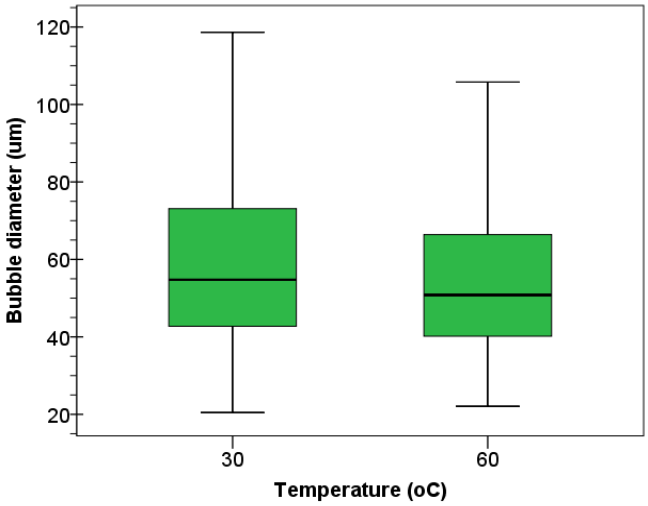


**Figure 5.9** Effect of solution temperature on bubble size distribution (not including outliers)

### *Anode age*

The experimental results shown in Figure 5.6 suggested that bubbles generated on an old anode were, on average, 2.0 µm (0.089 standard deviations) larger than those generated on a new anode. The ANOVA analysis resulted in a Pearson's r value of 0.15 for the anode age which meant this parameter had a small/medium effect on the final size of a bubble. It was postulated that anode age affected the detachment size of a bubble by influencing the liquid-solid-gas contact angle which in turn influenced the balance of the forces acted on the bubble. SEM images revealed that the surface of an old anode was highly uneven and covered with voids and micro cracks whereas the surface of a new anode was relatively smooth and even (Figure 5.10).

It was likely that the small cavities and cracks on the surface of the old anode provided much higher number of nucleation sites for the bubbles, leading to "forced" coalescence of the bubbles during their growth on the anode immediately prior to their detachment due to insufficient distances between neighbouring bubbles on the anode. Similar observations were reported by Huet where mean detachment radius of electrolytic bubbles increased with the surface roughness of nickel electrodes (Huet et al. 2004).

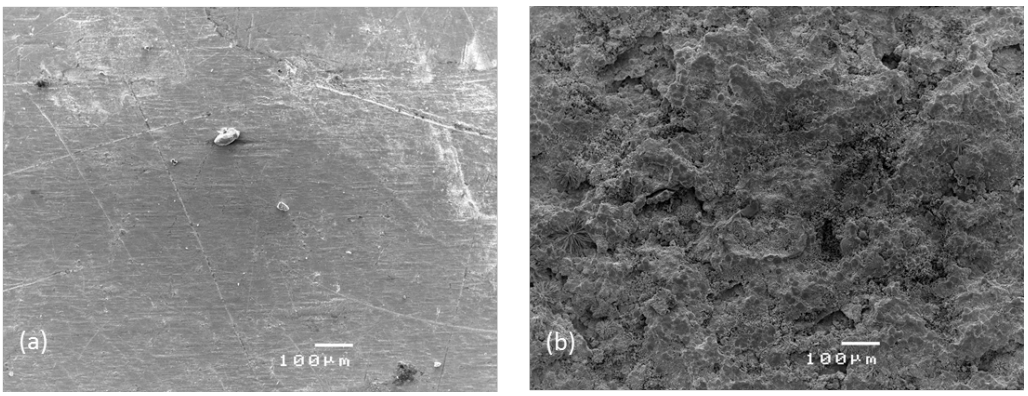


**Figure 5.10** The surface morphology of (a) a new anode (b) an old anode

It is important to note that, regardless of the age of the anodes or operating conditions, bubble size distribution was relatively large, ranging from 20 µm to more than 400 µm (Figure 5.4). The heterogeneities in both the chemical composition and the surface roughness of the anodes were believed to be the main reasons for such wide bubble size distributions. The anodes were Pb-Ca-Sn cold rolled alloys, either the surface roughness or the distribution of the three elements was very unlikely to be even on the surface of the anodes after the rolling process.

*Solution acidity and Current density*

It is worth noting that, within the ranges tested in this study, both the solution acidity and the current density had negligible influence on the bubble size. Solution acidity could affect the bubble size only through the change it could cause in the solution viscosity. Kazakis et al. (2008) reported a noticeable difference in the average bubble size only when the viscosities of the test solutions were considerably different, e.g. the difference between their viscosities was more than 600%. Rheological tests of the copper electrolyte solutions, however, showed that high acidity solutions were only 21% more viscous than low acidity solutions. Therefore, it was suggested that a much larger difference in the solution acidity, and hence the viscosity, was required to observe a noticeable difference in the average size of the bubbles generated during the copper electrowinning process.

Based on Faraday's law, increasing the electrical current density would increase the amount of oxygen produced at the anode (Harris 2007). Consistent with our results presented previously, within the range of 200 and 400 A $m^{-2}$, a change in the current density had caused only a change in the bubble nucleation rate and hence the number of bubbles generated per unit time. The final sizes of the bubbles changed little with current density as discussed previously in Section 4.3.1 (Al Shakarji et al. 2010).

### 5.3.3. Effect of parameters' interaction on bubble size

Few publications in this field studied the interactions that exist among the test parameters. The full factorial ANOVA analysis showed that more than 22% of variations in bubble sizes recorded in the test series were due to the interactions between the test parameters.

With a Pearson's r value of 0.20, the anode age-temperature interaction (G*T) was identified as the most significant parameter interaction. The results are shown in Figure 5.11.

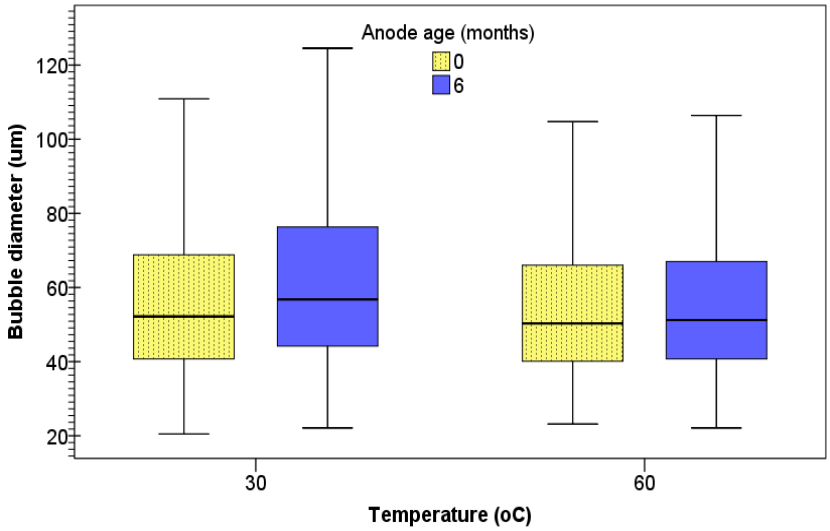


**Figure 5.11** The interaction between anode age and temperature

It can be seen that, on an old anode, increasing the temperature of the solution from 30 $^{o}$C to 60 $^{o}$C resulted in a relatively large decrease (more than 0.247 standard deviations) in the average bubble diameter. In contrast, the same increase in the solution temperature resulted in a much smaller decrease (about 0.049 standard deviations) in the average bubble diameter on a new anode.

The G*T interaction not only affected the average size but also the size distribution of bubbles. Size distribution of bubbles formed on the old anode was much wider at low solution temperature in comparison to that of high solution temperature (i.e. larger box and whiskers at low solution temperature). In contrast, the temperature of the solution had a relatively small effect on the size distribution of bubbles formed on a new anode (i.e. similar box and whiskers sizes at low and high temperatures).

The decrease in the average bubble size and its distribution with temperature rise was due to surface tension reduction as explained earlier. Consistent with observations made by other researchers (Drelich and Miller 1994, Meiron et al. 2004), the strong interaction between anode age and solution temperature was believed to be mainly due to the effect of anode's surface morphology on the three phase contact angle.

The effect of the anode's surface morphology (i.e. anode age) on bubble size and its distribution was much more evident at low solution temperature (Figure 5.11) since the overall surface tension was higher at lower temperature.

One of the other important interactions was the T*A interaction. The decrease in the average bubble size and its distribution due to temperature rise was not the same for the low and high acidity solutions (Figure 5.12). The average size and size distribution of bubbles were more strongly affected by temperature rise in low acidity solutions than in high acidity solutions.

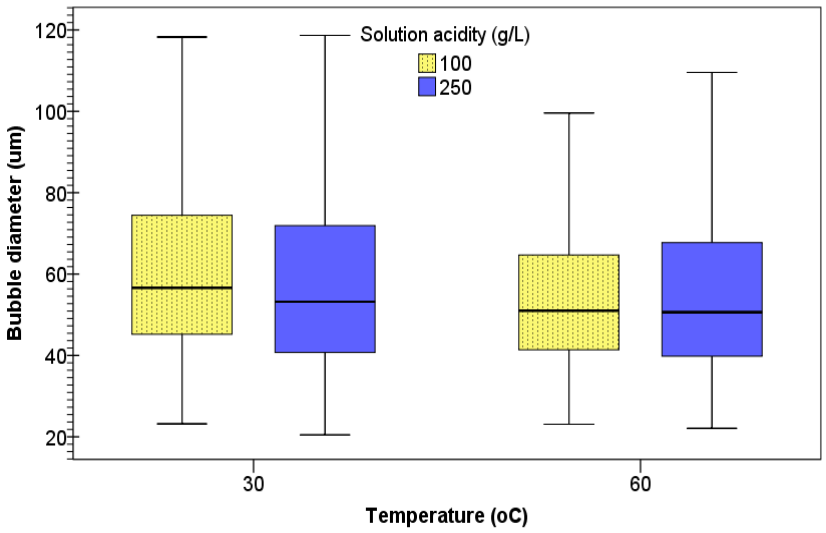


**Figure 5.12** The interaction between temperature and solution acidity

Surface tension and viscosity were both known to influence the final size of a bubble (Xie et al. 2009, Xu et al. 2009). Temperature affected both surface tension and viscosity whereas acidity only affected viscosity. Therefore, the T*A interaction was expected to be the result of surface tension and viscosity interaction. The surface tensions of low and high acidity solutions were measured at two different temperatures (Figure 5.13).

It is general knowledge that surface tension of a liquid is a function of not only its composition but also its temperature. Measurements showed that surface tension of a low acidity solution was higher than that of a high acidity solution at 30 °C (Figure 5.13). However, surface tensions of the two solutions were almost the same at 60 °C. In other words, temperature had a more profound effect on the surface tension of low acidity solutions than that of high acidity solutions. These observations were similar to those seen in Figure 5.12 in that, in low acidity solutions, the differences in the average bubble size and bubble size distribution caused by temperature rise were much larger. Both figures demonstrated a strong interaction between temperature and solution acidity.

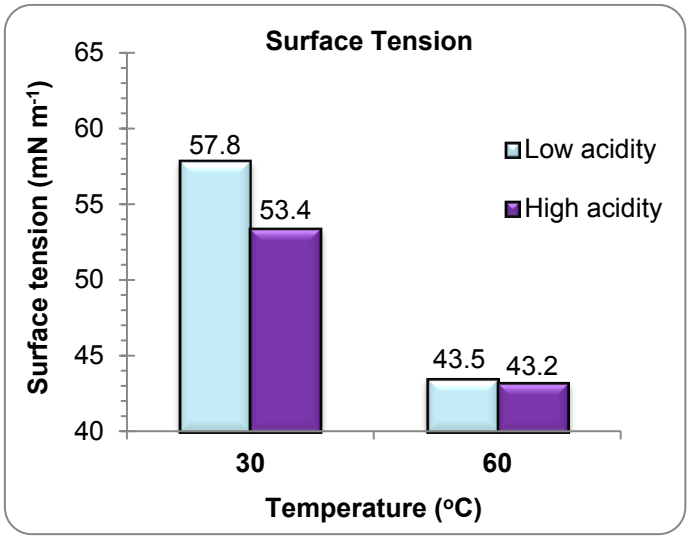


**Figure 5.13** Effect of temperature and acidity on surface tension

The surfactant-solution acidity (S*A) interaction had a Pearson's r value of 0.13. The interaction between FC-1100 and solution acidity is illustrated in Figure 5.14.

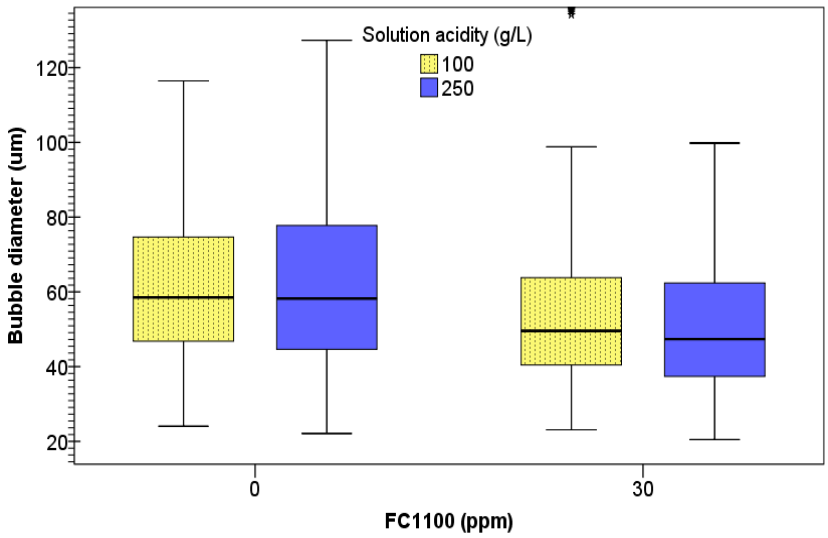


**Figure 5.14** The interaction between FC-1100 and solution acidity

In the absence of FC-1100, although bubble size distribution was slightly larger in high acidity solutions, the average bubble sizes generated in the low and high acidity solutions were very similar. In the presence of FC-1100, bubbles generated in high acidity solutions were on average 0.101 standard deviations smaller in diameter than those generated in low acidity solutions. Xu et al. also reported similar observations when studying the effect of NaCl concentrations on bubbles generated from a sparger in the presence of fixed amounts of sodium dodecyl sulphate surfactant (Xu et al. 2009). The higher ionic concentration at high acidity solutions was speculated to result in closer

packing of the surfactant molecules by reducing the repulsive forces between them (Xu et al. 2009). In our case, bulk concentration of FC-1100 in high acidity solutions might be lower, resulting in more FC-1100 molecules packing at the interface. This can be inferred from the fact that the average surface tension of low acidity solutions is higher than that of high acidity solutions. The closer packing of the surfactant molecules at the oxygen/solution interface lowers the surface tension and results in smaller bubbles.

## 5.4 Conclusions

A high-speed camera and image analysis software were used to measure the size of the bubbles generated during the copper electrowinning process. Measurements, made under a variety of operating conditions, showed that of the five test parameters, FC-1100 and solution temperature had the most significant effect on the average size of the oxygen bubbles. Bubble size and bubble size distribution were noticeably reduced in the presence of FC-1100 or when the solution temperature was increased. FC-1100 and solution temperature both influenced bubble sizes by reducing the overall surface tension of the solution. To a lesser extent, anode age also influenced the detachment size of bubbles. Older anode generated larger bubbles and wider bubble size distributions mainly due to its surface roughness variations.

The data produced by the present work can be used to investigate the correlation between bubble size and the amount of acid mist, facilitating the design of strategies for minimizing acid mist generation in the tankhouse. The data can also be used to calculate the rate of bubble generation and release under a variety of operating conditions. Such information would be extremely useful in simulating the flow pattern of electrolyte solution between electrodes, which can be utilized to enhance the design of the electrodes and cells leading to improved electrolyte flow and copper quality at higher current densities.

# Chapter 6: Acid mist and Bubble size Correlation

## Abstract

The average bubble size and the amount of acid mist generated during copper electrowinning were measured under a variety of operating conditions. In the absence of surfactants, the amount of generated acid mist decreased as the average bubble size increased. In contrast, in the presence of FC-1100, a surfactant typically used to supress acid mist, acid mist showed little correlation with the average bubble size. The significant change in the bubble burst mechanism, due to the presence of surfactant molecules in the solution/air interface, is believed to be the reason for the suppression of the effect of bubble size on acid mist.

*Keywords:* Copper electrowinning; Bubble size; Acidic mist; Surfactant; Surface elasticity

## 6.1 Introduction

The effect of five different parameters on the amount of acid mist and on the size of oxygen bubbles were discussed, separately, in Chapters 3 and 5 respectively. In this chapter, we discuss the effect of the average bubble size on the amount of acid mist and seek to establish whether the two phenomena are correlated.

## 6.2 Methodology

The copper electrowinning process was replicated in a bench scale tank as explained in Section 3.2.1. In total, 64 tests were conducted under 32 different operating conditions to examine the effects of five parameters. The five test parameters were anode age, current density, solution temperature, FC-1100 (a typical surfactant used in industry to suppress acid mist), and solution acidity. Details of the experimental setup, acid mist measurements, and bubble sampling and size analyses can be found in Sections 3.2 and 4.2.

## 6.3 Results and Discussion

The average acid mist and bubble size measurements from 64 experiments are shown in Figure 6.1. The test results are divided into two groups. The first group belongs to tests that were conducted with solutions containing no FC-1100 (shown by diamonds in

Figure 6.1). The second group is the result of tests conducted with solutions containing 30 ppm of FC-1100 (shown by squares in Figure 6.1).

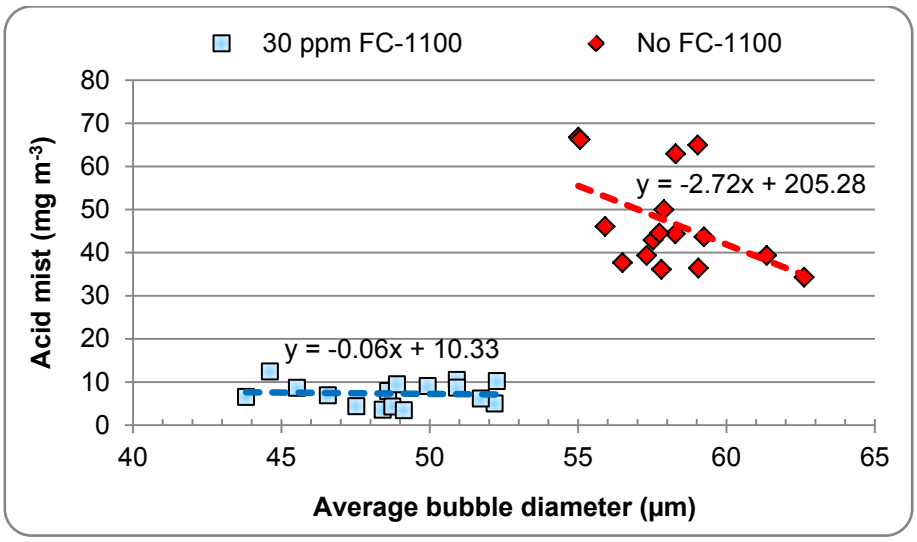


**Figure 6.1** Effect of FC-1100 on acid mist and bubble size

In electrowinning, both bubble size and acid mist are strongly influenced by the presence of a surfactant such as FC-1100 (Al Shakarji et al. 2011b, Al Shakarji et al. 2011a). The important thing to note in Figure 6.1 is that the amount of acid mist correlates to the average bubble size very differently depending on the presence or the absence of FC-1100 molecules in the solution. When FC-1100 is present, the average bubble size has almost no effect on the amount of acid mist. In contrast, when no FC-1100 is used, the amount of acid mist decreases with increasing bubble sizes.

When a bubble bursts at the free surface of a solution, it usually produces two types of drops: film drops and jet drops. Film drops are created from the shattering of the film cap of the bubble whereas jet drops are created from the disintegration of a liquid jet which is formed after the collapse of the bubble cavity (Spiel 1998). For bubbles smaller than 1.8 mm in diameter, which includes all the bubbles generated in copper electrowinning, jet drop formation is predominant (Resch and Afeti 1991). In oceanography, where the amount of surface active agents is negligible, it has been shown that as the diameter of the bubble increases (in the range of 200-1000 µm), the average size of jet drops also increases but the number of jet drops decreases exponentially (Rossodivita and Andreussi 1999). These findings are consistent with our results presented in Figure 6.1 with no FC-1100, which shows a negative correlation of acid mist amounts to bubble size. When larger bubbles burst, the generated droplets are fewer in number and larger in size in

comparison to droplets of smaller bubbles. The larger droplets are heavier and slower than small droplets and it is less likely for them to become airborne, hence the decrease in the total amount of acid mist with the increased average bubble size.

When FC-1100 is present, Figure 6.1 shows that the average bubble size is smaller, due to a reduction in surface tension. The amount of acid mist is also significantly reduced. It must be stressed, however, that the significant reduction in acid mist is not due to a reduction in surface tension of the solution. While there is a direct correlation between the average bubble size and the surface tension of the solution, i.e. the lower the surface tension, the smaller the bubble size, the amount of acid mist is hardly related to the bubble size when FC-1100 was used.

Contrary to one of the most widely accepted understanding, a reduced surface tension will not necessarily lead to less acid mist. For example, Figure 6.2 shows that although surface tension is reduced to 43 mN $m^{-1}$ when solution temperature is raised to 60 $^{o}$C, the amount of acid mist increases by nearly 7 folds. This is because an increase in the temperature of the solution not only reduces the surface tension but also the viscosity of the solution, making it easier for the bubble burst to produce finer droplets, which are more likely to become airborne.

Figure 6.3 shows that addition of FC-1100 to the solution also results in a large surface tension reduction, similar to that of temperature rise. The amount of acid mist, however, is reduced by nearly 7 folds. As will be seen later, such a reduction in acid mist amount is not due to reduction in surface tension, but a change in the bubble burst mechanism caused by the presence of the surfactant.

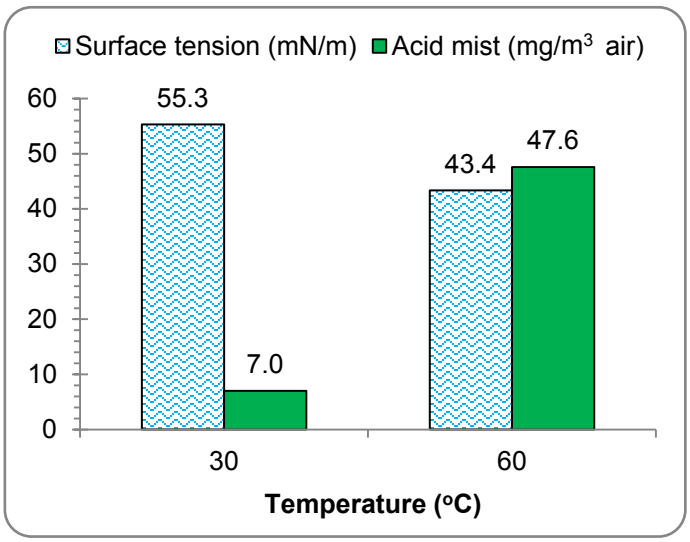


**Figure 6.2** Effect of temperature on surface tension and acid mist

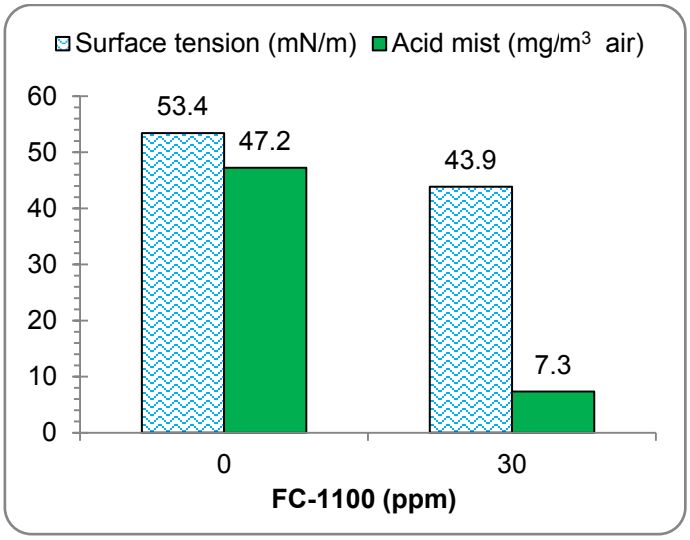


**Figure 6.3** Effect of FC-1100 on surface tension and acid mist

When a surfactant is present in a solution, surface viscosity and surface elasticity are two measurable parameters and are often utilized to characterize the dynamics of monolayer. Surface viscosity represents the resistance to deformation of the film to a stress imposed on the system (Pugh 1996). In other words, surface viscosity is a measure of energy dissipation in the surface. Surface elasticity, on the other hand, is a measure of the energy stored in the surface layer (Pugh 1996).

In the absence of a surfactant, such as FC-1100, surface viscosity in the solution/air interface does not exist or is negligible. Hence, the bubble film offers little resistance to burst. Consequently, only a small portion of a bubble's kinetic energy, which is due to its buoyancy force, is required to produce high number of fine droplets. The remainder of the bubble's kinetic energy is transferred to the droplets that are generated upon its collapse. This leads to the generation of droplets with higher initial velocities, increasing their chances of becoming airborne (i.e. generation of higher amounts of acid mist). This is why bubble size has a noticeable effect on the amount of acid mist in the absence of surfactant molecules.

In the presence of surfactant molecules, when a bubble reaches the free surface of the solution, the thinning of the liquid film that is formed between the bubble and the ambient air leads to the creation of a gradient in the concentration of the surfactant molecules. To balance the concentration gradient, the surfactant molecules move towards the thinner section of the film, presenting resistance to the film thinning process in the form of surface viscosity and/or surface elasticity. A large portion of the bubble's kinetic energy is therefore dissipated to overcome the surface viscosity and surface elasticity of the

solution. Hence, the liquid droplets produced from the burst have less energy and travel at lower speeds in comparison to those generated in the absence of a surfactant leading to lesser amounts of airborne droplets (i.e. lesser amounts of acid mist). In addition, the resistance to burst also implies fewer number but larger volume of droplets. In summary, the presence of a surfactant in the solution changes the bubble burst behaviour to the extent that the effect of bubble size on the amount of acid mist becomes negligible, hence the near horizontal trend line for the No FC-1100 data in Figure 6.1.

In the copper electrowinning industry there are two frequently asked questions in regard to acid mist. The first question is whether smaller bubbles generate less acid mist or big bubbles? The second question, which follows naturally, is that how the process parameters can be changed to favour the generation of bubbles that will result in less acid mist?

In our studies, we have shown that in the absence of surfactants, an increase in the average bubble size does indeed decrease acid mist generation. However, it should be noted that even most extreme changes in the process parameters, within operational limits, can only result in at most 10-20 μm change in the average bubble diameter (Al Shakarji et al. 2011a), which is insufficient to achieve satisfactory level of acid mist reduction. In contrast, if a surfactant such as FC-1100 is used, the size of the bubbles becomes irrelevant.

## 6.4 Conclusions

In the absence of a surfactant, bubble size has a noticeable negative correlation with the amount of acid mist being generated in that larger bubbles result in less acid mist. In the presence of a surfactant, however, the effect of bubble size on acid mist becomes negligible. The change in the bubble burst mechanism, due to the presence of surfactant molecules at the solution/air interface, is proposed to be the reason for the suppressed effect of bubble size on the amount of acid mist.

# Chapter 7: The Mechanism of Acid Mist Generation


## Abstract

This chapter investigates the dispersion of acid mist, generated during copper electrowinning, at (and above) the solution/air interface. Theoretical assessment of the source of acid mist suggests that acid mist is formed almost entirely from airborne jet drops and not film drops as generally understood. Jet drops are created from the disintegration of a liquid jet which is formed after the collapse of the bubble cavity.

The size distribution and number frequency of the jet drops, generated during copper electrowinning, is estimated based on size distribution and frequency data of oxygen bubbles from our previous work. The maximum acid mist concentration, for a given air suction rate, is shown (theoretically and experimentally) to occur not at the solution/air interface but rather at a certain height above the solution line.

Almost all the generated jet drops are predicted to become airborne at air velocities less than 100 mm $s^{-1}$. Therefore, it can be concluded that forced ventilation systems, such as hoods and suction fans, increase acid mist generation by increasing the air flow rate above the solution which in turn increases the number of airborne jet drops. In contrast, acid mist barriers such as floating balls and mats reduce the natural convection of air above the solution which in turn reduces the number of airborne jet drops.


*Keywords:* Acid mist; Jet drops; Aerosol; Electrowinning; Oxygen evolution

## 7.1 Introduction

Literature data on acid mist in electrowinning is scarce. Information on the nature of the ejected droplets, their size distribution, and their dependency on bubble sizes is virtually non-existent. The number of the airborne droplets (i.e. acid mist concentration) changes with the height above the solution. General understanding is that the concentration of acid mist is at its maximum at the vicinity of the free surface of the solution and decreases further height above the solution.

In many of the electrowinning tankhouses, forced ventilation or hoods are used to reduce the concentration of acid mist in the air. The acceptable level of acid mist in the breathing zone is usually less than 1 mg of sulphuric acid per $m^3$ of air (OSHA 2003). The effectiveness of forced ventilation and hoods in reducing acid mist strongly depends on their installation position and also on their air flow rate. Currently, due to the absence

of quantitative information about the parent of acid mist and its concentration at different heights, ventilation fans and hoods are installed at arbitrary heights and run at arbitrary air flow rates.

This chapter provides crucial quantitative information about the nature and size distribution of the airborne acid-containing droplets, the change in acid mist concentration with the height above the solution, and the effect of air flow rate on acid mist concentration.

## 7.2 Theory

When a bubble bursts at the free surface of a liquid, it usually produces two types of drops: film drops and jet drops. As mentioned in Section 2.3.2, the type and the number of these droplets depend on the size of the parent bubble.

The majority of copper electrowinning bubbles have a diameter of 20-180 μm and a few are in the range of 180-400 μm (Al Shakarji et al. 2011a). Therefore, according to equations 2.7 and 2.8, the airborne acidic drops (i.e. acid mist) in copper electrowinning are almost entirely jet drops and not film drops as previously thought.

The number of jet drops, based on equation 2.8, increases exponentially as the diameter of the bubble decreases. The size of a jet drop, on the other hand, increases with bubble size (Spiel 1997). Furthermore, the first drop generated from the disintegration of a given liquid jet is usually the largest and the consequent drops decrease in size (Spiel 1997). The following empirical correlations were derived, from the experimental work of Spiel (1997) on sea water bubbles at 27-29 °C, to predict the radius of the first three jet drops ($R_{drop}$ in μm) generated after the collapse of a micro bubble of radius $R_{bubble}$:

$$R_{drop1} = 0.0345 R_{bubble}^{1.206} \quad (7.1)$$

$$R_{drop2} = 0.0172 R_{bubble}^{1.316} \quad (7.2)$$

$$R_{drop3} = 0.000679 R_{bubble}^{1.796} \quad (7.3)$$

Generally, the ejection speed of a jet drop decreases as its size increases. Moreover, the first jet drop has the highest velocity and the consequent drops, generated from the same bubble, are ejected at lower speeds (Rossodivita and Andreussi 1999). The following empirical equations can be used to approximate the speed of ejection of a jet drop ($s_e$ in m $s^{-1}$) based on the size of the bubble it is produced from (Spiel 1997):

$$s_{e\,drop1} = 12.12\exp(-1.390 \times 10^{-3} R_{bubble}) \quad (7.4)$$

$$s_{e\,drop2} = 9.64\exp(-2.806 \times 10^{-3} R_{bubble}) \quad (7.5)$$

$$s_{e\,drop3} = 6.53\exp(-2.916 \times 10^{-3} R_{bubble}) \quad (7.6)$$

Equations 7.1-7.6 come from studies conducted on bubble collapse in seawater or freshwater. The estimations made throughout this chapter are based on the assumption that the collapse mechanism of bubbles in the copper electrolyte solution is not significantly different from that of bubbles in seawater as justified in Section 2.3.2.

For a given bubble size, the first jet drop is the largest and the consequent drops decrease in size. In copper electrowinning, although 6-7 jet drops are expected from the collapse of each bubble (according to equation 2.8), no correlations could be found in the literature to estimate the size of droplets produced after the third drop. Figure 7.1 shows the estimated size of the first three jet drops (based on equations 7.1-7.3) produced after the collapse of a bubble under typical copper electrowinning conditions.

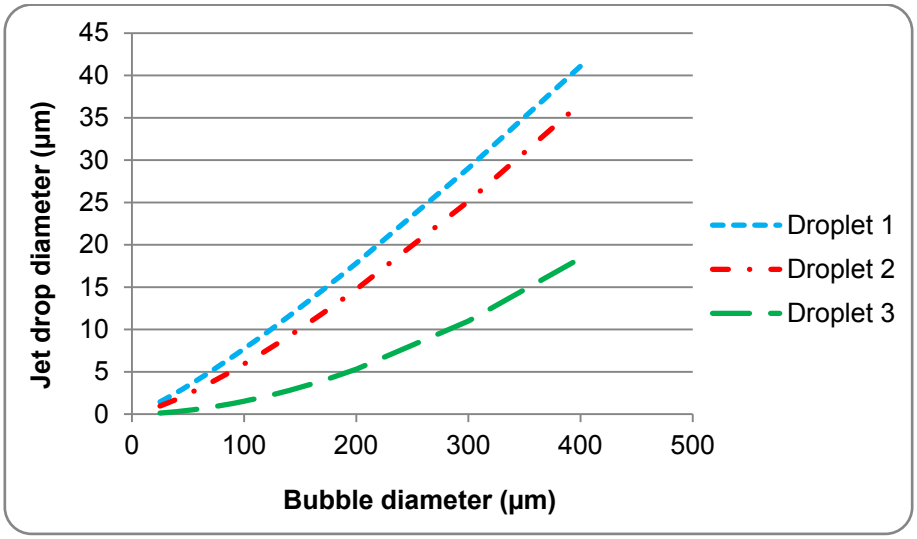


**Figure 7.1** Estimated jet droplet sizes based on the actual bubble sizes in copper electrowinning

A number frequency plot was obtained for the first three jet drops (Figure 7.2) by combining bubble size distribution data from Chapter 5 and jet drop size estimations of Figure 7.1. By assuming 6 drops are generated after the collapse of each bubble, an estimated 569 million jet drops are produced per second for every $m^2$ of immersed anode when operating at a nominal current density of 300 A $m^{-2}$.

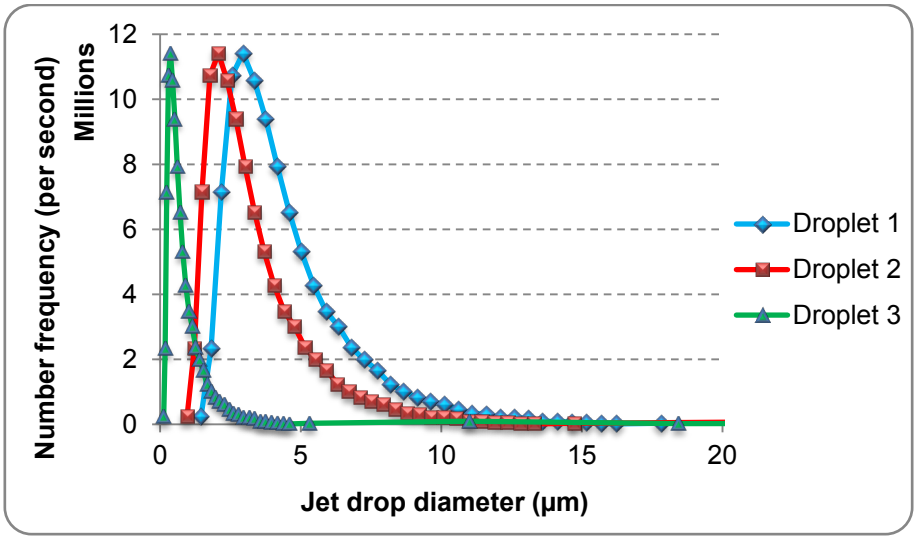


**Figure 7.2** Estimated number frequency plot for the first three jet droplets (per $m^2$ of immersed anode)

To calculate velocity and position profiles of a jet drop (assuming stagnant air and no mass variation of droplet with time), droplet's acceleration ($a$) was calculated as the vector sum of deceleration/acceleration due to gravity ($a_g$) and deceleration due to air drag ($a_d$):

$$a = a_g + a_d \qquad (7.7)$$

where

$$a_g = -9.81 \text{ m s}^{-2} \qquad (7.8)$$

and

$$a_d = -\frac{3}{4}.C_d.\frac{\rho_{air}}{\rho_{drop}}.\frac{u|u|}{D_{drop}} \qquad (7.9)$$ (Rossodivita and Andreussi 1999)

The drag coefficient, $C_d$, is a function of Reynolds number and for a droplet it can be calculated as (Edson and Fairall 1994):

$$C_d = \frac{24}{Re} \quad \text{for } Re < 0.5 \qquad (7.10)$$

$$C_d = \frac{24(1+0.19)}{Re} \quad \text{for } 0.5 \leq Re < 2 \qquad (7.11)$$

$$C_d = \frac{24(1+0.15Re^{0.687})}{Re} \quad \text{for } 2 \leq Re \qquad (7.12)$$

The velocity and position profiles were then calculated by integrating instantaneous acceleration and velocity over time, respectively:

$$u = u_0 + \int a\, dt \qquad (7.13)$$

$$z = z_0 + \int u\, dt \qquad (7.14)$$

The velocity and position profiles of a typical 5 µm jet drop, ejected from a 70 µm bubble, are shown in a semi-log graph in Figure 7.3. The 5 µm jet drop is ejected at a noticeably high speed of 11.4 m $s^{-1}$. The droplet comes to full stop (i.e. reaches its maximum height of 1.04 mm) after only 0.8 milliseconds due to the enormous air drag force opposing its upward motion. The same air drag force slows down the fall of the droplet. The droplet reaches its very low terminal velocity (-0.9 mm $s^{-1}$) 2.0 milliseconds after ejection and falls back to the bulk solution after 1150 milliseconds.

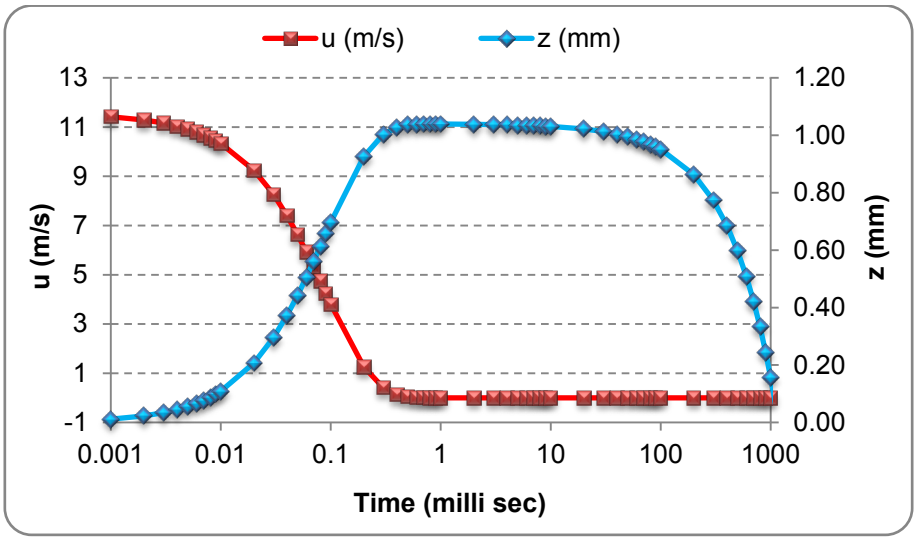


**Figure 7.3** Velocity and position profiles of a typical 5 µm jet drop

Similar calculations were carried out to determine the maximum height reached by each droplet in stagnant air according to its size and ejection speed. The results of these calculations were then combined with the number frequency plots (Figure 7.2) to estimate the total weight of the drops (considering the average solution density of 1200 kg $m^{-3}$) present at a certain height above the solution line (Figure 7.4).

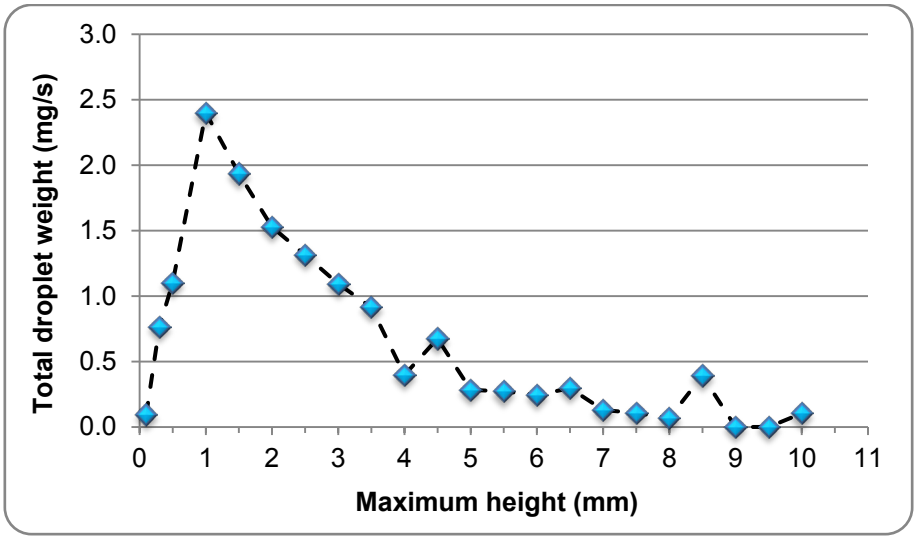


**Figure 7.4** Estimated total weight of acid drops present at certain heights above the solution (per $m^2$ of anode)

The most noticeable feature of Figure 7.4 is that the concentration of acid mist is not the highest at the vicinity of the solution/air interface, contrary to one of the most widely believes in the industry. Initially, acid mist concentration increases with height and only beyond a certain height it starts to decrease. This specific height is estimated to be 1-2 mm above the solution assuming stagnant air above the cell.

It is important to note that stagnant air is not a realistic assumption and it was used to simplify the otherwise extremely complex calculations. In industry, there is a considerable air flow rate above the cell due to natural and forced convections. Oxygen gas liberated after the collapse of bubbles, relatively high temperature gradient between solution and ambient air, and ventilation fans are examples of the sources of natural and forced air convection that are present in almost all the copper electrowinning tankhouses.

## 7.3 Methodology

### 7.3.1. Equipment setup

The copper electrowinning process was replicated in a clear acrylic bench-scale tank (Figure 7.5). For each set of experiments, a fresh batch of solution was synthesized with composition similar to the electrolyte solutions found in most copper electrowinning tankhouses worldwide. The electrolyte solution contained 45 g $L^{-1}$ Cu, 170 g $L^{-1}$ sulphuric acid, 15 mg $L^{-1}$ Guar gum, 20 ppm Cl, and 100 ppm Co.

Acid mist was captured by a nitro cellulose filter (HAWP04700 by Millipore) with a pore size of 0.45 µm to ensure the capture of very fine acidic droplets. Air was drawn through the filter at controlled flow rates and acid mist concentration was calculated as the grams of sulphuric acid, captured by the filter, per $m^3$ of air drawn. Full details of acid mist measurement technique are described in Section 3.2.

Clear flexible PVC sheets were used as curtains to isolate the atmosphere above the cell, up to 1 m, from the outside disturbances. To prevent pressure drop above the cell, due to air suction through the filter, the PVC curtains were open from the bottom allowing the ambient air to flow through freely. The main purpose of PVC curtains was to prevent dangerous acid mist from scattering throughout the lab. In addition, PVC curtains eliminated the effect of uncontrolled external factors, such as the air flow from the laboratory's air conditioning system, leading to more repeatable results.

The nitrocellulose filter and PVC curtains were fixed to a rectangular lid whose surface area was the same as that of the electrolysis tank. The height of the lid could be adjusted freely allowing the filter to be operated at a desired height above the solution line for the duration of each experiment.

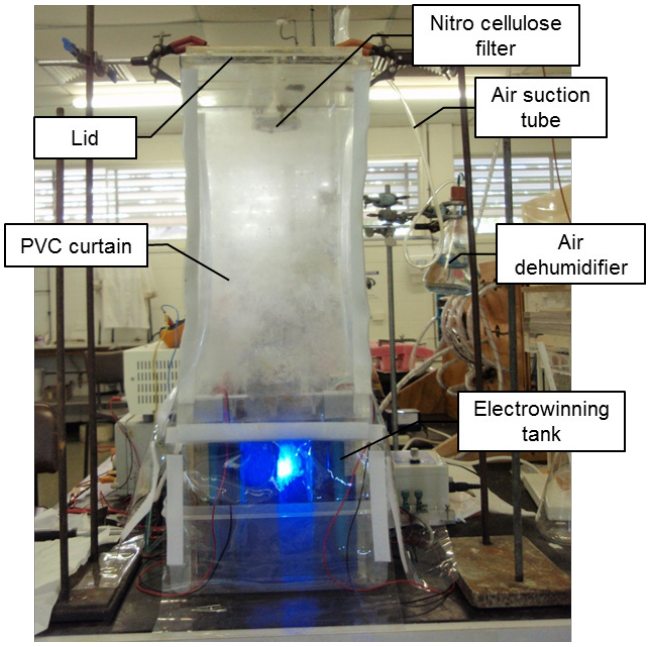


**Figure 7.5** Equipment setup

### 7.3.2. Experimental design

The effects of two factors on acid mist concentration were tested in present work: the air flow rate through the filter, and the height at which the filter was installed. The air drawn through the filter was varied between 0.24 and 3.5 L $min^{-1}$. For a given air flow rate, the height of the filter was varied between 100 and 1000 mm above the solution line. Tests were conducted in 45 $^{o}$C solution with an electrical current density of 300 A $m^{-2}$.

## 7.4 Results and Discussion

In total, 125 experiments were conducted to investigate the effect of height above the solution and effect of air flow rate on acid mist concentration.

### 7.4.1. Effect of air suction rate

The terminal velocity of each of the generated droplets, falling back to the solution, was calculated similar to the example shown in Figure 7.3. For a droplet to become airborne, the velocity of the air moving upward has to be larger than the droplet's terminal velocity. By using these data and droplet size distribution estimates (Figure 7.2), the weight percentage of the airborne drops was calculated as:

$$Weight\ fraction_{airborne} = \frac{\text{Weight}_{\text{airborne drops}}}{\text{Weight}_{\text{generated drops}}} \qquad (7.15)$$

For a given air speed, when air is moving upward, Figure 7.6 shows the maximum size of a droplet that can become suspended in the air. Figure 7.6 also shows the fraction of droplets that would become airborne at a given air speed. For example, at a low air speed of 48 mm $s^{-1}$, droplets up to 37 µm in diameter can become airborne which represents 75 wt% of the total jet drops generated at the solution/air interface.

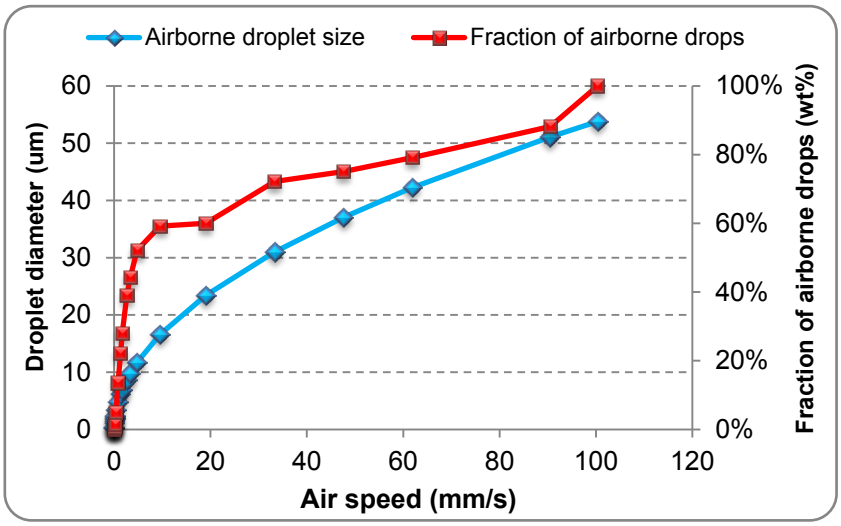


**Figure 7.6** Effect of air speed on making jet drops airborne

Figure 7.6 predicts an exponential increase in the weight of the airborne drops, and therefore in the amount of acid mist, with air velocity.

In theory, in stagnant air situation, jet drops reach no further than 70 mm above the free surface of the solution and all the ejected droplets eventually return to the bulk solution within seconds. Therefore, acid mist should not exist in the absence of air flow. In reality, considerable amount of acid mist is formed even without forced ventilation.

Based on Figure 7.6 estimations, nearly 60 wt% of the droplets that are generated upon the collapse of bubbles will become airborne with air velocities less than 10 mm $s^{-1}$. Such extremely low air velocity could easily occur via natural convection. The hot electrolyte solution (45-50 $^{o}$C) alone can cause a considerable temperature gradient in the surrounding air, resulting in noticeable natural air draft which can carry the jet drops to the breathing zone.

The rate of acid mist generation can be estimated by using the data given in Figure 7.6 and the concentration of sulphuric acid in the solution. Figure 7.7 shows an example of such calculation with acid concentration of 170 grams per litre of the solution which is typical of that of copper electrowinning electrolyte solution.

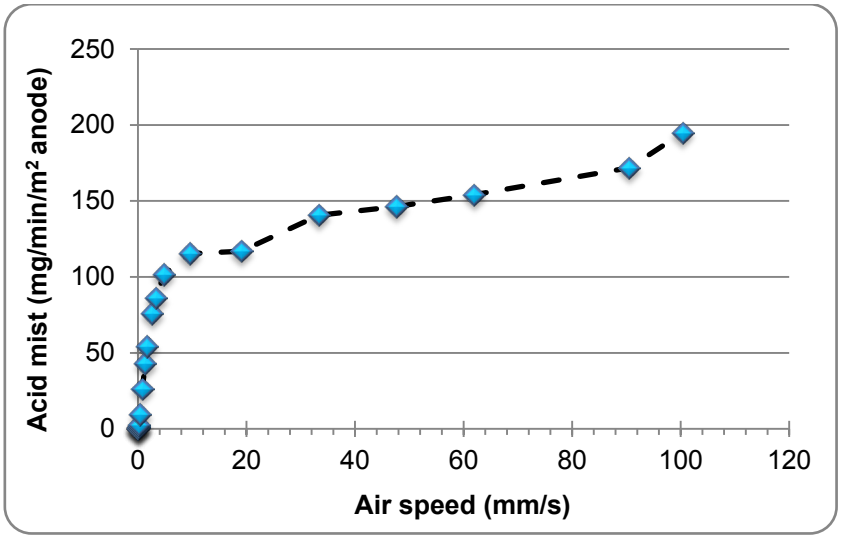


**Figure 7.7** Predicted acid mist generation based on air velocities near the surface of the solution

Data such as those shown in Figure 7.6 and Figure 7.7 can be of great help in designing more effective and more efficient acid mist reduction systems such as hoods and forced ventilations. To illustrate the accuracy of our theoretical work, the actual acid

mist measurements from lab scale tests (Figure 7.9) are used to estimate the air velocities near the surface of the solution for each test. These air velocities are then utilized to predict the maximum size of the airborne drops (similar to Figure 7.6 calculations) and hence the total weight of the airborne acid. A comparison between the actual and theoretical acid mist concentrations is shown in Figure 7.8.

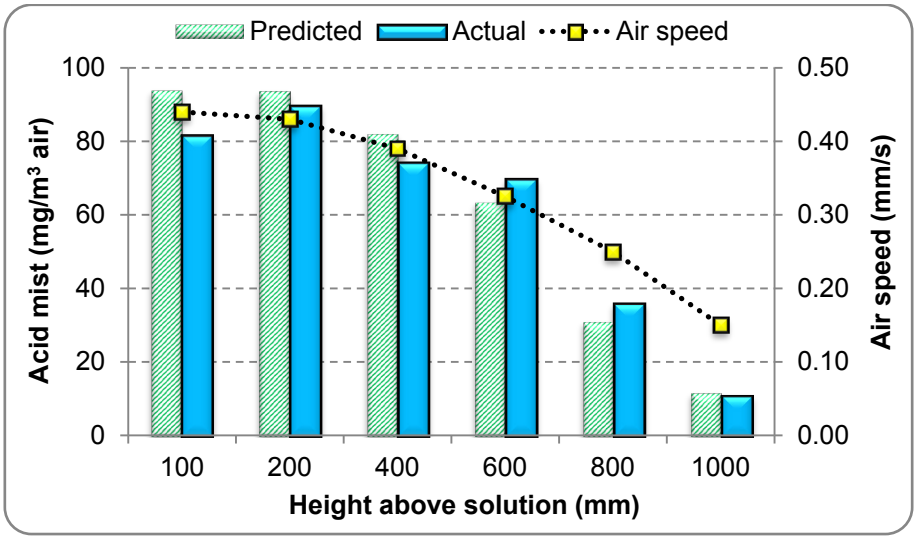


**Figure 7.8** Predicted and actual acid mist concentrations at different heights for a sampling rate of 3.5 L $min^{-1}$

As can be seen in Figure 7.8, the predicted acid mist concentrations are very close to the experimental data. The relative difference between the two sets of data is, on average, 9.4% at various heights above the solution.

### 7.4.2. Effect of height above the solution line

Figure 7.9 shows the results of acid mist measurements at various heights above the solution line for three different air flow rates. It can be seen that as predicted by our theoretical calculations, Section 7.2, the highest acid mist concentration does not occur at the solution/air interface. Instead, the maximum acid mist concentrations exist at 200-400 mm above the free surface of the solution depending on the air suction rate (Figure 7.9).

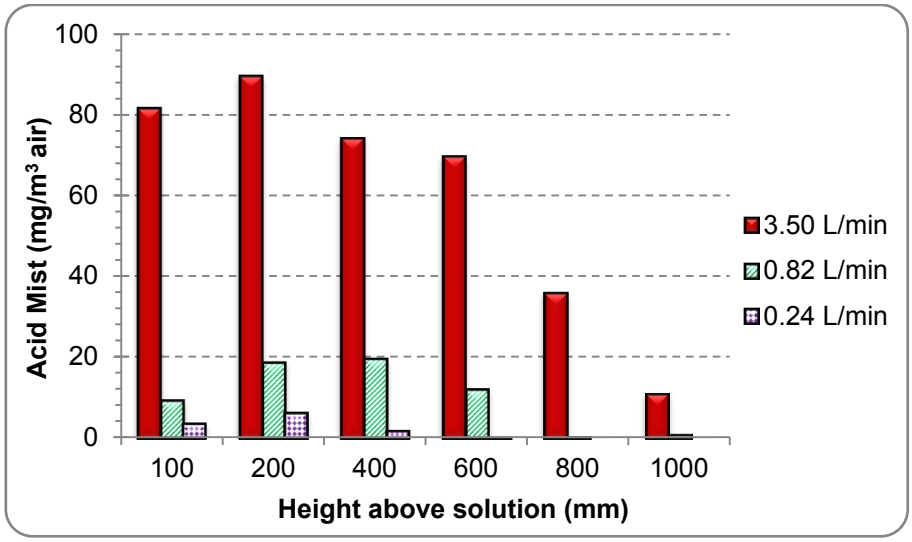


**Figure 7.9** Effect of height and air flow rate on acid mist concentration (experimental data)

Figure 7.9 shows that acid mist concentration gradually decreases beyond the 200-400 mm height and becomes hard to detect at heights more than 1000 mm. In addition, it can be seen that the concentration of acid mist increases exponentially with air flow rate at various heights as predicted by Figure 7.7. The increase in air flow rate from 0.24 to 0.82 L $min^{-1}$ (a 3.4 fold increase), for example, results in a 27 fold increase in the total amount of acid mist and a 14.6 fold increase in the air suction rate (from 0.24 to 3.5 L $min^{-1}$) results in a 650 fold increase in the total amount of acid mist.

## 7.5 Conclusions

Acid mist generated during electrowinning is predicted to be the result of airborne jet drops and not film drops as generally understood. These jet drops are the result of the disintegration of jets that are formed after the collapse of bubbles at the free surface of the solution.

The size distribution and number frequency of the jet drops in copper electrowinning is estimated based on size distribution data of oxygen bubbles from our previous work. Nearly 60 wt% of the generated jet drops is predicted to become airborne at air velocities as low as 10 mm $s^{-1}$. Forced ventilation systems, such as hoods and suction fans, will therefore increase acid mist generation by increasing the air flow rate above the solution which in turn increases the number of airborne jet drops. In contrast, acid mist barriers such as floating balls and mats reduce the number of airborne jet drops by reducing the convection of air above the solution.

The amount of acid mist varies at different heights above the solution. The maximum acid mist concentration, for a given air sampling rate, is shown (theoretically and experimentally) to occur not at the solution/air interface but rather at a certain height above the solution line.

# Chapter 8: Performance Evaluation of Acid Mist Reduction Techniques


## Abstract

The effectiveness of various acid mist suppression techniques has been analysed in the present work. The two important factors that influenced the performance of a floating barrier were its coverage of the solution's surface area and its height above the solution line. When comparing single layered floating barriers, spherical shaped barriers reduced acid mist the most due to their higher buoyancy and higher coverage of the solution surface. In general, barriers made of high density polyethylene were 3.4% more effective in reducing acid mist than those made of polypropylene due to their lower density which enabled them to be more buoyant in the solution and intercept acid mist more effectively.

Acid mist was reduced noticeably with the addition of FC-1100 (a chemical reagent widely used to suppress acid mist) to the solution up to 30 ppm. Further addition of FC-1100 made much less difference in the suppression of acid mist. When FC-1100 was used in combination with floating barriers (such as spheres), the reduction in acid mist improved by an average of 29% in comparison to the use of FC-1100 alone.


*Keywords:* Acid mist; Copper electrowinning; Floating barriers; Surfactant; FC-1100; Current density

## 8.1 Introduction

In many of the electrowinning tankhouses, plastic balls or beads are employed to reduce the formation of acid mist in the tankhouse. More than 56% of the electrowinning plants worldwide use plastic balls to reduce acid mist (CTI-ANCOR 2001). These plastic objects float on the surface of the electrolyte providing a barrier that prevents the acidic droplets, caused by the burst of oxygen bubbles, from becoming airborne.

These floating objects are good mist eliminators only in thick layers (Mella et al. 2006). Using thick layers of plastic balls or beads, however, often results in thin upper cathode deposit making it difficult to strip the produced copper from the cathode. Another disadvantage of using balls and beads is difficult housekeeping. The floating barriers are small, 2-20 mm in diameter, and easily slip into the pipes and pumps blocking the flow of electrolyte and damaging the equipment (Mella et al. 2006). Moreover, it is very hard to maintain a thick layer of these floating objects covering the entire free surface of the solution. On the large scale, often there are sections where very few or no balls at all are

present at the surface of the solution and acid droplets are directly ejected into the air by the bursting bubbles.

Despite the wide spread use of these floating barriers, their effectiveness has not been quantified and documented. In this chapter, the performance of different floating barriers in reducing acid mist has been quantified and the reasons for their differences discussed. In addition, the effects of the barrier's material type (high density Polyethylene versus Polypropylene) and the electrical current density on the operation of the floating barriers have also been investigated.

A chemical reagent known as FC-1100 (Fluorad$^{TM}$ manufactured by 3M) is also widely used in electrowinning tankhouses to suppress acid mist. No publications could be found, except for the brochures supplied by the manufacturer of FC-1100, that quantifies the effectiveness of this reagent in comparison to other mist suppression techniques. In this chapter, we have examined not only the effect of FC-1100 concentration on acid mist, but also have quantified its effectiveness when used in combination with other acid mist reduction techniques.

## 8.2 Methodology

### 8.2.1. Equipment setup

The copper electrowinning process was replicated in a clear acrylic bench-scale tank (Figure 8.1). Four submersible heaters, with variable heat output, were used to keep the temperature of the solution at 45±1 $^{o}$C. The electrolyte solution used for the experiments was synthesized to be similar to those used in the copper electrowinning industries. Concentrations of major chemicals in the electrolyte were 45 g $L^{-1}$ Cu, 170 g $L^{-1}$ sulphuric acid, 15 mg $L^{-1}$ Guar gum, 15 ppm Cl, and 100 ppm Co.

Clear flexible PVC sheets were used as curtains to isolate the atmosphere above the cell from the outside disturbances. Acid mist was captured by nitro cellulose filters (HAWP04700 by Millipore). Air was drawn through the filters at controlled flow rates and acid mist concentration was calculated as the grams of sulphuric acid, captured by the filters, per $m^3$ of air drawn. Full details of acid mist measurement technique and equipment setup are described in Sections 3.2.1 and 7.3.1.

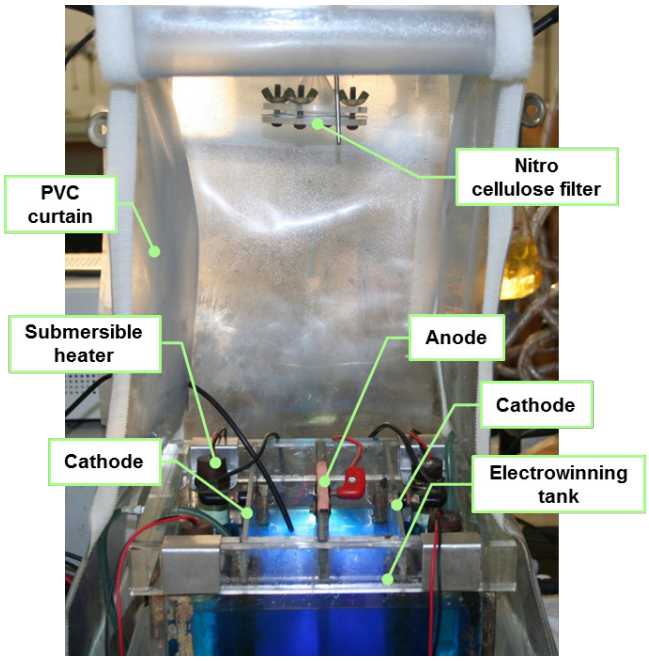


**Figure 8.1** Equipment setup

### 8.2.2. Experimental design

Floating barriers and chemicals reagents are commonly used in the industry to reduce acid mist. In this study, the performances of four different floating barriers and a chemical reagent (FC-1100) were quantified and compared.

The floating barriers were utilized to study the effect of a barrier shape and also material type on acid mist reduction. Material type and dimensions of each barrier are shown in Table 8.1. Figure 8.2 shows the four different floating barriers used in the experiments. To maintain consistency and to accurately observe the effect of a test parameter, one layer of each of the floating barriers was artificially arranged to give a maximum surface coverage for each given experiment.

**Table 8.1** The selected test variables and their values (PE: Polypropylene, HDPE: High density Polyethylene)

| Barrier | Material | Dimensions | |
|---|---|---|---|
| | | Diameter (mm) | Height (mm) |
| Bio balls (solid) | PP | 39 | 31 |
| Spheres (hollow) | PP, HDPE | 19.5 | -- |
| Discs (hollow) | PP, HDPE | 34 | 12 |
| Beads (solid) | PP | 4.5 | 3 |
| | HDPE | 3 | 2 |

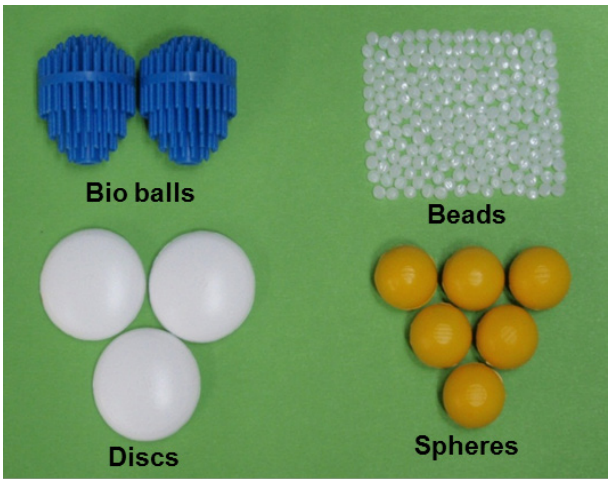


**Figure 8.2** Different shapes of the utilized floating barriers

To examine the effect of current density on the performance of these floating barriers, two different current densities of 200 A $m^{-2}$ and 400 A $m^{-2}$ were used throughout the test series.

The chemical reagent (FC-1100) was tested at various concentrations ranging from 3 ppm to 100 ppm. A combination of FC-1100 with floating spheres is often used in electrowinning tankhouses to supress acid mist. This combination was also replicated in the laboratory and tests were conducted at a nominal current density of 300 A $m^{-2}$.

The acid mist sampling rate (i.e. air flow rate through filters) was set at 3.0 L $min^{-1}$. This sampling rate was higher than that used in the industry (usually 0.2-1.0 L $min^{-1}$) to enhance the resolution of the test results. Since the actual amount of captured acid mist (per $m^3$ of air) could be higher than those observed in the industry (due to higher sampling rate and enclosed test area), the percentage reduction in mist in addition to the actual amounts of captured acid mist are both reported throughout this chapter.

## 8.3 Results and Discussion

The primary goal of the present work was to compare the effectiveness of various acid mist reduction techniques. In total, 105 tests were conducted to investigate the effect of barrier shape and material, current density, and FC-1100 on the amount of airborne acid-containing droplets (i.e. acid mist).

### 8.3.1. Effect of barrier shape and size

The effect of a barrier was calculated by averaging the test results from different current densities and material types. As can be seen in Figure 8.3, one layer of the floating barrier reduced the acid mist amount by 30-60% when compared to the control tests where no chemical or mechanical suppressor were used (labelled as "None" in Figure 8.3). Spheres provided the highest reduction in acid mist followed by discs and bio balls. In comparison, beads were the least effective in preventing acid mist from escaping the surface of the cell to the atmosphere above.

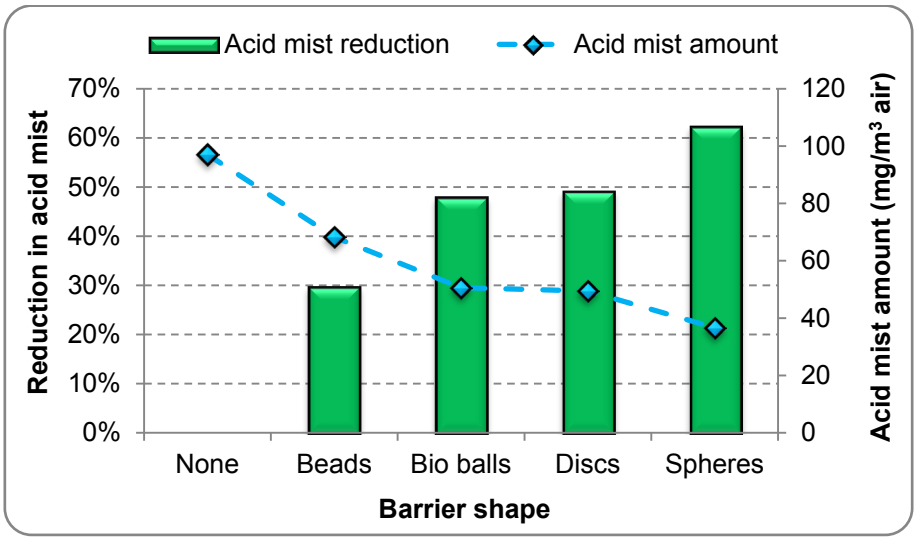


**Figure 8.3** The effect of barrier shape (single layer) on reducing acid mist

Based on the ANOVA analysis, the difference made in the amount of acid mist was statistically significant for all barriers in comparison to the control test with no barriers (based on the 95% confidence interval). Moreover, the reduction in acid mist by spheres was also considered significantly different from that by beads.

Based on the observed results, it was speculated that the exposed area of the free surface of the solution could be the reason for the differences observed in the acid mist amounts when using different barriers. To examine this theory, the portion of the solution surface covered by a barrier (i.e. surface coverage) was calculated for each type of barrier. ImageJ, an open source image analysis software, was used to analyse images taken from the top of the cell to estimate the surface coverage. For example, the total free surface of the solution between the two electrodes was 4197 $mm^2$. A total of 10 spheres were used between the two electrodes to block the acid mist. The total area of the solution blocked by the spheres was estimated (by ImageJ) to be 2924 $mm^2$. Therefore, the surface coverage was calculated as

$$\text{Surface coverage}_{spheres} = \frac{2924}{4197} = 0.697 \qquad \textbf{(8.1)}$$

Surface coverage and acid mist reduction exhibited a linear relationship except when beads were used (Figure 8.4). Although beads provided the highest surface coverage (i.e. least exposed solution), the amount of acid mist detected was the highest.

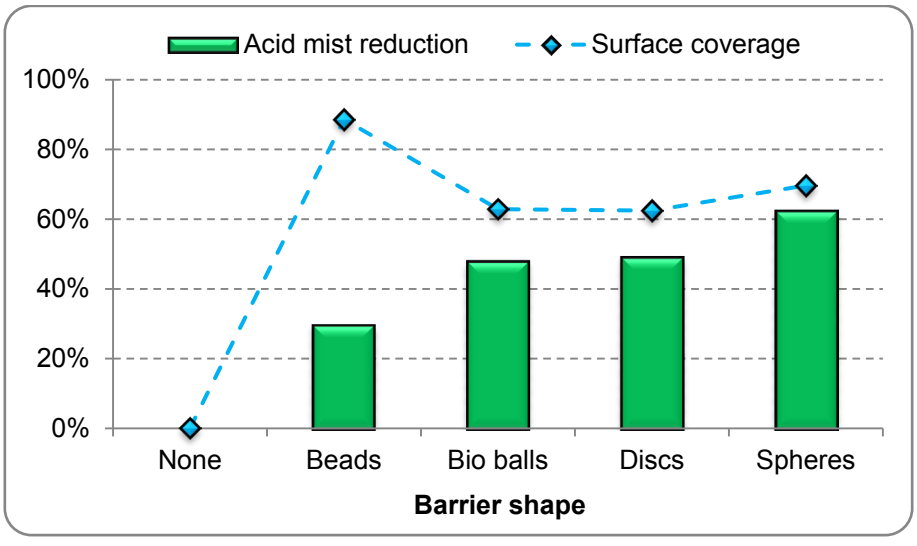


**Figure 8.4** Acid mist reduction and surface coverage comparison of different barriers

Results in Figure 8.4 suggested that surface coverage was not the only factor influencing the amount of acid mist but that the height of a barrier above the surface of

the electrolyte also played a role. Intuitively, one would expect that the more buoyant a barrier, the better chance it would have in intercepting the acidic droplets ejected by the bursting bubbles at the surface of the solution. Consequently, less acid mist is expected to become airborne.

To test this theory, the total volume of a barrier floating above the free surface of the solution was calculated by using top view and side view images of each floating barrier. This calculated volume was then plotted alongside the percentage of acid mist reduction for each barrier (Figure 8.5).

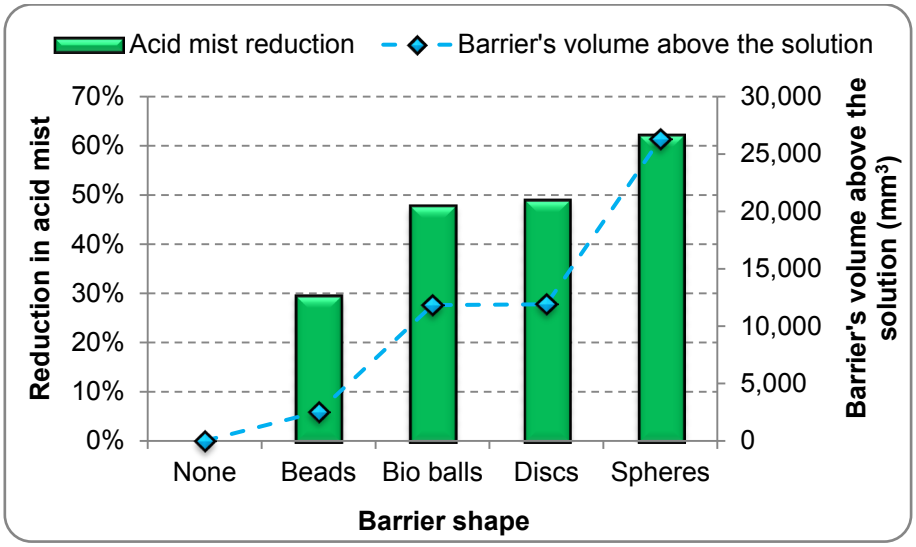


**Figure 8.5** Effect of barriers' volume (single layer) above the solution on acid mist reduction

It can be seen that the effectiveness of a barrier in reducing acid mist was closely related to the total volume of a barrier above the free surface of the solution. In other words, the thickness of a barrier and its surface coverage were two important factors in determining its ability to prevent acid mist.

Multiple layers of a floating barrier are often used in the industry to improve the suppression of acid mist. The change in acid mist suppression power is clearly demonstrated in Figure 8.6 where spheres, discs, and beads were applied in one, two, and three layers. The reduction in acid mist increased with the number of layers applied, as expected. Furthermore, the rate of improvement in acid mist suppression decreased with the number of layers. For example, on average, one layer of a floating barrier decreased acid mist by 47% whereas the addition of second and third layers only resulted in an

overall reduction in acid mist of 69% and 77%, respectively (i.e. 22% and 8% acid mist reduction improvement per layer added, respectively).

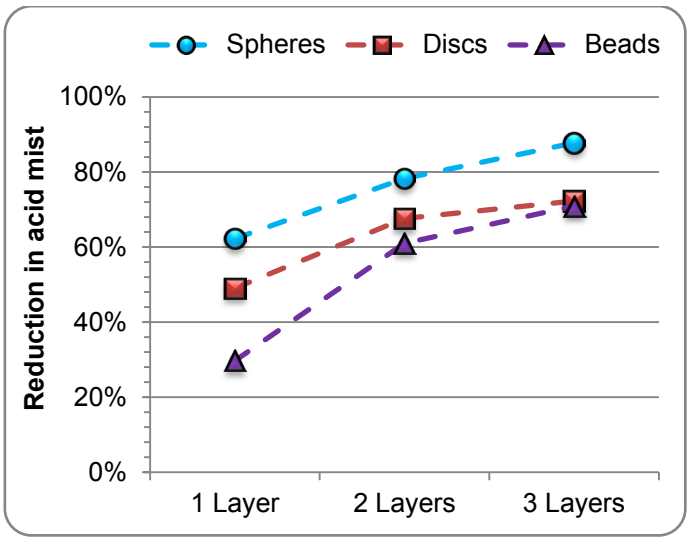


**Figure 8.6** Effect of using multiple layers of a floating barrier

### 8.3.2. Effect of barrier material

Spheres, discs and beads were available in polypropylene (PP) and high density polyethylene (HDPE). All the 6 different barriers were examined to observe the effect of material type (Figure 8.7).

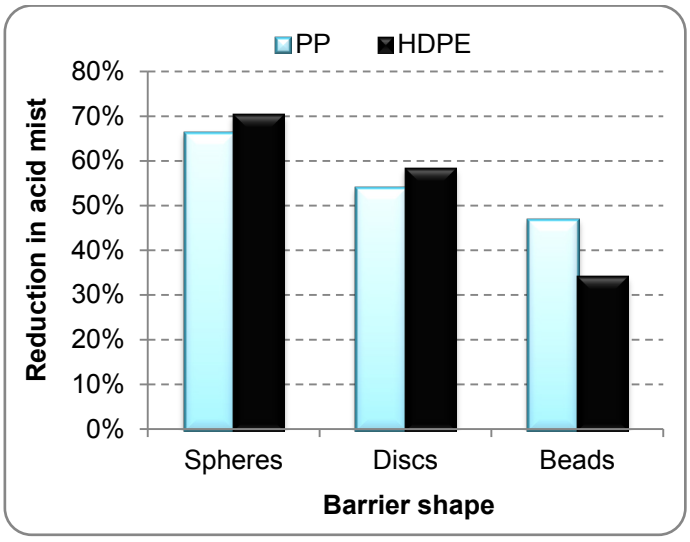


**Figure 8.7** Effect of barrier's material type on acid mist reduction

The relative difference in reducing acid mist due to material type was about 4% for spheres and discs. The buoyancy of a floating barrier and its coverage of the free surface of the solution were two important characteristics in the reduction of acid mist, as

established in Section 8.3.1. On the other hand, PP and HDPE had similar densities (0.946 and 0.941 g $m^{-3}$ respectively). Therefore, two barriers of the same shape would have similar thickness (height above the free solution) and similar coverage of the solution surface. These similarities led to the similarities in acid mist reduction power observed for similar shaped barriers made of PP or HDPE materials. The slightly better performance of HDPE spheres and discs in comparison to their PP counterparts was attributed to the lower density of HDPE (in comparison to PP) barriers which resulted in slightly better buoyancy and therefore a better mist suppression.

Beads, in contrast to spheres and discs, made of PP reduced 13% more acid mist than those made of HDPE. Closer examination of the shape and size of beads revealed that PP beads were on average 1.5 mm wider and 1 mm thicker than HDPE beads. Although the surface coverage of both types of beads were very similar, due to their very small sizes, the height above the solution of PP beads was about 1.4 mm whereas that of HDPE beads was about 0.7 mm. Thus, the better performance of PP beads in comparison to HDPE beads was attributed to their higher height above the solution line.

### 8.3.3. Effect of current density

Based on Faraday's law, the total volume of oxygen gas liberated during electrolysis is directly related to the amount of electrical current flowing through the anode. On the other hand, current density has a negligible effect on the detachment size of bubbles (Al Shakarji et al. 2010). Therefore, doubling the electrical current density doubles the number of oxygen bubbles generated per unit time. Consequently more acid mist is expected to be produced as a result of more bubbles bursting at the free surface of the solution.

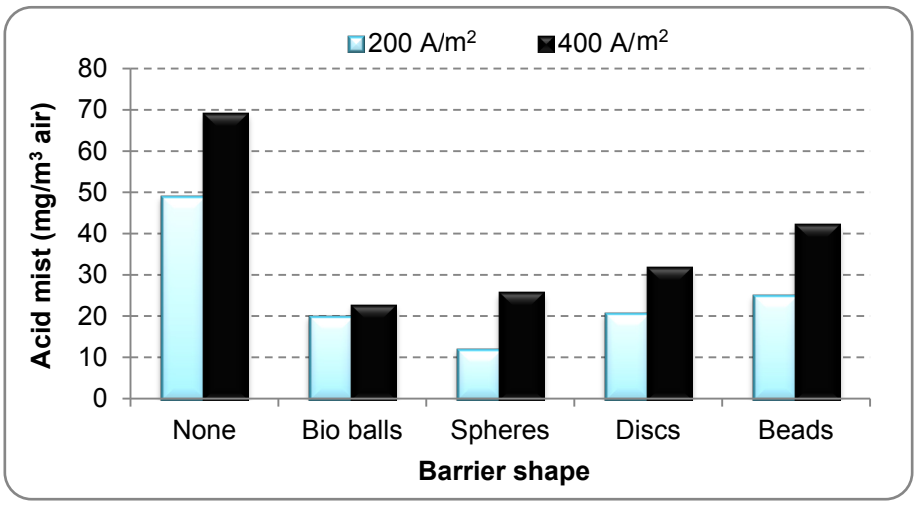


**Figure 8.8** Effect of current density on acid mist amount

Figure 8.8 confirmed that more acid mist was indeed generated at higher current density regardless of the barrier type. However, doubling the current density from 200 to 400 A $m^{-2}$ did not double the amount of acid mist as one would expect. On average, doubling the current density resulted in only 59% increase in the amount of acid mist. The reason was that acid mist was produced from the burst of bubbles that ejected droplets into the air of which some became airborne. The amount of mist generated from the simultaneous bursts of two neighbouring bubbles is known to be less than the sum of mist amount from the bursts of two individual bubbles separately, due to interferences between the bursts of the bubbles (Al Shakarji et al. 2011b). At a higher current density, the number of neighbouring bubbles bursting simultaneously is higher. Therefore, even though the number of oxygen bubbles is doubled when current density is doubled, the acid mist amount is less than double.

### 8.3.4. Effect of FC-1100

A series of tests were conducted to determine the effect of FC-1100 concentration on acid mist reduction. The reduction percentage in acid mist in addition to the actual amounts of captured acid mist is shown in Figure 8.9. The reduction percentage in acid mist was calculated based on the amount of acid mist generated in the absence of barriers and FC-1100.

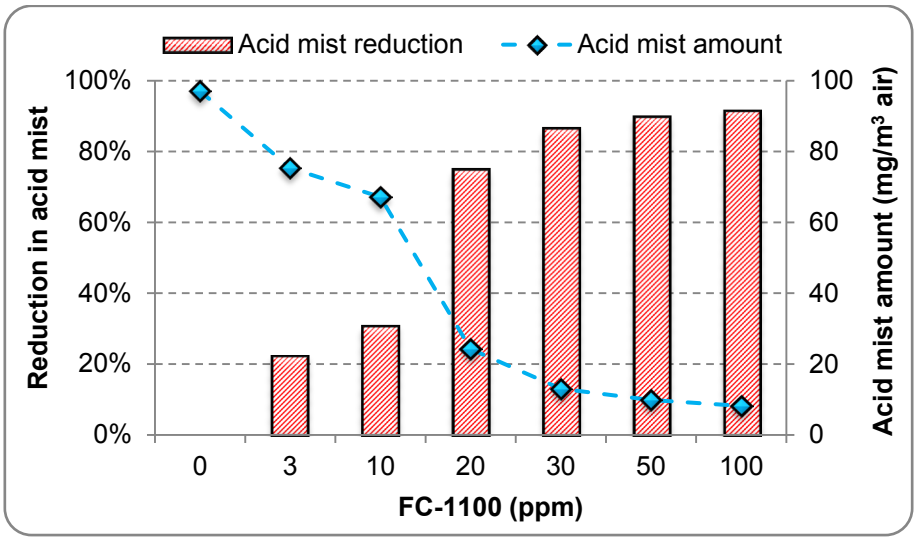


**Figure 8.9** Effect of FC-1100 concentration on acid mist

The decrease in the amount of acid mist with increased FC-1100 was noticeably high up to 30 ppm concentration and became much less thereafter. It should be noted that, in contrast to the general understanding, FC-1100 does not reduce acid mist by reducing the

surface tension of the solution. Acid mist is reduced because FC-1100 molecules change the bubble burst mechanism and slow down the drainage rate of the thin film that is formed when a bubble reaches the free surface of the solution (Al Shakarji et al. 2011b, Al Shakarji et al. 2012).

The Occupational Safety & Health Administration (OSHA) and American Conference of Governmental Industrial Hygienists (ACGIH) both recommend a Permissible Exposure Limit (PEL) of 1 mg sulphuric acid per $m^3$ of air. When 3-10 ppm of FC-1100 was added to the solution, based on the manufacturer's recommendation, the amount of acid mist was still much higher than PEL (67-75 mg $m^{-3}$). Even at 100 ppm concentration, the actual amount of acid mist (8.2 mg $m^{-3}$) was still noticeably higher than PEL. This is why in industry, FC-1100 is almost always used in combination with one or more other mist suppression techniques such as floating barriers, mats, or hoods.

### 8.3.5. Combined effect of FC-1100 and spheres

In the electrowinning tankhouses, typically 2-3 layers of balls are applied for effective acid mist reduction. A set of experiments were conducted to examine the improvement in acid mist reduction when 3 layers of spheres utilized at various FC-1100 concentrations. The results are demonstrated in Figure 8.10.

Figure 8.10 shows that in the absence of FC-1100, 3 layers of spheres can still provide a good reduction in acid mist (nearly 88%). A consistent improvement in the performance of the floating spheres was observed with the increase in the concentration of FC-1100 in the solution. The amount of acid mist was reduced by 95% when spheres were used in combination with 10 ppm of FC-1100.

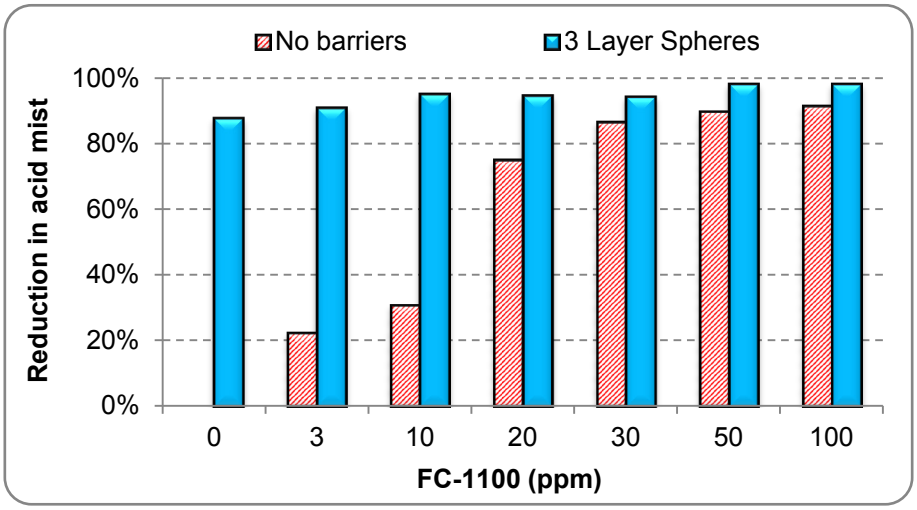


**Figure 8.10** Effectiveness comparison of different barriers

## 8.4 Conclusions

The effectiveness of a floating barrier in reducing acid mist was strongly influenced by two parameters: its coverage of the free surface area of the solution, and its height above the solution line. When comparing one layer of a floating barrier, spherical shaped barriers performed the best (62% acid mist reduction) followed by discs (49%) and bio balls (48%). Beads provided the lowest reduction in acid mist (30%).

Overall, barriers made of high density polyethylene (HDPE) were 3.4% more effective in reducing acid mist than those made of polypropylene (PP). It was hypothesized that the lower density of HDPE enabled HDPE barriers to be more buoyant in the solution resulting in more effective coverage and interception of acid drops and preventing them from becoming airborne.

The amount of acid mist was increased by 59%, on average, when current density was increased from 200 to 400 A $m^{-2}$. The amount of acid mist, although increased, did not double when current density was doubled. This was attributed to the interaction between bubbles bursting simultaneously at the free surface of the solution, resulting in lesser than expected number of airborne acid droplets.

Acid mist was reduced noticeably with the addition of FC-1100 to the solution up to 30 ppm. Considerable reductions in acid mist (91-98%) were achieved 3 layers of spheres were used in combination with FC-1100.

# Chapter 9: General Conclusions

The PhD thesis was accomplished by conducting a total of 429 experiments and utilizing 158 batches of synthesized electrolyte solutions of various compositions. Overall, more than 112,000 bubble images were captured containing an estimated 16.8 million bubbles. 512 of these photos (containing 64,000 bubbles) were carefully analysed for bubble size measurements.

## 9.1 Amount of acid mist

Acid mist still is a serious issue in the purification of non-ferrous metals (such as copper, zinc and nickel) via the electrowinning process. Prior to this study, little quantitative information was available on acid mist generation mechanism and the process parameters that affect the amount of acid mist. In addition, although oxygen bubbles that are generated at the anode were known to be the major contributor to acid mist, no systematic studies had been conducted to investigate the nucleation, growth and burst mechanism of these bubbles.

The present work shows that the total amount of acid mist generated is heavily influenced by the temperature of the solution and the presence of FC-1100 (a mist suppressing reagent commonly used in industry) in the solution. To a lesser extent, electrical current density and solution acidity also affect the total amount of acid mist generated. Acid mist increases with temperature and current density and decreases with the addition of FC-1100 to the solution. Counter intuitively, solutions with higher sulphuric acid concentrations generate less acid mist.

Contrary to the general understanding, FC-1100 does not reduce acid mist generation because of its ability to reduce surface tension of the solution. Instead, it is the ability of this surfactant to increase the surface elasticity and surface viscosity that is responsible for the reduction of acid mist generation. The bubble burst mechanism at the free surface of the solution, which is mainly influenced by surface elasticity and surface and bulk viscosity of the solution, is a critical factor in determining the amount of acid mist generated.

The amount of acid mist is increased, on average, by only 59% when current density is doubled from 200 to 400 A $m^{-2}$. This less than expected increase in acid mist amount is attributed to the interaction between bubbles bursting simultaneously at the free surface of the solution.

Floating barriers such as balls and beads are widely used to supress acid mist. The effectiveness of a floating barrier in reducing acid mist is strongly influenced by two parameters: its coverage of the free surface area of the solution, and its height above the solution line. Barriers made of high density polyethylene (HDPE) are, on average, 3.4% more effective in reducing acid mist than those made of polypropylene (PP). The lower density of HDPE is believed to enable HDPE barriers to be more buoyant in the solution, resulting in more effective coverage and interception of acid drops and preventing them from becoming airborne.

Acid mist is reduced noticeably with the addition of FC-1100 to the solution up to 30 ppm. Further addition of FC-1100 makes much less difference in the suppression of acid mist. When FC-1100 is used in combination with floating barriers (such as spheres), the reduction in acid mist improves further by an average of 29% in comparison to the use of FC-1100 alone.

## 9.2 Source of acid mist

Oxygen bubbles, which are electrolytically generated during copper electrowinning, are the major contributors of acid mist. These bubbles exist in a wide size distribution ranging from less than 20 μm to more than 400 μm in diameter. The heterogeneous surface of the anode is believed to be the main factor for such wide bubble size distribution. Regardless of the applied operating conditions, 95% of the generated bubbles are less than 106 μm in diameter.

FC-1100 and solution temperature have significant effect on the average size of the oxygen bubbles. Bubble size and bubble size distribution are noticeably reduced in the presence of FC-1100 or when the solution temperature is increased. FC-1100 and solution temperature both influence bubble sizes by reducing the overall surface tension of the solution. To a lesser extent, anode age also influences the detachment size of bubbles. Older anodes usually generate larger bubbles and wider bubble size distributions mainly due to their higher surface roughness variations.

In the absence of a surfactant, bubble size has a noticeable negative correlation with the amount of acid mist being generated in that larger bubbles result in less acid mist. In the presence of a surfactant, however, the effect of bubble size on acid mist becomes negligible. The change in the bubble burst mechanism, due to the presence of surfactant molecules at the solution/air interface, is proposed to be the reason for the suppressed effect of bubble size on the amount of acid mist.

Theoretical assessment of the source of acid mist suggests that acid mist is formed almost entirely from airborne jet drops and not film drops as generally understood. These jet drops are the result of the disintegration of liquid jets that are formed after the collapse of bubbles at the free surface of the solution. The diameter of these jet drops is estimated to range from about 0.1 μm up to 54 μm. Nearly 60 wt% of the generated jet drops are predicted to become airborne at air velocities as low as 10 mm $s^{-1}$. Forced ventilation systems, such as hoods and suction fans, will therefore increase the total acid mist generation by increasing the air flow rate above the solution which in turn increases the number of airborne jet drops, although the concentration of the acid mist is lower. In contrast, acid mist barriers such as mats and floating balls reduce the number of airborne jet drops by mechanically blocking the majority of the drops.

## 9.3 Future work

The data produced by the present work can be used to facilitate the design of strategies for minimizing acid mist generation in the tankhouse. The data can also be used to calculate the rate of bubble generation and release under a variety of operating conditions. Such information would be extremely useful in simulating the flow pattern of electrolyte solution between electrodes, which can be utilized to enhance the design of the electrodes and cells leading to improved electrolyte flow and copper quality at higher current densities.

The present work has identified the most influential parameters in acid mist generation. The next step is to measure the change in acid mist when changing these influential parameters in a full sized tankhouse. Such measurements will facilitate the derivation of empirical equations that can be used to accurately estimate the dependence of acid mist generation on the operating conditions of a tankhouse, which is essential in designing effective acid mist suppression techniques that suit the needs of individual tankhouses.

New anodes, such as Ti based anodes, are emerging as alternatives to the conventional lead alloy anodes. Much attention has been given to the savings made in power consumption when using these new anodes but no research has been undertaken to determine their effect on acid mist generation. Anode material can influence acid mist by affecting the bubble size distribution and hence the rate of bubble generation. It is strongly recommended to examine the effect of anode material on the amount of acid mist generated before commercializing a new type of anode.

To design effective and efficient ventilation systems, it is imperative to consider the size of the acid droplets that are generated upon the burst of bubbles at the solution/air interface. In this thesis, the source of acid mist has been identified as jet drops and their size distribution has been estimated theoretically. Appropriate experiments need to be conducted to verify these estimations. In addition, to gain a more in depth understanding of acid mist generation mechanism, the effect of solution properties (such as surface tension, surface elasticity, and surface viscosity) on the ejection speed and size of these jet drops has to be investigated. Such information, could unlock the secret of completely eradicating acid mist.

# Appendix A: Supplementary data

Due to the high volume of the experimental data, the supplementary materials are provided electronically on the attached DVD. Detailed information of all the experimental work (such as test conditions, dates they were conducted, test results, and statistical analyses) are provided in clearly labelled folders corresponding to the chapters of this thesis.

# Bibliography

3M 2007, *Acid Mist Suppressant FC-1100* Powerpoint presentation, 3M.

Al Shakarji, R, He, Y & Gregory, S 2010, 'Measurement of Bubble Size Distribution in Copper Electrowinning Process by Image Analysis', *7th International Copper Conference*, GDMB, Germany, vol. 4, pp. 1237-1251.

Al Shakarji, R, He, Y & Gregory, S 2011a, 'The sizing of oxygen bubbles in copper electrowinning', *Hydrometallurgy,* vol. 109**,** pp. 168-174.

Al Shakarji, R, He, Y & Gregory, S 2011b, 'Statistical analysis of the effect of operating parameters on acid mist generation in copper electrowinning', *Hydrometallurgy,* vol. 106**,** pp. 113-118.

Al Shakarji, R, He, Y & Gregory, S 2012, 'Acid mist and bubble size correlation in copper electrowinning', *Hydrometallurgy,* vol. 113–114**,** pp. 39-41.

Alfantazi, A M & Dreisinger, D B 2003, 'Foaming behavior of surfactants for acid mist control in zinc electrolysis processes', *Hydrometallurgy,* vol. 69**,** pp. 57-72.

Bailey, M, Gomez, C O & Finch, J A 2005a, 'Development and application of an image analysis method for wide bubble size distributions', *Minerals Engineering,* vol. 18**,** pp. 1214-1221.

Bailey, M, Gomez, C O & Finch, J A 2005b, 'A method of bubble diameter assignment', *Minerals Engineering,* vol. 18**,** pp. 119-123.

Bender, J T 2010, 'Evaluation of Mist Suppression Agents for Use in Copper Electrowinning', *7th International Copper Conference*, GDMB, Germany, vol. 4, pp. 1271-1280.

Blanchard, D C & Syzdek, L D 1988, 'Film drop production as a function of bubble-size', *Journal of Geophysical Research-Oceans,* vol. 93**,** pp. 3649-3654.

Cheng, C Y, Urbani, M D, Miovski, P, Kittelty, D, Otero, A F & San Martin, R M 2004, 'Evaluation of saponins as acid mist suppressants in zinc electrowinning', *Hydrometallurgy,* vol. 73**,** pp. 133-145.

Cohen, J 1988, *Statistical power analysis for the behavioural science,* Lawrence Erlbaum Associates Inc., New Jersey.

CTI-ANCOR 2001, 'Electrolytic copper electrowinning', in *World 2001 tankhouse operating data*, University of Arizona, USA, pp. 1-48, viewed 12 May 2008.

Davenport, W G, King, M, Schlesinger, M & Biswas, A K 2002, *Extractive Metallurgy of Copper,* Elsevier Science Ltd, London.

Davis, J A & Eng, P 2002, *Budget quotation for a Cross Flow Ventilation System of Sepon Copper Ltd*. Quote. DESOM Systems Inc.

Drelich, J & Miller, J D 1994, 'The Effect of Solid Surface Heterogeneity and Roughness on the Contact Angle/Drop (Bubble) Size Relationship', *Journal of Colloid and Interface Science,* vol. 164**,** pp. 252-259.

Edson, J B & Fairall, C W 1994, 'Spray droplet medeling', *Journal of Geophysical Research-Oceans,* vol. 99**,** pp. 25295-25311.

Field, A P 2005, *Discovering statistics using SPSS,* SAGE Publications Ltd, London.

Frazer, A 2006, 'The effect of bubble size on acid mist concentration in electrowinning plants', Bachelore of Engineering Honours, James Cook University, Townsville Australia.

Girgin, E H, Do, S, Gomez, C O & Finch, J A 2006, 'Bubble size as a function of impeller speed in a self-aeration laboratory flotation cell', *Minerals Engineering,* vol. 19**,** pp. 201-203.

Grau, R A & Heiskanen, K 2002, 'Visual technique for measuring bubble size in flotation machines', *Minerals Engineering,* vol. 15**,** pp. 507-513.

Grau, R A & Heiskanen, K 2005, 'Bubble size distribution in laboratory scale flotation cells', *Minerals Engineering,* vol. 18**,** pp. 1164-1172.

Grau, R A, Laskowski, J S & Heiskanen, K 2005, 'Effect of frothers on bubble size', *International Journal of Mineral Processing,* vol. 76**,** pp. 225-233.

Harris, D C 2007, *Quantitative chemical analysis,* Freeman and Co, New York.

Henry, C L, Dalton, C N, Scruton, L & Craig, V S J 2006, 'Ion-Specific Coalescence of Bubbles in Mixed Electrolyte Solutions', *The Journal of Physical Chemistry C,* vol. 111**,** pp. 1015-1023.

Hernandez-Aguilar, J R, Coleman, R G, Gomez, C O & Finch, J A 2004, 'A comparison between capillary and imaging techniques for sizing bubbles in flotation systems', *Minerals Engineering,* vol. 17**,** pp. 53-61.

Hiemenz, P C 1977, *Principles of Colloid and Surface Chemistry,* Marcel Dekker Inc, New York.

Holmberg, K, Jonsson, B, Kronberg, B & Lindman, B 2003, *Surfactants and polymers in aqueous solution,* John Wiley & Sons Ltd, London.

Hooper, G 2008, *Quotation on 3M Matting*. Quote. Blackwoods Townsville.

Hosny, A Y 1993, 'Electrowinning of zinc from electrolytes containing anti-acid mist surfactant', *Hydrometallurgy,* vol. 32**,** pp. 261-269.

Houlachi, G E, Edeards, J D & Robinson, T G 2007, *Copper Electrorefining and Electrowinning,* Canadian Institute of Mining, Metallurgy and Petroleum, Quebec Canada.

Hrussanova, A, Mirkova, L, Dobrev & Vasilev, S 2004, 'Influence of temperature and current density on oxygen overpotential and corrosion rate of Pb-Co3O4, Pb-Ca-Sn, and Pb-Sb anodes for copper electrowinning: Part I', *Hydrometallurgy,* vol. 72**,** pp. 205-213.

HSIS 2009, *Exposure standard documentation*, National Occupational Health and Safety Commission, viewed 3 April 2008, <http://hsis.ascc.gov.au/DocumentationES.aspx?ID=578>.

Huet, F, Musiani, M & Nogueira, R P 2004, 'Oxygen evolution on electrodes of different roughness: an electrochemical noise study', *Journal of Solid State Electrochemistry,* vol. 8**,** pp. 786-793.

Hunter, R J 2001, *Foundation of Colloid Science,* Oxford University Press Inc, New York USA.

ICSG 2010, 'The World Copper FactBook', in International Copper Study Group, Lisbon Portugal, pp. 1-58, viewed 11 April 2010.

Jones, S F, Evans, G M & Galvin, K P 1999, 'Bubble nucleation from gas cavities - a review', *Advances in Colloid and Interface Science,* vol. 80**,** pp. 27-50.

Kazakis, N A, Mouza, A A & Paras, S V 2008, 'Experimental study of bubble formation at metal porous spargers: Effect of liquid properties and sparger characteristics on the initial bubble size distribution', *Chemical Engineering Journal,* vol. 137**,** pp. 265-281.

Lin, B, Recke, B, Knudsen, J r K H & Jŕgensen, S B 2008, 'Bubble size estimation for flotation processes', *Minerals Engineering,* vol. 21**,** pp. 539-548.

Liow, J L, Frazer, A, He, Y, Eastwood, K & Phan, C 2007, 'Acid mist formation in the electrowinning of copper', paper presented at 35th Australasian Chemical Engineering Conference, Melbourne Australia, 23-26 September.

Liow, J L & Gray, N B 1996, 'Experimental study of splash generation in a flash smelting furnace', *Metallurgical and Materials Transactions B-Process Metallurgy and Materials Processing Science,* vol. 27**,** pp. 633-646.

Meiron, T S, Marmur, A & Saguy, I S 2004, 'Contact angle measurement on rough surfaces', *Journal of Colloid and Interface Science,* vol. 274**,** pp. 637-644.

Mella, S, Rodrigo, V & Lillo, A 2006, 'Copper electrowinning in the absence of acid mist', in SAME Ltd, Santiago Chile, pp. 1-13, viewed 12 July 2009.

Miller, L A 2012, '2010 Minerals Yearbook (Zinc)', in USGS, pp. 12, viewed 7/7/2012.

Montgomery, D C 2005, *Design and Analysis of Experiments,* John Wiley & Sons, Inc.

Moskalyk, R R, Alfantazi, A, Tombalakian, A S & Valic, D 1999, 'Anode effects in electrowinning', *Minerals Engineering,* vol. 12**,** pp. 65-73.

Najafi, A S, Xu, Z & Masliyah, J 2008, 'Single micro-bubble generation by pressure pulse technique', *Chemical Engineering Science,* vol. 63**,** pp. 1779-1787.

Nguyen, T, Guresin, N, Nicol, M & Atrens, A 2008, 'Influence of cobalt ions on the anodic oxidation of a lead alloy under conditions typical of copper electrowinning', *Journal of Applied Electrochemistry,* vol. 38**,** pp. 215-224.

O'Connor, C T, Randall, E W & Goodall, C M 1990, 'Measurement of the effects of physical and chemical variables on bubble size', *International Journal of Mineral Processing,* vol. 28**,** pp. 139-149.

Oguz, H N & Prosperetti, A 1993, 'Dynamics of bubble-growth and detachment from a needle', *Journal of Fluid Mechanics,* vol. 257**,** pp. 111-145.

OSHA 2003, *Sulfuric Acid Exosure Limits*, Occupational Safety & Health Administration, viewed 6 October 2011, <http://www.osha.gov/dts/chemicalsampling/data/CH_268700.html>.

Permprasert, J & Devahastin, S 2005, 'Evaluation of the effects of some additives and pH on surface tension of aqueous solutions using a drop-weight method', *Journal of Food Engineering,* vol. 70**,** pp. 219-226.

PMOS 2003, 'Solvent Extraction Systems', Drawing, viewed 5 January 2012, <http://www.postmixing.com/mixing%20forum/Macro/Liq-Liq/Mixer-Settlers/cfd%20design/background.htm>

Porter, M R 1994, *Handbook of Surfactants,* Blackie Academic and Professional, UK.

Pugh, R J 1996, 'Foaming, foam films, antifoaming and defoaming', *Advances in Colloid and Interface Science,* vol. 64**,** pp. 67-142.

Resch, F & Afeti, G 1991, 'Film drop distribution from bubbles bursting in seawater', *Journal of Geophysical Research-Oceans,* vol. 96**,** pp. 10681-10688.

Rigby, G D, Grazier, P E, Stuart, A D & Smithson, E P 2001, 'Gas bubble induced mixing in electrowinning baths', *Chemical Engineering Science,* vol. 56**,** pp. 6329-6336.

Robinson, T, Lang, J & Isbell, L 1994, *Cerro Colorado Copper Company SX-EW Plant,* Commissioning report, ISA PROCESS Tankhouse.

Rossodivita, A & Andreussi, P 1999, 'Spray production by air bubbles bursting on a water surface', *Journal of Geophysical Research-Oceans,* vol. 104**,** pp. 30059-30066.

San Martin, R M, Otero, A F & Cruz, A 2005a, 'Use of quillaja saponins (Quillaja saponaria Molina) to control acid mist in copper electrowinning processes: Part 2: pilot plant and industrial scale evaluation', *Hydrometallurgy,* vol. 77**,** pp. 171-181.

San Martin, R M, Otero, A F, Figueroa, M, Escobar, V & Cruz, A 2005b, 'Use of quillaja saponins (Quillaja saponaria Molina) to control acid mist in copper electrowinning processes: Part 1. Laboratory scale evaluation', *Hydrometallurgy,* vol. 77**,** pp. 163-170.

Sigley, J L, Johnson, P C & Beaudoin, S P 2003, 'Use of nonionic surfactant to reduce sulfuric acid mist in the copper electrowinning process', *Hydrometallurgy,* vol. 70**,** pp. 1-8.

Simison, S, Pellicano, A, Brust, M & Schiffrin, D J 1999, 'Detection of near-wall hydrodynamic effects by electrochemiluminescence', *Journal of Electroanalytical Chemistry,* vol. 470**,** pp. 89-94.

Song, A, Dong, S, Hao, J, Liu, W, Xu, G & Wang, H 2005, 'Functions of fluorosurfactants 1: Surface activities-improved and vesicle formation of the short-tailed chain sulfonate salt mixed with a fluorosurfactant', *Journal of Fluorine Chemistry,* vol. 126**,** pp. 1266-1273.

Spiel, D E 1994a, 'The number and size of jet drops produced by air bubbles bursting on a fresh water surface', *Journal of Geophysical Research-Oceans,* vol. 99**,** pp. 10289-10296.

Spiel, D E 1994b, 'The sizes of the jet drops produced by air bubbles bursting on sea-water and fresh-water surfaces', *Tellus Series B-Chemical and Physical Meteorology,* vol. 46**,** pp. 325-338.

Spiel, D E 1997, 'More on the births of jet drops from bubbles bursting on seawater surfaces', *Journal of Geophysical Research-Oceans,* vol. 102**,** pp. 5815-5821.

Spiel, D E 1998, 'On the births of film drops from bubbles bursting on seawater surfaces', *Journal of Geophysical Research-Oceans,* vol. 103**,** pp. 24907-24918.

Subbaiah, T, Singh, P, Hefter, G, Muir, D & Das, R P 2000, 'Sulphurous acid as anodic depolarizer in copper electrowinning Part II', *Journal of Applied Electrochemistry,* vol. 30**,** pp. 181-186.

Sunwest 2004, *The most comprehensive solution to tankhouse emmissions problems*, Sunwest Supply, viewed 13 April 2008, <http://www.sunwesttec.com/brushes.html>.

Tucker, J P, Deglon, D A, Franzidis, J P, Harris, M C & O'Connor, C T 1994, 'An evaluation of a direct method of bubble size distribution measurement in a laboratory batch flotation cell', *Minerals Engineering,* vol. 7**,** pp. 667-680.

Valkovska, D S, Danov, K D & Ivanov, I B 1999, 'Surfactants role on the deformation of colliding small bubbles', *Colloids and Surfaces A: Physicochemical and Engineering Aspects,* vol. 156**,** pp. 547-566.

Vogt, H, Aras, O & Blazer, R J 2004, 'The limits of the analogy between boiling and gas evolution at electrodes', *International Journal of Heat and Mass Transfer,* vol. 47**,** pp. 787-795.

Volanschi, A, Olthuis, W & Bergveld, P 1996, 'Gas bubbles electrolytically generated at microcavity electrodes used for the measurement of the dynamic surface tension in liquids', *Sensors and Actuators A: Physical,* vol. 52**,** pp. 18-22.

von der Höh, A 2010, 'Red jet generated by water droplet*',* Photo, viewed 21 December 2011, <http://www.voidphase.com/media/2010/12/waterdrops_red1_1920.jpg>

Wallace, G J 2011, '2009 Minerals Yearbook (Nickel)*',* USGS, pp. 30, viewed 7 July 2012.

Wedin, R, Davoust, L, Cartellier, A & Byrne, P 2003, 'Experiments and modelling on electrochemically generated bubbly flows', *Experimental Thermal and Fluid Science,* vol. 27**,** pp. 685-696.

Xie, G X, Luo, J B, Liu, S H, Guo, D, Li, G & Zhang, C H 2009, 'Effect of liquid properties on the growth and motion characteristics of micro-bubbles induced by electric fields in confined liquid films', *Journal of Physics D-Applied Physics,* vol. 42**,** pp.

Xu, Q, Nakajima, M, Ichikawa, S, Nakamura, N, Roy, P, Okadome, H & Shiina, T 2009, 'Effects of surfactant and electrolyte concentrations on bubble formation and stabilization', *Journal of Colloid and Interface Science,* vol. 332**,** pp. 208-214.